Deltares

Morphological model for the river Rhine

First (v0.5) model of the IJssel branch

Morphological model for the river Rhine
First (v0.5) model of the IJssel branch

Author(s)
Ana Luisa Nunes de Alencar Osorio
Anke Becker
Anna Kosters
Willem Ottevanger
Victor Chavarrias

Morphological model for the river Rhine
First (v0.5) model of the IJssel branch

Client	-
Contact	Arjan Sieben, Michiel Reneerkens, Dénes Beyer
References	
Keywords	Morphological model, Rhine, DVR

Document controle	
Version	1.0
Date	13-12-2024
Project nr	11210364-003
Document ID	11210364-003-ZWS-0005
Pages	91
Classification	
Status	final

Author(s)

	Ana Luisa Nunes de Alencar Osorio Anke Becker Anna Kosters Willem Ottevanger Victor Chavarrias	

Summary

The riverbed (main channel and flood plains) of the Rhine branches is dynamic and changes over time under the influence of morphological processes and human intervention. Currently, morphodynamics in the Rhine branches can be predicted and assessed with the so-called DVR model. For three reasons, this model is however outdated:

- The calibration is based on periods before realization of several important interventions (Room for the River, Water Framework Directive).
- RWS is moving to a new model generation in new software (the 6th generation models in the D-HYDRO Suite software package).
- There are new data and insights regarding morphological developments.

Therefore, a new model and set of tools is being developed to replace the old one.

The model developments take place over the course of several years and started in 2023. The current report is a progress report on the work that was carried out in 2023 and 2024 and resulted in model version v0.5 (partially 1D calibrated). Choices made in 2023 and 2024 may be changed in the following years to further improve model performance. Once the model of the entire Rhine branches is ready, a final report will be made that contains a full description of all data, methods and results used for the final version v1 of the model.

In 2023 and 2024, a first version of the morphological model of the IJssel (v0) was set-up based on existing 6th generation hydrodynamic models. Some modifications of the hydrodynamic schematizations were needed to make them suitable for morphological simulations (constant roughness, bed level in cell centers). The influence of the way the bed level is schematized is significantly larger in the IJssel model than in the Waal model. This is because the grid resolution on the IJssel is much lower than on the Waal (only 6 cells across the width on the IJssel, while there are about 12 cells across the width on the Waal). The influence of the change in bed level schematization could partly be removed by an appropriate choice of summer bed roughness.

Schematizations for two moments have been made: j02 (start of calibration period) and j16 (start of validation period). First calibration runs have been carried out with j02, leading to model version v0.5. Outputs of the model are compared to offline sediment transport computations and data measurements. The results for width averaged bed level changes and sediment transport are quite good already. Local deviations between model behavior and reality need to be removed in the next phase during more detailed (2D) calibration.

However, varying the parameters of the transport formula has shown that the model is close to ill-posedness. Any small change in the model, such as an update to a more recent geometry or the implementation of an intervention, can lead to instability. It is therefore recommended to implement the possibility to add extra diffusion to the model into the software.

All steps in model development and the main steps in analysis of model results have been defined in Matlab scripts to make them reproducible and re-usable for model development for other branches or future scenarios.

Content

1 Introduction

1.1 Background and motivation

The riverbed (main channel and flood plains) of the Rhine branches is dynamic and changes over time under the influence of morphological processes and human intervention. Currently, morphodynamics in the Rhine branches can be predicted and assessed with the so-called DVR model (Duurzame Vaardiepte Rijndelta – sustainable fairway Rhine delta). For three reasons, this model will be outdated in the foreseeable future:

- The calibration is based on periods before realization of several important interventions (Room for the River, Water Framework Directive).
- RWS is moving to a new model generation in new software (the 6th generation models in the D-HYDRO Suite software package).
- There are new data and insights regarding morphological developments.

An up-to-date and reliable model is however needed for river management issues such as:

- project design of interventions in/along the summer bed (normalisation, sediment management),
- impact assessment for evaluation of measures (river engineering assessment framework / licensing),
- analyses of/after monitoring in pilots (sediment management, eroding banks, river widening such as by longitudinal dams, etc.),
- system analyses for long-term scenarios with management variants, e.g. for IRM (Integraal RivierManagement – Integrated River Management) so that estimates can be made of the morphological development on the different river functions.

These are reasons to replace the current modelling instrument for the Rhine branches with a new set of models and tools.

1.2 Objective

The objective of this project is the development of a new modelling instrument that simulates the complex spatial riverbed dynamics in the Rhine branches, enabling us to predict developments and effects of interventions in the riverbed, examine options for long-term (2050-2100) management and policy decisions, and thus shape the river management of the future.

1.3 This report

The development of such a modelling instrument for the entire Rhine branches will take several years. In 2023, a start was made with model developments for the Waal river branch. In 2024 the model set up for the IJssel was initiated. This report presents the model developments for the IJssel, leading to model version v0.5. Chapter 3 presents the data used. Chapter 4 to 8 describe the model set-up and present calibration and validation preliminary results. Chapter 9 shows conclusions and recommendations for the following steps to be taken in the model development. For the sake of completeness, the recommended next steps in the development of the models of the other Rhine branches are mentioned as well.

This report is a progress report. Choices presented here may be changed in the following years to further improve model performance. Once the models for all branches are finished completely, a series of final reports will be made as follows:

1. main report for all Rhine branches together, summarizing the definitive choices and results
2. calibration reports per branch
3. brief synthesis report, which summarizes, per Rhine branch, the information used in the model and what the model can be used for. This report needs to be easy to read, also by non-experts on morphological modelling.
4. manual, with sections on
   a. tutorial for setting up a new model
      i. how to change model input, if needed specified per branch or river section
      ii. which input is the user allowed to modify, and which not
      iii. how to use the available scripts for modifying input and for visualizing model output
   b. how to apply the model in applications for permits (“vergunningaanvragen”) according to the “Rivierkundig Beoordelingskader (RBK)”
      i. which hydrograph to use
      ii. how many years to simulate
      iii. which standard figures to produce and analyse
      iv. etc.
   c. how to apply the model for policy studies, such as “Integrated River Management (IRM)”
      i. which hydrograph to use
      ii. how many years to simulate
      iii. which standard figures to produce and analyse
      iv. etc.
5. factsheets, for use on the IPLO website, via which model schematizations can be requested. These need to support the choice of model for a specific question.
6. Transfer protocol – “Protocol van Overdracht (PvO)” - the questionnaire to be answered before the model can formally become part of the official set of RWS models

1.4 Software

Within this project, the following software is used:

Software package	Version	Used for
D-HYDRO Suite	2.26.15.78894 (hydrodynamic spin-up and “offline” calibration) 2.27.03.79079 (final morphological simulations)	Hydrodynamic simulations Morphological simulations
Baseline	6.3.2	Schematization of model geometry
ArcGIS	10.6	In combination with Baseline

2 Approach for model set-up

2.1 General approach of the long-term model development

Spruyt (2023) has made an inventory of the intended use of the new modelling instrument and its required functionality. Based on this, she presents a general approach, which foresees a model development in several steps. These steps are extended as follows for this project:

- v0 This version is a basic model that contains the most important functionality, with the main goal to have a running but not yet too complex model. Within this step, we further distinguish the following sub-steps:
  - v0.5: after offline calibration
  - v0.8: after 1D calibration
  - v1: after 2D-calibration, so fully calibrated
- v1 Building on v0, the first model version replaces the existing DVR model. It covers the same functionality, but is based on the latest available data and insights.
- v2 The second model version is based on v1 but extended with new functionality to make the model suitable for more types of applications (e.g. finer grids, exchange of sediment between main channel and flood plains, bank erosion processes, etc.).
- v3 The third model version is used to develop new insights and functionality.

To give structure to this long-term development, several activity areas are defined as presented in Table 2-1 and linked to the stages of model development (v0-v3). The starting point is formed by the existing hydrodynamic model schematizations of RWS (the so-called 6th generation hydrodynamic models).

To effectively carry out the model set-up and associated calibration, we start by setting up submodels for different river branches, which can then relatively easily be merged into an overall model. The intended coverage of the final model is presented in Figure 2.1.

In each year of the model development, specific activities are identified for the different areas of activity per submodel.

Figure 2.1 Coverage of the sixth-generation hydrodynamic Rhine branches model (orange) and the current DVR instrument (purple areas, the different purple colors indicate the subdomains of which that model consists). Light and dark blue areas are water bodies that are not part of aforementioned models.

2.2 Overview of the activities carried out in 2024

In 2023, a start was made with the development of the first basic models (v0) of the Waal and IJssel branches. The Waal model was used as example to test methodologies and develop the necessary scripts. Both the Waal and IJssel models helped to identify issues in the existing tools and software used as well as in the model schematizations. Based on the model experiences from the Waal, the IJssel morphodynamic model was set up in 2023 and 2024, leading to model version v0.5 (partially 1D calibrated) with the following steps:

- collection of the data needed to carry out the next steps (Chapter 3),
- modification of the existing hydrodynamic model to make it suitable for morphodynamic simulations (Chapter 4),
- hydrodynamic validation of the modified model (Chapter 5),
- set-up of basic morphodynamic schematizations (v0) of the IJssel branch (Chapter 6)
- “offline calibration” of the IJssel branch to get a first impression of the performance of the chosen transport formula in combination with the model schematization (i.e. (gradients in) flow velocities, roughnesses and grain sizes) (Chapter 7)
- first steps in the 1D calibration of the IJssel branch, including the choice of calibration and validation periods (Chapter 8).

Model schematizations representing the geometry of two different years were prepared for the IJssel (see section 4.1 for more detail):

- 2002: This will be the start of the calibration period (2002-2012, section 8.2).
- 2016: This will be the start of the validation period (2016-2022, section 8.2).

Furthermore, the Waal model was refined and calibrated further towards version v0.5 (see Kosters et al., 2024), and decisions on the calibration and validation periods for the next model extension – with Boven-Rijn, Pannerdensch Kanaal and Neder-Rijn-Lek – were taken.

Table 2-1 Steps in model development.

activity areas	associated activities	model version	done in 2023/2024
data collection	• Collection of all data needed to set-up a model, e.g. boundary conditions, calibration data hydrodynamics and sediment transport and morphology, bed composition, etc.	v0 v1	boundary conditions; 1D calibration data; discharge distribution; bed composition
morphodynamic model schematization: towards a well-working basic model (v0)	• set-up of a first running model including: a. dynamic river bed b. representative initial bed elevation (e.g. smoothing of bed forms) c. suitable roughness formulation for morphology d. sediment (grain sizes and sediment layers, with focus on active/upper layer) e. secondary flow f. first choice of transport formula and parameters (uncalibrated) g. non-erodible and less erodible layers h. suitable grid resolution • testing phase v0 model, identification of problems and modification of the schematization accordingly	v0	IJssel v0: set-up and testing of calibration and validation schematizations
extending the basic model to a v1 model	• more sophisticated description of a. main channel roughness b. composition and thickness of underlayers, including non-erodible layers • set-up of a dredging and dumping module • testing phase v1 model, and iterative modification of model schematization if necessary	v1	-
development of methodologies and tools for running the model	• approach and tools for model simulation (i.e. Simulation Management Tool) • strategy for model spin-up • strategy and tools for model evaluation and presentation of results • strategy and tools for simplification of model set-up and improving reproducibility	v0 v1	IJssel v0.5: Pre- and postprocessing tools
model calibration and validation	• calibration and validation strategy • adapting the hydrodynamic model to make it suitable for morphodynamic simulations • hydrodynamic validation • “offline” calibration giving a first estimate of morphological response based on the flow field in the hydrodynamic simulations • 1D morphodynamic calibration and validation (focusing on width-averaged, large-scale and long-term trends) • 2D morphodynamic calibration and validation (focusing on 2D patterns in the river bed, such as bank patterns and bend profiles) • validation of dredging and dumping module	v1	IJssel v0.5: “offline” calibration, start of 1D calibration
exploring model uncertainties	• influence of unknown physical variables (e.g. roughness in transport, bed composition, active layer thickness) • influence of model settings (e.g. initial geometry/composition and boundary conditions) or modelling concepts (e.g. Hirano model)	v1-v3	-

activity areas	associated activities	model version	done in 2023/2024
	• influence of simulation strategy and approaches (e.g. methods for optimizing simulation time, schematization of the hydrograph, choice of simulation period)		
development of modeling strategies and development for future use of the model	• identifying types of application and requirements • development of strategies for application of the model (e.g. choice of scenarios, choices for model settings and geometry, type of interventions) • identifying needs for further development of the model schematization (including needs for knowledge development and data requirements) • implementation and testing	v1-v3	-
verification of model application	• testing the model application in test cases of a. effect of interventions b. planning study (“planstudie”) c. (long-term) forecast of system behaviour • improvement of the model schematization, modeling strategies, methodologies and tools based on the outcomes of the test cases	v1-v3	-
Implementation of new functionality in D-HYDRO	• Identifying requirements of new functionality • functional design of needs • design of implementation • implementation and testing • updating user manuals	v2-v3	-

3 Data

3.1 Observed discharges and water levels

Observed discharges and water levels (daily values) have been delivered by RWS. For the IJssel, the data covers the period of 2002-2022. For Lobith, discharges and water levels are available from 1999-2022. For calibration and validation of the IJssel model, representative hydrographs were developed based on the discharge at Lobith and the discharge distribution across the Rhine branches (paragraph 3.2). This process is described in detail in paragraph 4.4. For most of the test simulations, the discharge hydrograph from the DVR model in Delft3D 4, the predecessor of the new model, was used (see section 3.2), because the calibration and validation hydrographs were not available yet. In the future, the discharge and water level data can be used to refine the approach for the upstream and/or downstream model boundaries.

3.2 Discharge distribution

The initial version (v0) of the new morphodynamic model of the IJssel still makes use of approaches that were derived for its predecessor, the “DVR model” in Delft3D 4. This also applies for the hydrodynamic upstream boundary condition, which is a standardized yearly hydrograph consisting of several stages with constant discharges. The same hydrograph is used for test simulations with v0 of the new model. For calibration and validation, two hydrographs that are representative for those periods (see chapter 8) have been derived (paragraph 4.4).

Both the DVR hydrograph as the calibration and validation hydrograph for the Rhine branches (Waal and IJssel so far) are defined for Lobith on the Boven-Rijn, so that they are valid for all branches. For use in the separate branch models, such as the IJssel model, they were translated to the corresponding values on the branches. For this translation, information on the discharge distribution for a range of discharges at Lobith, as computed by RWS-ON, was used. Since the discharge distribution at Pannerdensche Kop and IJsselkop has changed in the past decades due to continuous incision of the river bed of especially the Waal on the one hand and man-made modifications in the river geometry (e.g. Room for the River measures) on the other hand, it was decided to use two different discharge distributions for the different periods that are to be modelled, i.e. one distribution for more recent periods starting from 2016, and another one for the period between 2002 and 2013.

The distribution for 2016 and later is based on the current Qf-relation (Qf18 stationair), corrected for weir operation, bed level changes (until 01/01/2023), and a closed mass balance at the bifurcation points (‘vereffening’) as described in Van Putten (2023). The IJssel discharges corresponding to the nine discharge levels at Lobith were derived based on linear interpolation between the Lobith discharges for which the discharge distribution was computed. The distribution for 2002-2013 was derived in the same way but based on the QH-relation 2000.1 (including corrections to get a closed mass balance at the bifurcation points). The resulting values for both relations are given in Table 3-1 and Table 3-2.

Table 3-1 Translation of DVR discharge levels to upstream boundary conditions for the IJssel pilot model (v0).

Discharge level no.	Q Boven-Rijn (DVR levels) [m^3/s]	Q IJssel based on "vereffende afvoerverdeling 2023" [m^3/s]
1	1020	169
2	1203	207
3	1635	299
4	2250	330
5	3053	422
6	3824	527
7	4717	649
8	6151	839
9	8592	1169

Table 3-2 Translation of calibration and validation discharge levels to upstream boundary conditions for the IJssel model (v0.8).

Discharge level no.	Q Boven-Rijn (DVR levels) [m^3/s]	Q IJssel 1999-2012 (QH 2000.1) [m^3/s]	Q IJssel from 2016 ("vereffende afvoerverdeling 2023") [m^3/s]
1	1020	171	169
2	1400	263	247
3	1630	297	298
4	2020	305	332
5	2500	359	353
6	3220	459	445
7	4350	617	599
8	5800	813	793
9	8400	1212	1141

3.3 Grain sizes

Grain size data that covers the entire IJssel up to km 1001 is available from measurement campaigns from 1951 to 2020 (Figure 3.1). The campaigns of 1984 and 1995 also contain data for the Keteldiep (km 1001.5 – 1006). For the new model, the 2020 data will be used. It fully covers the current model extent (IJssel up to km 1001 only). In that campaign, samples have been taken at a distance of 500 m (full and half river kilometers) along the river axis and at a distance of 1.000 m (full river kilometers) along two parallel lines +/-70 m from the river axis (Table 3-3) using a "Hamon happer".

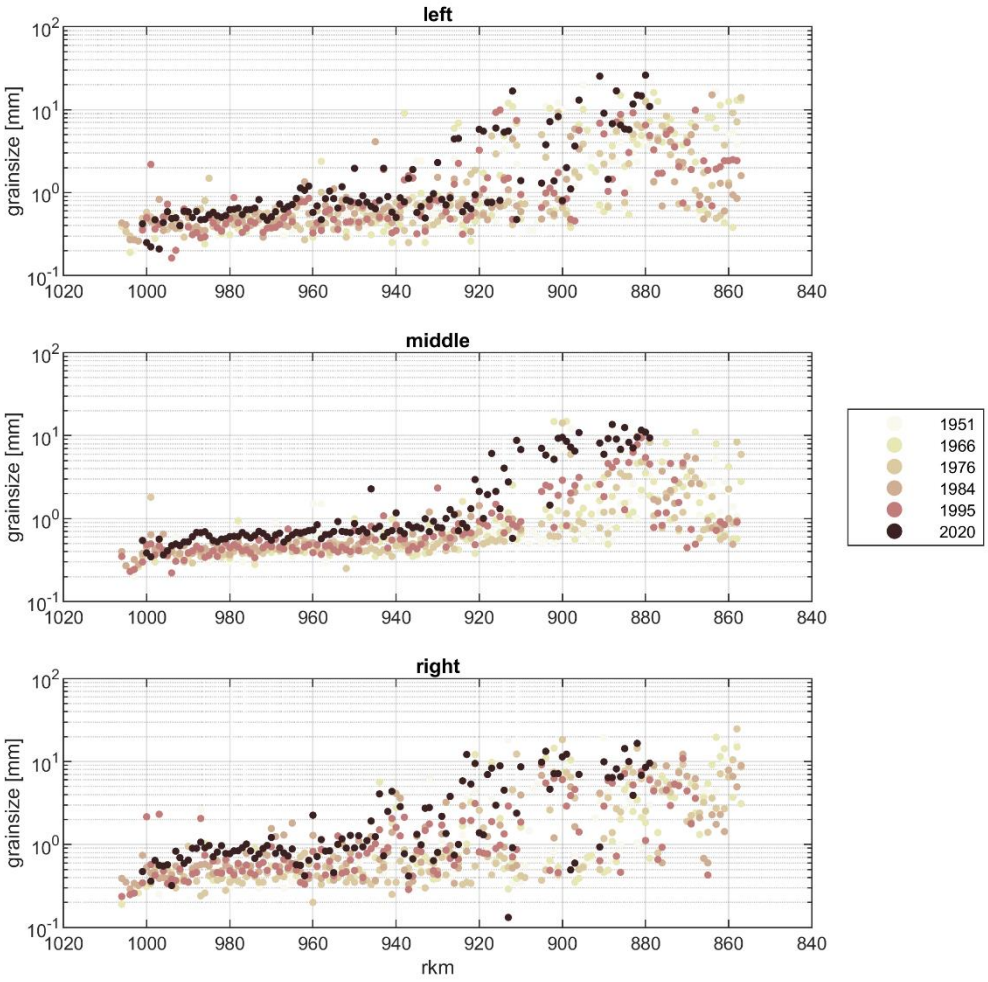

Figure 3.1 Available D_{50} grain size data for the IJssel. Top: 70 m to the left of the river axis; middle: on the river axis; bottom: 70 m to the right of the river axis. The data from the 2020 campaign (dark dots) was used in the model set-up.

Table 3-3 Location of data points with sieve curves from the 2020 measurement campaign.

Location	Streamwise coordinates	Transverse coordinate
Left bank	879, 880, … 1001, 1001	-70 m
Axis	879, 879.5, 880, … 1000, 1000.5, 1001	0 m
Right bank	879, 880, … 1001, 1001	70 m

3.4 1D calibration data

The following data is available for the 1D calibration, which focusses on long-term and large-scale trends in bed level development as well as yearly sediment transport rates. Furthermore, celerity of bed disturbances is used as a more-easy-to-measure proxy for sediment transport rates.

3.4.1 Trends in bed level change

De Joode (2023) has projected all available multibeam bed level measurements (1 m x 1 m) of the period 1999-2021 onto a grid, which has been defined as (Figure 3.2):

- The length of the cells is 100 m on the river axis and varies slightly towards the outer edges of the main channel due to its curvature.
- The width of the main channel (in between 'normaallijnen') is divided into 8 cells, 4 of which to the left of the river axis (labelled L4-L1) and the other 4 to the right of the river axis (labelled R1-R4).

De Joode (2023) processed the multibeam data into cell averaged bed elevations and standard deviation per grid cell. This data is used as basis for 1D model calibration.

Figure 3.2 Extract from the grid used to analyze bed elevations (from De Joode, 2023).

The morphologically active zone (see section 6.3 for the definition of that) of the new model generally extends slightly into R3 and L3 (Figure 3.3). Analysis of the data has shown that data coverage is low in the groyne fields (R5 and L5) and around groyne heads, which mostly fall into R4 or L4 (Figure 3.4). Therefore, it was decided to use the data from L3 to R3 for model calibration. Figure 3.4 shows that the data also does not always fully cover the L3-R3 cells. In that case the data of the year that does not provide sufficient coverage is not used in the calibration dataset for the respective cells. For the Waal a threshold of 99 % coverage was employed for considering that the cell had sufficient data. However, for the IJssel such high coverage, as well as the presence of bridges under which bed elevation was not measured, led to a significant amount of data gaps (Figure 3.5 - left). As indicated by the red dots in Figure 3.6, in the location of bridges the data in that river kilometer was not used because it did not reach the needed coverage for the data to be considered. The strategy used in the IJssel was then to define polygons around bridges, that are excluded from the km-averaging of bed elevations, preventing the total exclusion of the river kilometer.

To further reduce the data gaps, the data coverage was decreased to 95%. Figure 3.5 (right) shows the width averaged measured bed level that will be used for 1D calibration.

As during 1D calibration the focus is laid on width-averaged and large-scale behavior of the model, the data of De Joode was averaged across L3-R3 cells and river sections of 1 km length.

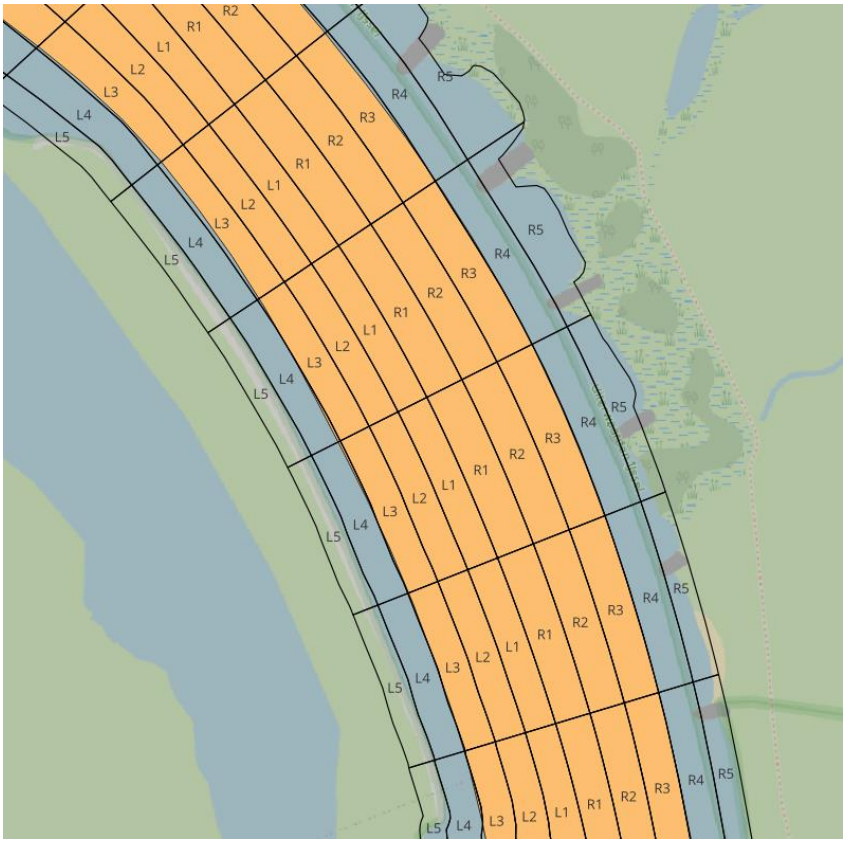

Figure 3.3 Morphologically active part of the river bed in IJssel-model v0 (orange area) compared to grid of De Joode (2023).

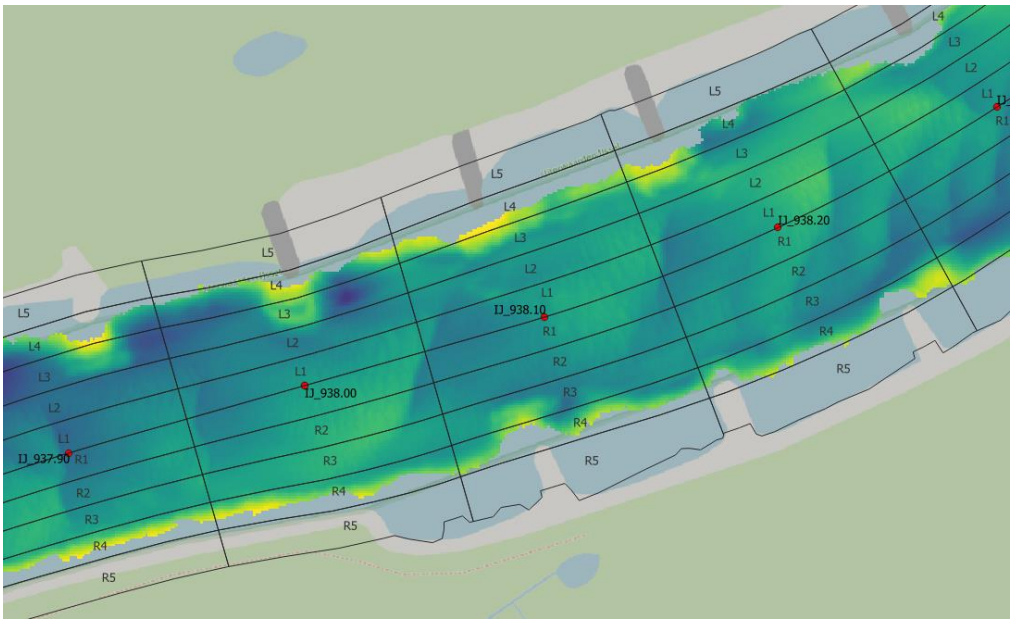

Figure 3.4 Data coverage of autumn 2020 multibeam measurements (yellow-green-blue colors represent the measured bed elevations), compared to grid of De Joode (2023, black polygons).

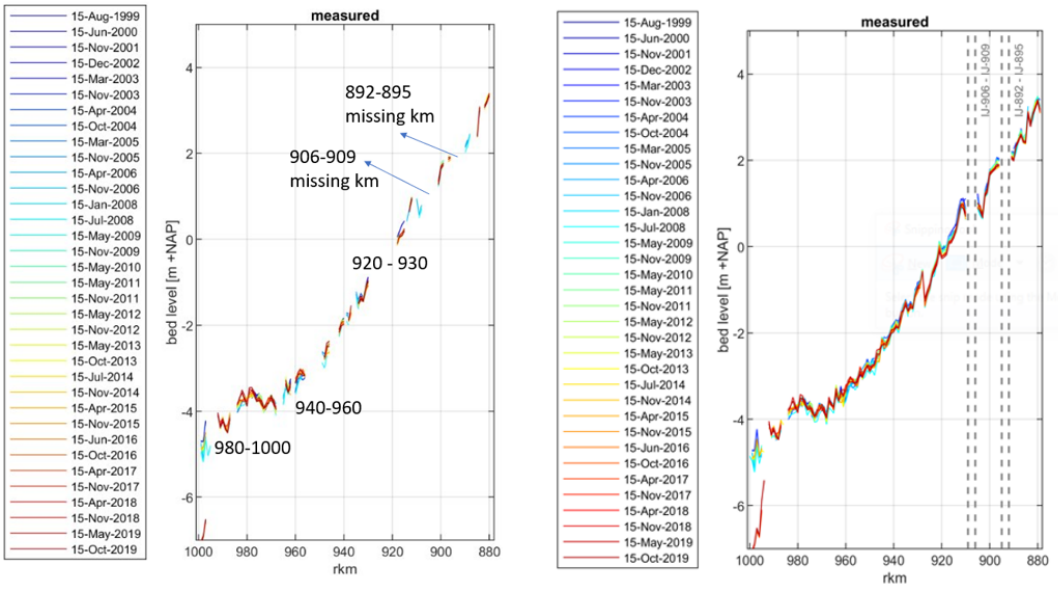

Figure 3.5 Available multibeam bed elevations, averaged over the width of the cross-section (L3R3), for the IJssel excluding (left) and including (right) the data around bridges. The data gaps are caused by river sections with no full data coverage across the entire width from R3 to L3 polygons.

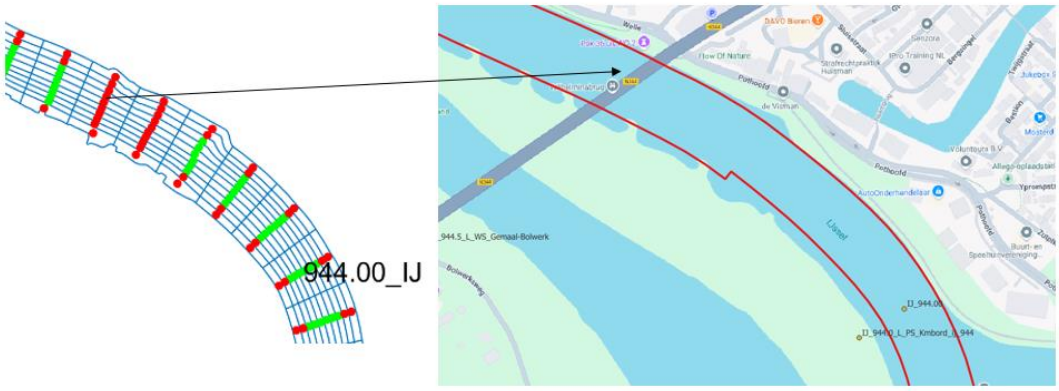

Figure 3.6 Data coverage of 99% for the IJssel. Red dots indicate cells without enough coverage.

3.4.2 Yearly sediment transport

Frings et al. (2019) estimated the yearly sediment transport per branch of the Rhine delta for a sediment balance of the Rhine (Table 3-4). In the framework of the IRM (Integraal Riviermanagement) project, Sloff (2019) derived sediment transport rates from the km- and width-averaged bed level changes of De Jong & Ottevanger (2020) [1] (Trend Pmap 20 years).

The bed level changes are influenced by fairway maintenance dredging and sand mining if the dredged material is not dumped back into the river at a location close-by. This needs to be taken into account in the interpretation of this yearly sediment transport estimate. The same applies to human interventions in the main channel.

[1] De Jong & Ottevanger (2020) derived a trend in bed level change per river kilometer section based on all available multibeam measurements between 1999 to 2018 (for the IJssel, the first available multibeam measurement is from 2002). They first made a linear fit through all data per 1x1m raster cell, and then averaged the trend within each river kilometer section. In the end, they did not use the Pmap data (in which data gasp are filled with data from the previous year) but only the available data per year. So the name “Pmap trend” is a bit misleading.

On the Ijssel, this can be seen clearly downstream, where in 2015 the main channel was lowered as part of the Room for the River project. That significant drop in bed level was interpreted as a large increase in sediment transport, which is not correct (and was therefore not taken into account in the log-term future trend that was also derived, see orange line in Figure 3.7.

The resulting longitudinal profiles for the IJssel are presented in Figure 3.7. The deviations between the estimates stress that these are rough estimates. They will be used in the 1D calibration as such.

Table 3-4 Annual sediment load of the Rhine branches estimated by Frings et al. (2019).

section	kilometers	gravel load (with pores) (m^3/y)	sand load (with pores) (m^3/y)	sum of gravel and sand load (with pores) (m^3/y)
Boven-Rijn	859-867	65.000	386.667	451.667
Boven-Waal	868-886	38.333	346.667	385.000
Midden-Waal	887-915	26.667	330.000	356.667
Beneden-Waal	916-951	10.000	308.333	318.333
Pannerdensch Kanaal	868-878	21.667	60.000	81.667
Boven-IJssel	878-930	3.333	28.333	31.667
Midden-IJssel	930-970	1.667	25.000	26.667
Beneden-IJssel	970-1000	1.667	25.000	26.667
Boven-Nederrijn	878-891	16.667	43.333	60.000
Beneden-Nederrijn	891-922	11.667	43.333	55.000
Lek	922-946	5.000	43.333	48.333

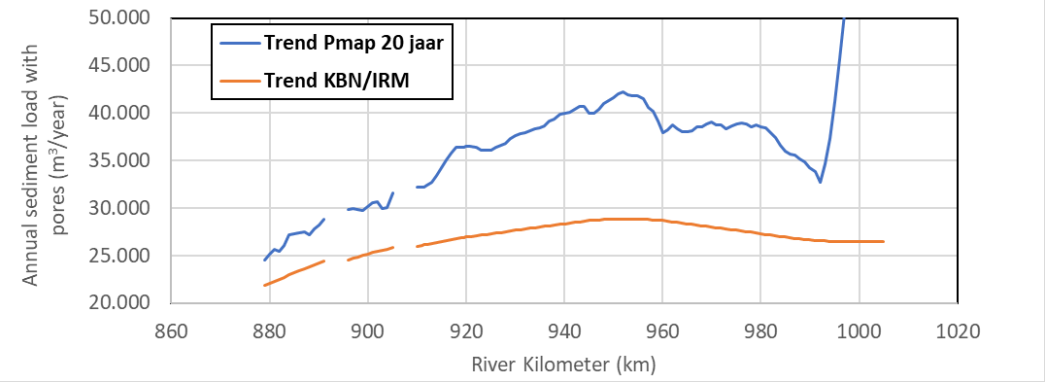

Figure 3.7 Estimate of the longitudinal profile of yearly sediment transport (including pores) for the IJssel (Sloff, 2019). Blue line: based on analysis of observed bed level changes; red line: based on estimated future trend in bed level development.

3.4.3 Celerity of bed disturbances

In the Rhine branches, bed perturbations should migrate downstream with a speed of approximately 1 km/y according to Sieben et al. (2005). In an update of this work (Sieben, 2020), specific values were derived per section of the different branches (Table 3-5).

Table 3-5 Observed celerities of bed disturbances for the IJssel.

section	year						
	1955	1965	1975	1985	1995	2005	2015
878-890	1.05	0.78	1.21	0.68	0.62	0.48	0.88
896-904	1.04	0.79	1.07	1.33	0.84	0.87	0.76
910-930	0.93	0.87	0.94	0.99	0.87	0.8	0.82
931-952	0.86	0.75	1.02	0.84	0.95	0.68	0.81
953-972	0.87	0.89	0.87	0.91	1.02	0.65	0.61
973-993	0.71	0.56	0.77	0.96	0.9	0.54	0.76
994-1005	1.05	1.08	0.76	0.97	0.88	0.97	0.84

3.5 Dredging and Dumping

An inventory of available data on dredging volumes and locations was made for the IJssel (Excel-sheet by J. Krabbendam, v10-07-2024). Figure 3.8 gives an overview of the data sources and total volumes per year. RWS assumes that in the periods 2002-2003, 2005-2009 and 2011-2013, no maintenance dredging was carried out (see metadata of the delivered Excel file with dredging volumes). In general, fairway maintenance is checked three times per year on the IJssel. The fairway has to be sufficiently deep (2.5 m below reference plane OLR) on 15th May, 1st August, and 15th December.

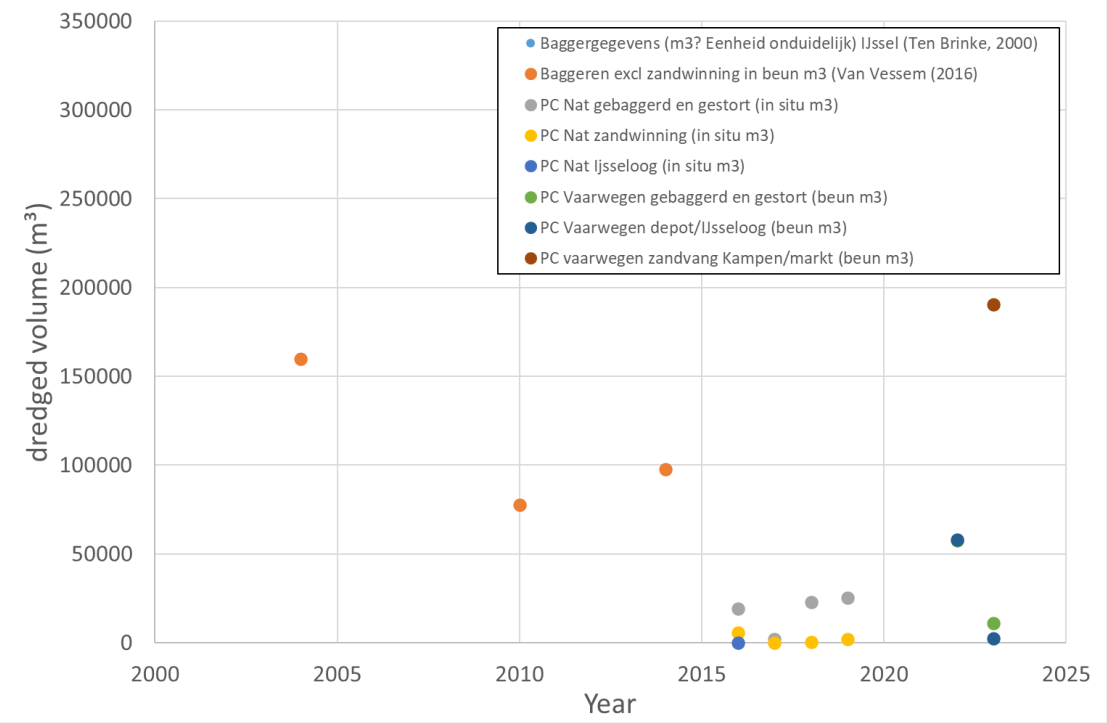

Figure 3.8 Available data on dredging volumes and locations for the IJssel (Excel-sheet by J. Krabbendam, v10-07-2024).

4 Hydrodynamic model schematization

4.1 Overview of different schematizations

Two different model schematizations have been prepared for the pilot in 2024:

D-HYDRO model schematization	Derived from Baseline schematization
dflowfm2d_dmor-ijssel-j02_6-v1a	baseline-rijn-j02_6-v1
dflowfm2d_dmor-ijssel-j16_6-v2a	baseline-rijn-j16_6-v2

These schematizations are representative for the situation of 2002 and 2016, respectively, and will be used to model morphological development in the period 2002-2012 (calibration period) and 2016-2020 (validation period).

4.2 Baseline set-up and conversion to D-HYDRO

Baseline-rijn-j16_6-v2 was already available at the beginning of this project. It is equal to baseline-rijn-j16_6-v1, but converted from Baseline 6.1.1 to Baseline 6.3.2. Baseline-rijn-j02_6-v1 is the result of mixing 6 measures, provided by RWS-ON, in baseline-rijn-j95_6-v1. In order to do this, baseline-rijn-j95_6-v1 was first converted to Baseline 6.3.2. The list of measures is included in Appendix A. All steps are schematized in Figure 4.1.

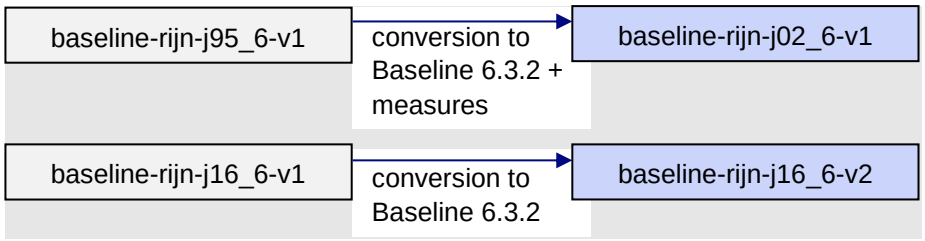

Figure 4.1 Steps to create Baseline schematizations.

The two resulting Baseline schematizations were converted to their corresponding D-HYDRO schematizations using the grid ‘rijntakken_final_v9_net.nc’. To convert only the data within the desired model domain (i.e. the IJssel), a shapefile containing the model boundary is used during the conversion from Baseline to D-HYDRO. These shapefiles were constructed by cutting of the model boundaries (or section polygons) of the entire j02 and j16 schematizations at the IJsselkop and the bifurcation into Keteldiep and Kattediep. Upstream, the model boundary excludes Hondsbroeksche Pleij, since there is only negligible flow through it at the discharge levels that are used in the morphological model. Downstream, it was agreed to keep the model extent the same as in the old DVR model for a first calibration. In a final model version, RWS would like to include the Keteldiep as well as the influence of Kattediep into the model. It still needs to be defined how to do that best.

During conversion from Baseline to D-HYDRO, the model boundaries for the IJssel are themselves converted to enclosure polygons, a model input file used to delineate the model domain at the start of the computation. By (manually) changing the enclosure polygon, the model domain can still be altered after conversion from Baseline (but only within the original model boundary, not outside of it).

4.3 Modifications within D-HYDRO

After the conversion from Baseline, the following elements of the model geometry have been modified:

4.3.1 Model domain

The IJssel model in its current version (and up to v1) extends from IJsselkop to the bifurcation between Keteldiep and Kattendiep branches, see Figure 4.2, which is the same extent as in the previous model in Delft3D 4. After calibration of the v1 model, it will be analyzed if the model can be extended further with the Keteldiep branch, up to about km 1006, because that branch is part of the area that RWS-ON is responsible for. This will then be a first step towards a v2 model. The extension is not implemented in in the v1 version yet to avoid problems with calibration due to inclusion of the bifurcation.

The upstream boundary is located just downstream of the bifurcation (Figure 4.3), to avoid violating the assumption that no sediment transport occurs across closed model boundaries as much as possible. As can be seen in Figure 4.3, a small part of the Neder-Rijn main channel is still included in this model extent. This has for now been corrected manually by changing the bed elevation of these cells to a high value to prevent them from getting wet. In reality, there is some flow across the dam between the two branches during high flow. This is neglected in the current model, which leads to overestimation of the flow velocities in the main channel. It could be considered to work with different lines for the boundary for different discharges to get the flow during high flow closer to reality. However, one needs to be conscious of the fact that, especially in a morphological model for long-term bed level development, the upstream boundary should be placed several kilometres (approximately one kilometre per year of simulation because of the celerity of bed disturbances, see section 3.4.3) upstream of the area of interest to avoid influences of boundary effects. If predictions have to be made for the most upstream part of the IJssel, a much larger model extent, including Pannerdensch Kanaal and the upstream part of Neder-Rijn, needs to be chosen. So a better representation of hydrodynamics locally around the boundary will not have a significant influence on the model results.

Figure 4.2 IJssel model domain (up to v1).

Figure 4.3 Upstream (left) and downstream (right) boundary location. The thick blue lines indicate the part of the boundary that is open.

4.3.2 Bed elevation

For the hydrodynamic model it was decided to define bed levels at grid cell corner points (`BedlevType = 3` and `Conveyance2D = -1`, see Figure 4.4, lower left).

The bed levels in these points are derived from Baseline by “picking” the elevation at that specific location. In the morphological model, we need to use `BedlevType = 1`[2] (Figure 4.4, top), which defines bed levels in cell centers. Minns et al. (2022) propose to derive the elevations in cell centers from a hydrodynamic simulation[3].

[2] There is no validated morphology functionality available for bed levels in corner points.

[3] Due to the staggered grid approach in D-HYDRO, bed elevations are needed at several locations in a cell to solve the hydrodynamic equations, including the cell center. Cell center bed elevations can therefore be exported from a hydrodynamic simulation that used elevations at corner points as input.

However, these elevations are the minimum of the values on cell edges (Figure 4.4, lower left) and this method therefore leads to structural overestimation of the depth along steep edges (e.g. fixed banks, “gestrekte oever”) and underestimation of water levels as was shown for the Waal in Becker et al. (2023). Larger differences are noticed in the IJssel compared to the Waal due to a narrower channel. Letting D-HYDRO determine the bed level in cell centers by the method illustrated in Figure 4.4, lower right, does not seem more promising either, because it still uses a minimum value.

As done for the Waal, it was decided to derive the mean value of the bed levels in the corner points[4] using a script, and impose it as cell center bed level in morphological simulations. Water level difference compared to the original hydrodynamic model was significantly reduced, as is shown during hydrodynamic validation in Chapter 5. Furthermore, an option picking the elevation at cell centers instead of corners became available in Baseline. This option was also tested since it could be used directly in the model. The results and final decision are presented in Chapter 5.

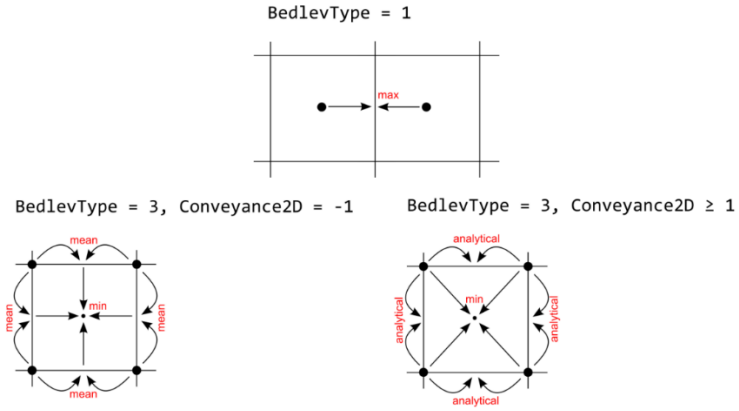

Figure 4.4 Schematic representation of options for representation of bed elevations on the staggered grid in D-HYDRO. The hydrodynamic model uses BedlevType = 3 and Conveyance2D = -1. The morphodynamic model has to use BedlevType = 1.

In Baseline, the bed elevation within the main channel of the IJssel is mainly based on multibeam measurements. The bed level in the two schematizations j02 and j16 is based on multibeam measurements carried out in December 2002 and October 2016, respectively. Hence, the bed elevation included in Baseline represents one moment in time (a ‘snapshot’) and contains small-scale features such as bed forms. Our large-scale model of the Rhine branches, however, is too coarse to properly resolve small-scale phenomena such as bed forms. Instead, these can be included in a “subgrid” way. It needs to be decided carefully for which processes that is relevant. The model is not made to predict small-scale bed forms in detail. However, it might be necessary to estimate the size of dunes by means of a bed form predictor and take it into account when deciding if dredging is needed or not.

Thus, the bed level in the model should be a representative bed level without these small-scale temporary phenomena. Therefore, the main channel part of the bed level from Baseline was smoothed using the following steps:

[4] i.e. the mean of the bed level values of all corner points was used, independent of the exact shape of the cell. In most cases, with rectangular cells, this is the mean of four corner cells, but there are some cells with more corner points as well.

1 averaging of the main channel bed level from Baseline in the polygons created by De Joode (2022) (see description in section 3.4.1). At the edge of the summer bed, the polygons were cut off to not exceed the extent of the morphologically active part (see section 6.3) in our model. This is important, because filtering will inevitably also remove part of the larger-scale phenomena from the bed level. These need to be brought back into the model during spin-up of the bed level, which is only possible in the morphologically active part.
2 calculating 1 km rolling means along each longitudinal section of De Joode (2023), i.e. L1-L3 and R1-R3 (with L3 and R3 polygons cut off as described above)
3 interpolating (Delaunay triangulation) the resulting values onto the 2D grid of our model (cell centre location).

The filter was only applied within the morphologically active zone of the model (section 6.3). Figure 4.5 shows that indeed this method filters out bed forms but not the large-scale patterns such as deep outer bends (blue line on top of red line).

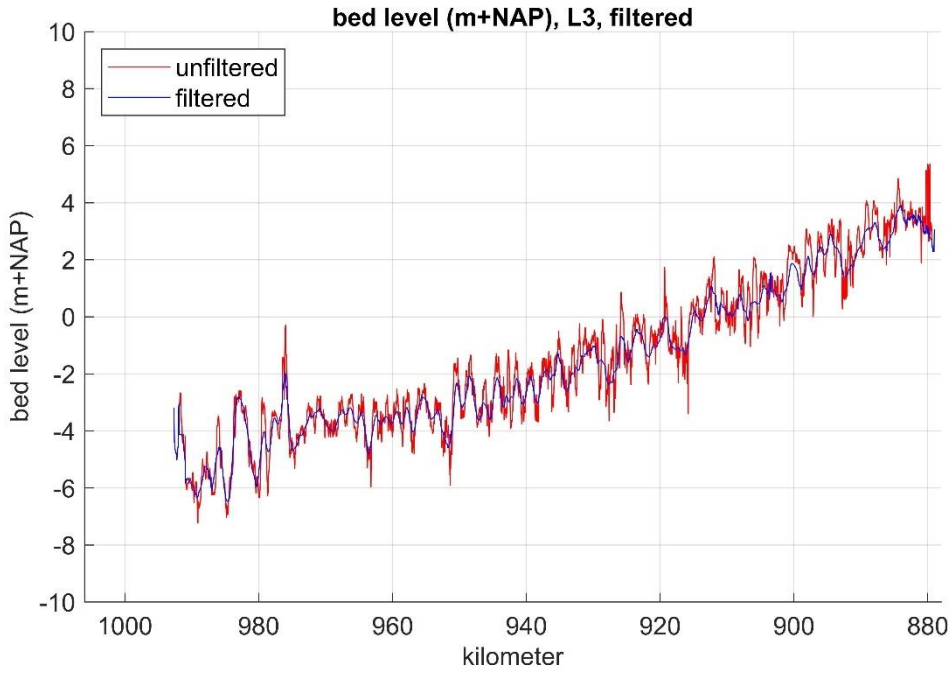

Figure 4.5 Comparison between filtered and unfiltered main channel bed level in the j16 model along a line approximately 70 m to the left of the river axis (L3). The unfiltered bed level is the bed level picked in cell centres by Baseline.

The impact of working with bed levels in cell centers instead of corner points and of the filtering for the main channel on calculated water levels is analyzed in a hydrodynamic validation of the model (Chapter 5).

On the longer term, we need to define, based on morphological model results for several branches, if filtering is indeed worthwhile. If yes, we also need to define how to get the procedure of determining bed levels in cell centers and filtering the main channel bed into Baseline and/or D-HYDRO, so that it can be used in the hydrodynamic model as well.

4.3.3 Main channel roughness

In the original hydrodynamic model, main channel roughness is defined by means of a base roughness that is multiplied by a calibration factor. Base roughness is constant per section, sections being between several kilometers to about 20 km long. Calibration factors are also defined per section, but the sections for the base roughness and calibration factors do not coincide. This is described in detail by Kosters et al. (2022). In Becker et al. (2023) it was observed in the Waal that abrupt changes in the roughness, as expected, create strong morphological reactions in the first (not yet calibrated) model runs.

Therefore, the roughness in the pilot model (v0) of the Waal was set to a constant Chézy value of 45 $m^{1/2}/s$. For the IJssel, the same approach was adopted. A fixed Chézy of 45 $m^{1/2}/s$ was chosen based on the comparison of hydrodynamic model results between the original and pilot model (see Chapter 5). The impact of the change in roughness and calibration factors on water levels and flow velocities is analyzed in the hydrodynamic validation of the model in Chapter 5. Note that for morphodynamic simulations a reasonable representation of flow velocities is much more important than correct water levels. Water levels, however, do determine the moment at which the flood plains and side channels are activated.

As done for the Waal branch the calibration factors were also deactivated, meaning that a constant value of 1 will be used in the entire model domain. In a next phase of model development, after a first calibration, we can experiment with more variability in main channel roughness and work towards a compromise between the input of the original hydrodynamic model and the needs of a morphodynamic model. A proposition for how to do that was made in Becker et al. (2023).

4.3.4 Discharge-dependent calibration factors

The modifications described in this section are only relevant for the simulations in which the original calibration factors from the hydrodynamic model are included. As described in Section 4.3.3, it was decided to apply a constant Chézy roughness coefficient in the morphodynamic simulations.

To each calibration section (see section 4.3.3), a calibration factor was assigned that is dependent on the local discharge (for more information, see Kosters et al., 2022). Because of this discharge dependency, a discharge cross-section must be assigned to each calibration section. These cross-sections are located as close as possible to the corresponding water level stations that were used for calibration. Calibration factors are defined for 5 (local) discharge levels. Between these discharges, the calibration factor is determined by linear interpolation.

In the IJssel model, the upstream boundary intersects with the smooth transition between calibration sections 2014 (Pannerdensch Kanaal) and 2024 (IJssel). Hence, a part of calibration section 2014 is present in the model. However, the corresponding discharge cross-section, PK_872.5_QR_Pannkop-IJsselkop, is not located within the model domain. In all model schematizations (j02 and j16), the discharge dependency was removed for section 2014. The same was done for calibration section 2015, which is present in the small piece of Neder-Rijn main channel that has accidentally been included in the current model version. This will not be necessary in later model versions, in which we will exclude the Neder-Rijn main channel completely. Appendix B gives an overview of the calibration factors (including the changes described in this section).

4.3.5 Other changes

Since the maximum discharge level to be simulated with this model is below 9000 m³/s, it was decided to exclude the flood channel at Veessen-Wapenveld from the model domain, as shown in Figure 4.6. Therefore, also the D-RTC rules for operation of the inlet structure were removed.

Figure 4.6 Model enclosure (red line) excluding the flood channel Veessen-Wapenveld. The original enclosure including the flood channel is defined by the thin black line.

4.4 Hydrodynamic boundary conditions

The model is forced with a discharge at the upstream boundary and a Qh-relation at the downstream boundary. The upstream model boundary is located on the IJssel at the IJsselkop (Figure 4.3).

4.4.1 Upstream boundary

The initial version (v0 till v1) of the new morphodynamic model of the IJssel still makes use of approaches that were derived for its predecessor, the “DVR model” in Delft3D 4. This also applies for the hydrodynamic upstream boundary condition, which is a standardized yearly hydrograph consisting of several stages with constant discharges (Figure 4.7). The same hydrograph is used in the first test simulations (v0) of the new model. For calibration and validation towards version v1, similar hydrographs have been derived that are representative for these two periods (2002-2012 and 2016-2022, see section 8.2). In that way, the calibration is valid for future simulations that are supposed to produce a long term trend in bed development. At a later stage, it can be decided to use a different type of upstream model boundary (e.g. a “normal” hydrograph), or to extend the methodology with different ways of forcing for different applications.

The discharge levels of the DVR model were translated from Lobith on the Boven-Rijn to the IJssel as described in paragraph 3.2.

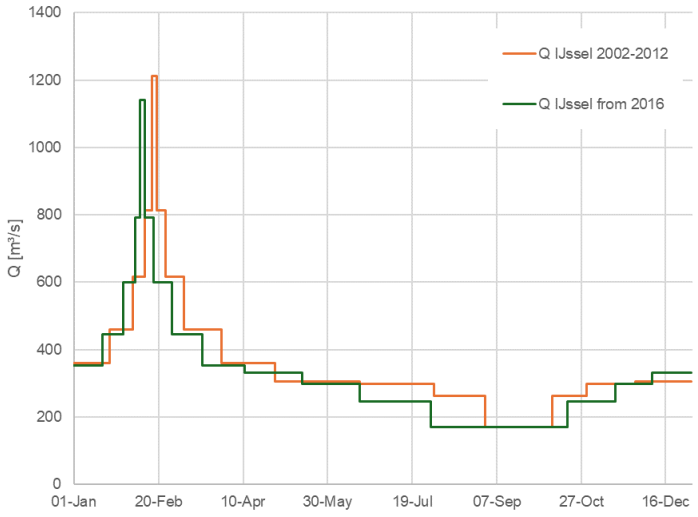

Q Lobith (m³/s)	no. of days	
	2002-2012	2016-2022
2500	21	17
3220	14	12
4350	7	7
5800	4	3
8400	3	3
5800	5	5
4350	11	11
3220	22	18
2500	32	25
2020	50	34
1630	44	34
1400	30	42
1020	40	81
1400	20	28
1630	29	22
2020	33	23

Figure 4.7 Standardized yearly hydrograph converted to the IJssel (left) and at Lobith (table on the right)

Average yearly discharge hydrographs were derived for the calibration and validation periods for the Waal and IJssel models:

- 1999 – 2012: calibration Waal
- 2002 – 2012: calibration IJssel
- 2016 – 2022: validation Waal and IJssel

The following sections describe how the hydrographs were derived for Lobith on the Boven-Rijn and present the resulting hydrographs (discharge levels and durations). The discharge levels were later translated to the upstream boundary location of the Waal and IJssel as described in paragraph 3.2.

4.4.1.1 Method

The approach to derive the discharge hydrographs is as follows:

- Observed discharges at Lobith for the respective calibration or validation period are used as input.
- These are ordered from small to high to obtain a probability density function (pdf, blue line in Figure 4.8).
- To keep the necessary modeling steps as limited as possible (e.g. hydrodynamic spin-up), it was decided to use the same discharge levels for all hydrographs. Nine suitable discharge levels have been determined in previous studies (“Uitwerking systeemmaatregelen beleidskeuze rivierbodemligging IRM” and “vaarweg Rijn grensregio”, both not yet published) based on relevant discharge regimes in the Rhine branches. The nine levels are presented in Table 4-1. Paragraph 4.4.1.2 discusses the discharge regimes.
- The moment of intersection of the levels with the pdf were determined (black points in Figure 4.8). The moment at which the hydrograph changes from one discharge level to the next was defined as halfway between these intersection points ($d_i/2$).
- In cases with relatively low high discharges, a minimum duration of the highest discharge level of 3 days was enforced at the cost of the duration of the level below. This was needed for the periods 2002-2012 and 2016-2022, which based on the procedure above received only 2 days of the highest discharge each.

- The nine levels and durations were then split into a hydrograph with 16 steps, as presented in Figure 4.7, that resembles a typical year with a flood event in winter and a low flow period during summer.

  Following the same procedure as for the DVR model, it is assumed that 40% of the higher discharges (levels 5-8) occur before the flood (100% of level 9), and 60% occur after the flood and before low flow season. Of the lower discharges (levels 2-4), 60% occur before the lowest discharge (level 1) and 40% after it. The resulting durations are rounded to full days.

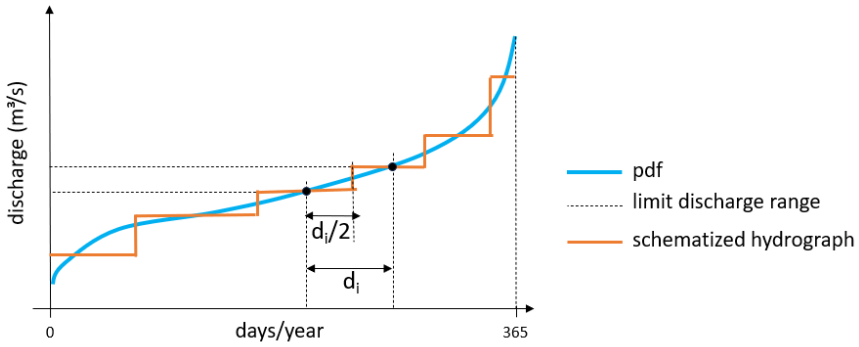

Figure 4.8 Approach to derive a schematized hydrograph from a pdf.

Table 4-1 Discharge levels and total duration for the three calibration and validation periods.

Discharge level (m³/s)	1999-2012 (d)	2002-2012 (d)	2016-2022 (d)
1020	32	40	81
1400	44	50	70
1630	68	73	56
2020	82	83	57
2500	60	53	42
3220	42	36	30
4350	23	18	18
5800	10	9	8
8400	4	3	3

4.4.1.2 Discharge regimes

The following discharge regimes have been identified as relevant regimes for the morphological development of the Rhine branches (based on the discharge at Lobith):

Table 4-2 Relevant discharge regimes in the Rhine branches based on the discharge at Lobith.

Q (from) (m³/s)	Q (to) (m³/s)	description discharge regime	Q levels (m³/s)
0	1770	weirs Nederrijn closed (impounded)	1020 1400 1630
1770	2740	weirs Nederrijn in transition from closed to open (impounded)	2020 2500
2740	3870	free flowing, discharge within main channel	3220
3870	ca. 5000	flow through flood plains starts to develop	4350
ca. 5000	18000	fully developed flow through flood plains	5800 8400

4.4.1.3 Hydrographs for Lobith

Figure 4.9 shows the resulting yearly hydrographs. Figure 4.10 presents the difference in volume under the pdfs compared to the schematized hydrographs. Note that the difference in volume is not a good indicator for the difference in yearly sediment transport, due to the non-linearity in the transport relation. For a proper assessment of how good the hydrographs are, one would have to compare morphological simulations using the hydrographs to fully unsteady simulations with the measured discharges series, or at least check convergence of model results for an increasing number of discharge levels. That does not fit into the current project, though.

Table 4-3 shows how the nine discharge levels were discretized further into hydrographs of 16 steps (see also Figure 4.7). That figure also show the resulting discharge levels for the IJssel, after translating the Lobith discharges into values for the upstream end of the IJssel. The Q-Q-relations 2000.1 (calibration period) and 2018 (*Qf18*, validation period) was used for this.

Table 4-3 Discretization into 16-step-hydrographs for the three different periods.

step	Q (Lobith) (m^3/s)	duration (d)		
		1999-2012	2002-2012	2016-2022
1	2500	24	21	17
2	3220	17	14	12
3	4350	9	7	7
4	5800	4	4	3
5	8400	4	3	3
6	5800	6	5	5
7	4350	14	11	11
8	3220	25	22	18
9	2500	36	32	25
10	2020	49	50	34
11	1630	41	44	34
12	1400	26	30	42
13	1020	32	40	81
14	1400	18	20	28
15	1630	27	29	22
16	2020	33	33	23
		365	**365**	**365**

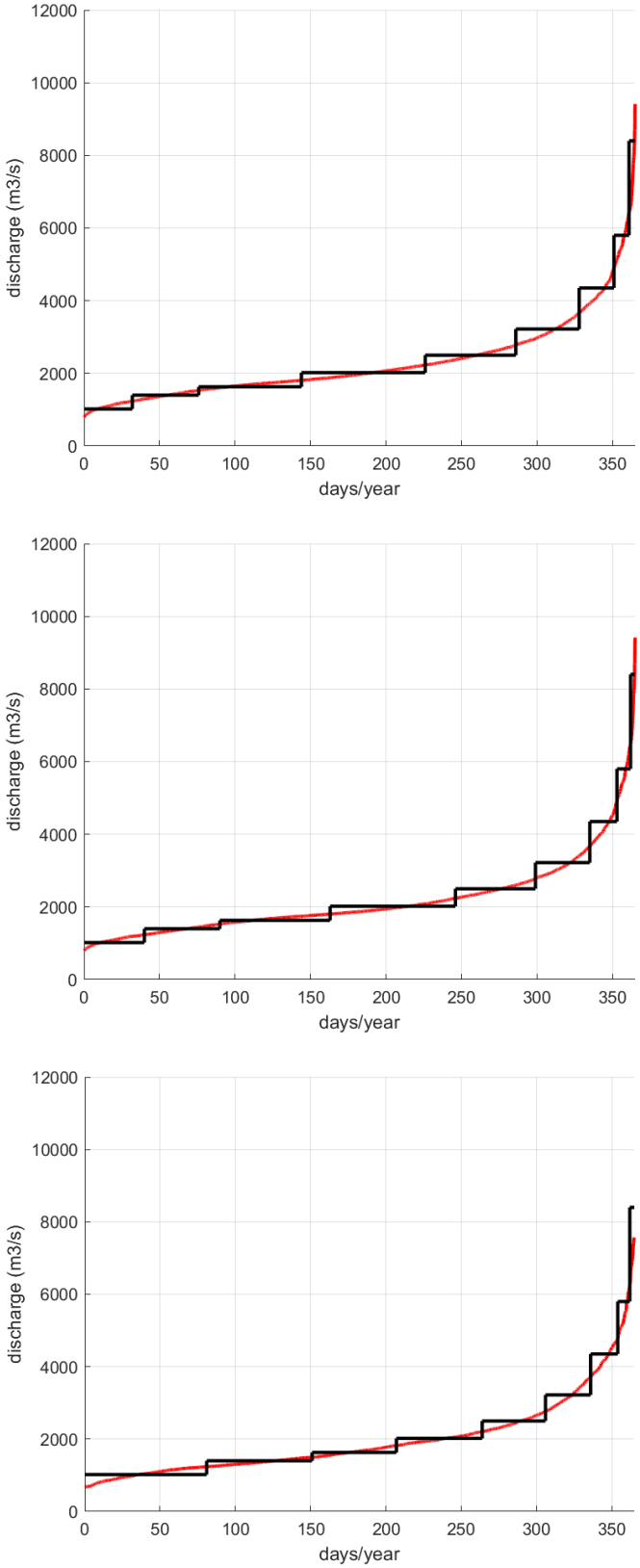

Figure 4.9 Pdfs (red lines) and duration of the discharge levels in the schematized hydrographs (black lines) for the calibration and validation periods 1999-2012 (top), 2002-2012 (centre), and 2026-2022 (bottom).

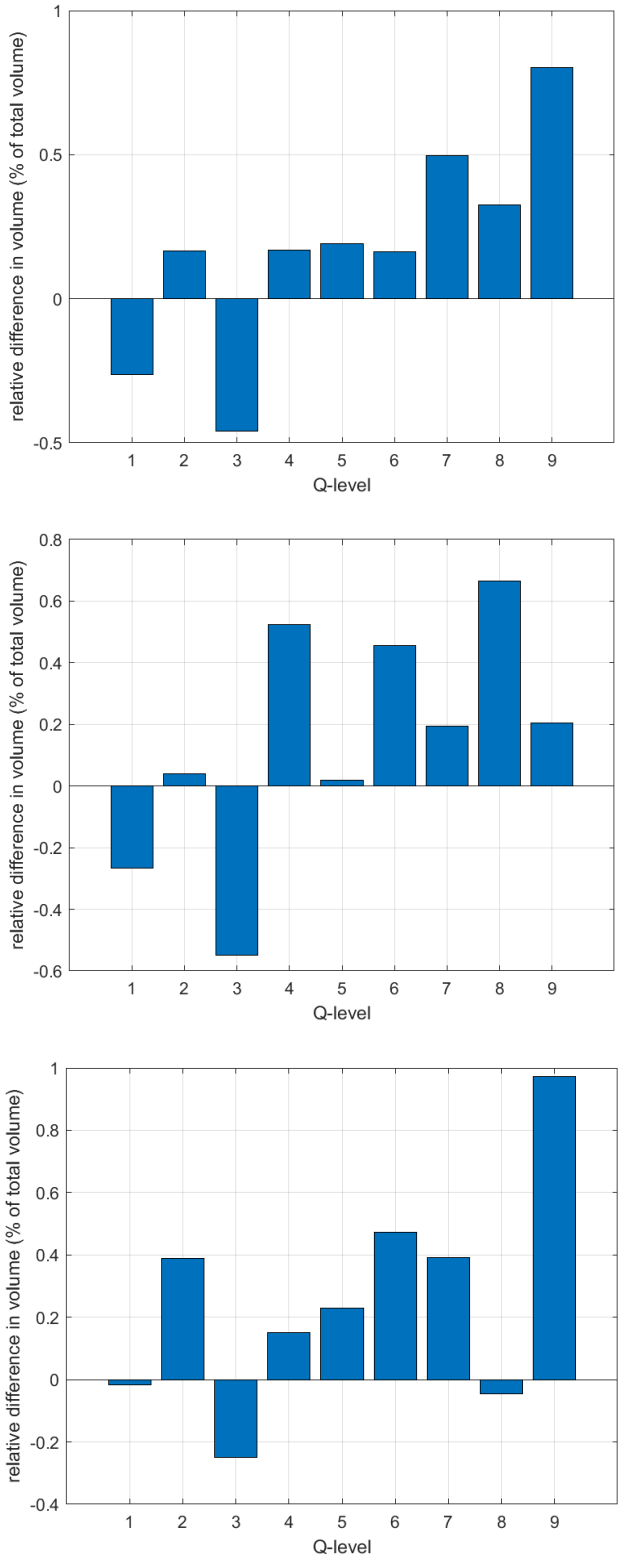

Figure 4.10 Relative difference in volume (% of the total year volume) between the pdf and the schematized hydrographs for the calibration and validation periods 1999-2012 (top), 2002-2012 (centre), and 2026-2022 (bottom).

4.4.2 Downstream boundary

The downstream model boundary is located at the bifurcation into Keteldiep and Kattendiep. For model schematizations j02 and j16, a Qh-relation was derived from the available standard simulations for the original hydrodynamic model j16 of the Rhine branches: S_600, S_1020, S_2000, S_4000, S_6000, S_8000, S10000, S13000, S16000. The new Qh-relation is composed of the sum of discharges through Keteldiep (cross-section IJ_1001.9_QO_Keteldiep) and Kattendiep (cross-section IJ_1001.9_QO_Kattendiep) and the water level at output location IJ_1002.00. The model interpolates linearly in between those values for the discharges of the hydrographs used in the morphological model.

By using a Qh-relation as downstream boundary, the model focusses on the influence of discharge, while excluding any effect of variation in IJssel Lake levels or wind set-up.

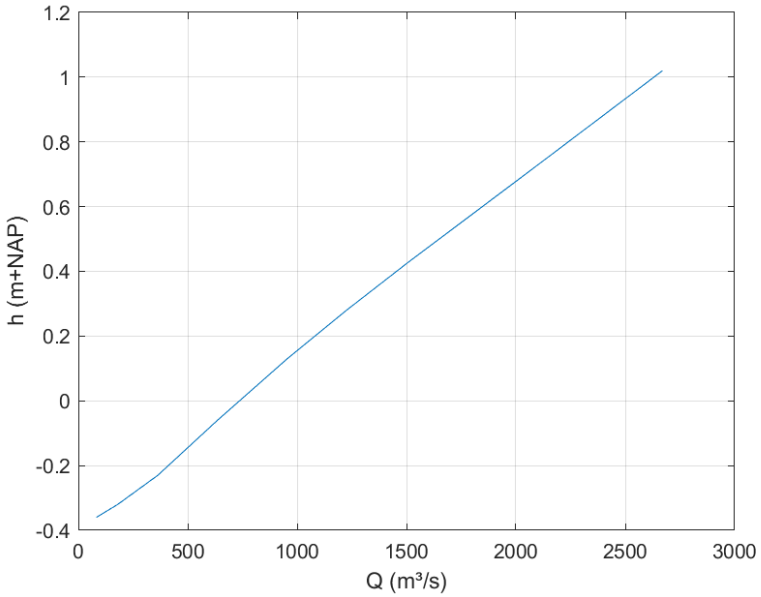

Figure 4.11 Qh relation at the bifurcation of the IJssel into Keteldiep and Kattendiep for j02 and j16

4.5 Initial conditions

For the 2002 and 2016 Rhine branches model (dflowfm2d-rijn-j16_6-v1a and dflowfm2d-rijn-j02_6-v2a), initial water levels from baseline are already available. The (initial) water level is derived using the land/water boundary as stored in the Baseline database (Baseline, 2024). With these initial conditions, stationary hydrodynamic simulations of 15 days were run to let the model adapt to the boundary conditions. The morphodynamic simulations are using the result of this hydrodynamic spin-up as initial conditions via restart files as well as a “local database” for use in the Simulation Management Tool (SMT).

5 Hydrodynamic validation

5.1 Validation simulations

With the IJssel branch model of the year 2016, of which the setup was described in chapter 4, nine stationary hydrodynamic simulations are carried out, corresponding to the discharge levels used to schematize the yearly hydrograph for morphodynamic simulations (in its v0 version, i.e. the levels already used in the DVR-model, see section 4.4). For these discharge levels, a hydrodynamic validation was carried out by comparing the model with the modifications as described in paragraph 4.3 to the original hydrodynamic model.

Each discharge level is simulated for a duration of 15 days, in order to achieve a stationary situation. Lateral inflow/outflow is not included in the model, just like in the predecessor of the morphodynamic model (the DVR model).

5.2 Effect of modifications to the original model

For the hydrodynamic validation, water levels and flow velocities along the river axis of the morphological model were compared to those of the original hydrodynamic model. In this way, the effect of the following modifications to the original model (see section 4.3) was visualized:

1 defining the bed levels in cell centers (bedlevel type 1) instead of at corner points (bedlevel type 3)
2 filtering the bed level
3 applying a constant main channel roughness instead of the combination of spatially varying base roughness and space and discharge dependent calibration factor
4 combining 1, 2 and 3.

The following sections present the effect of each of these modifications on water levels and flow velocities. Both parameters are taken on the output locations on full kilometers on the river axis.

5.2.1 Effect of defining the bed level in cell centers

Figure 5.1 and Figure 5.2 show the effect of changing the bed level definition from cell corners (bedlevel type 3) to cell centers (bedlevel type 1 using script averaging corner elevation and imposing in cell center), which is necessary for morphodynamic simulations (paragraph 4.3.2). Water levels are lowered by 5-25 cm, apart from in the simulation with the highest discharge level, where water levels become up to 5 cm higher. Larger water level differences are observed for lower flow values. The change in flow velocities remains limited (about 0.05 m/s on average, with peaks of up to 0.1 m/s).

Figure 5.3 and Figure 5.4 show the effect of changing the bed level definition from cell corners (bedlevel type 3) to cell centers (bedlevel type 1), but using the elevation at cell centers picked in Baseline as described in section 4.3.2. Differences in water levels between the two methods for estimating the bed level at cell centers can be seen in Figure 5.5. Differences range between -5 to 15 cm. Since the differences are small, elevations picked at cell centers from Baseline will be used. This saves one extra step to calculate the bed levels in cell centers as average from corner values by means of a script.

Compared to what Becker et al. (2023) saw for the Waal, the water levels differences resulting from the change in bed level definition (from corner points to cell centers) are a lot larger on the IJssel. In the Waal the maximum difference was 5 cm, whereas in the IJssel they reach 25 cm. This probably has to do with the fact that the main channel of the IJssel is narrower and has steeper banks and more straight banks (“gestrekte oevers”) than the Waal, while the computational grid is much coarser in terms of the number of cells across the width of the main channel.

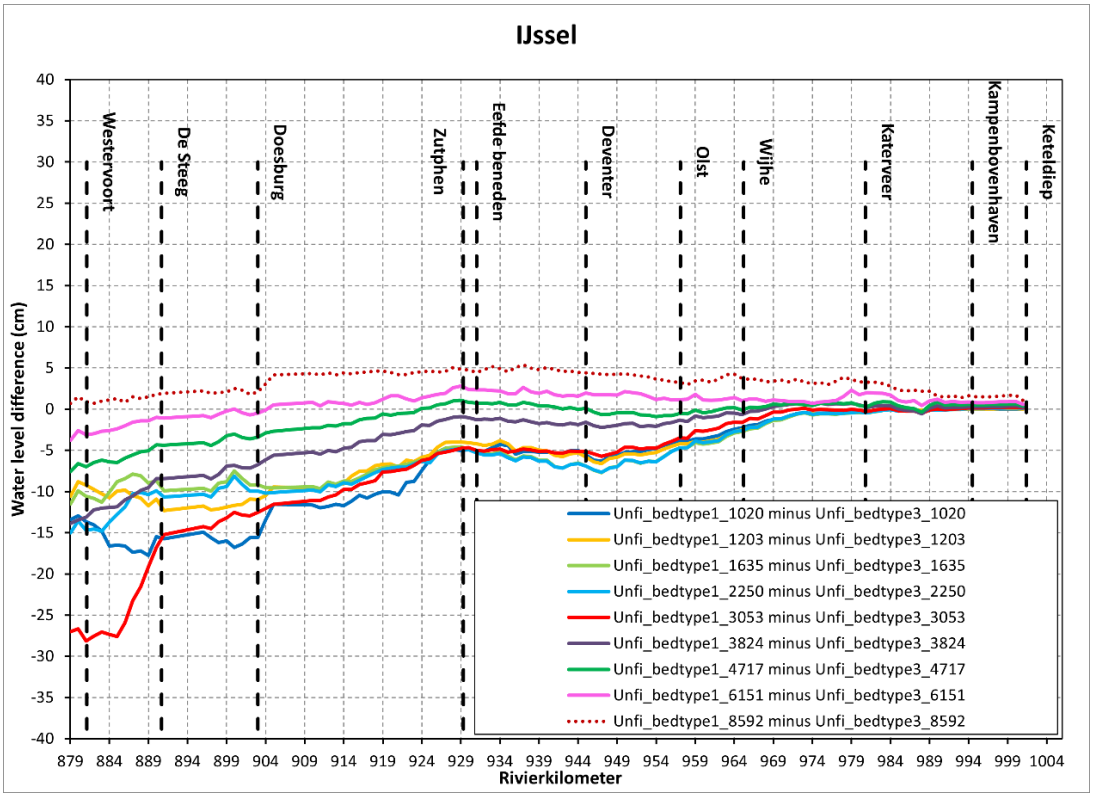

Figure 5.1 Difference in water levels along the river axis between simulations with bed levels in cell centers (“Unfilt_bedtype1”, morphological model) and bed levels in cell corners (“Unfi_bedtype3”, original hydrodynamic model).

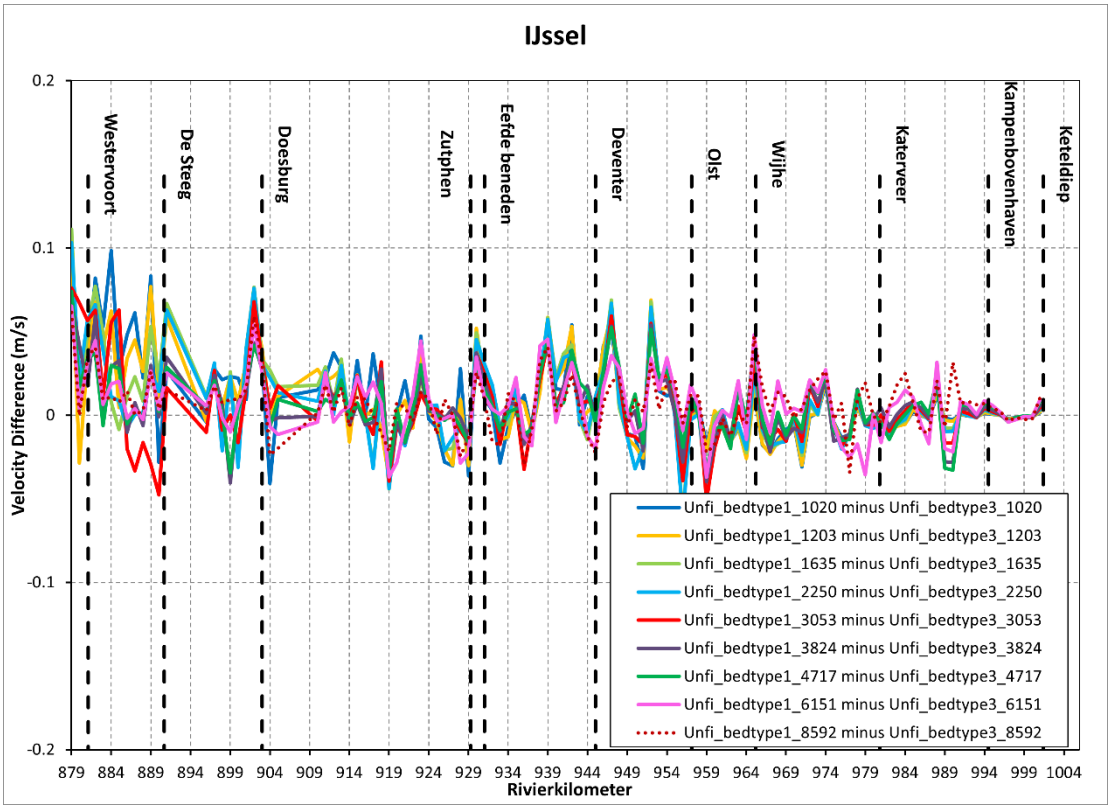

Figure 5.2 Difference in flow velocities (on the river axis) between simulations with bed levels in cell centers ("Unfilt_bedtype1", morphological model) and bed levels in cell corners ("Unfi_bedtype3", original hydrodynamic model).

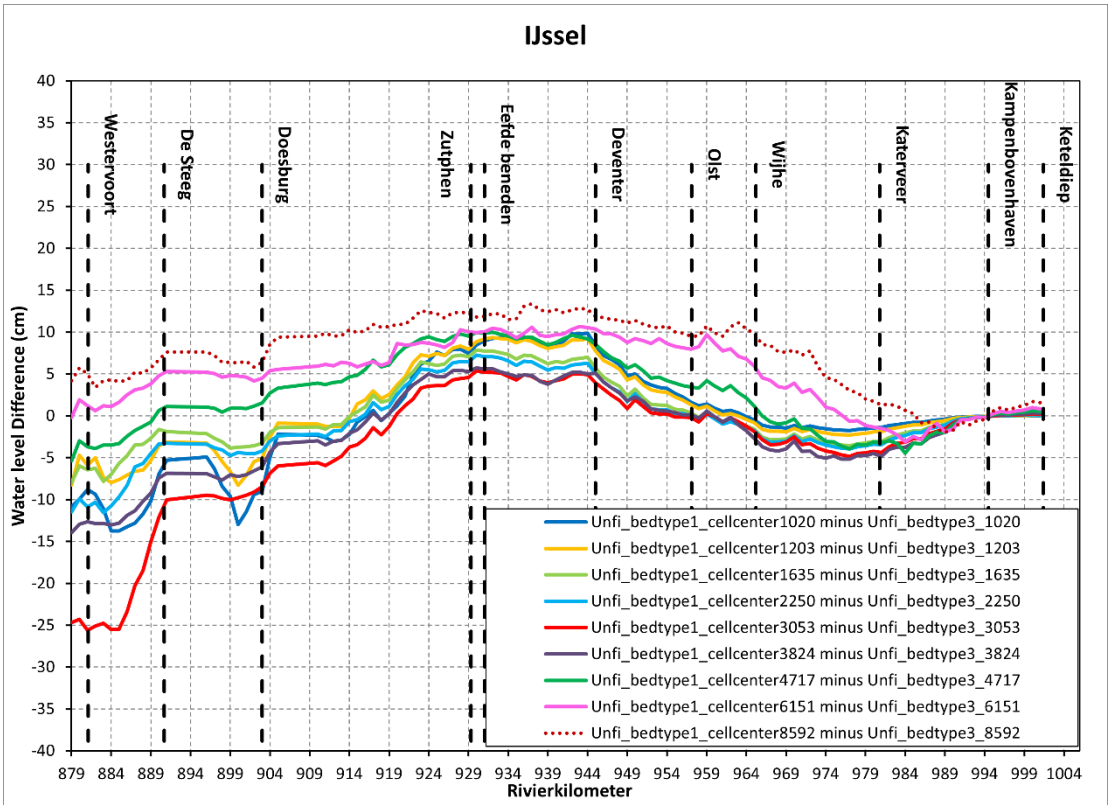

Figure 5.3 Difference in water levels along the river axis between simulations with bed levels in cell centers from baseline ("Unfilt_bedtype1 cellcenter", morphological model) and bed levels in cell corners ("Unfi_bedtype3", original hydrodynamic model).

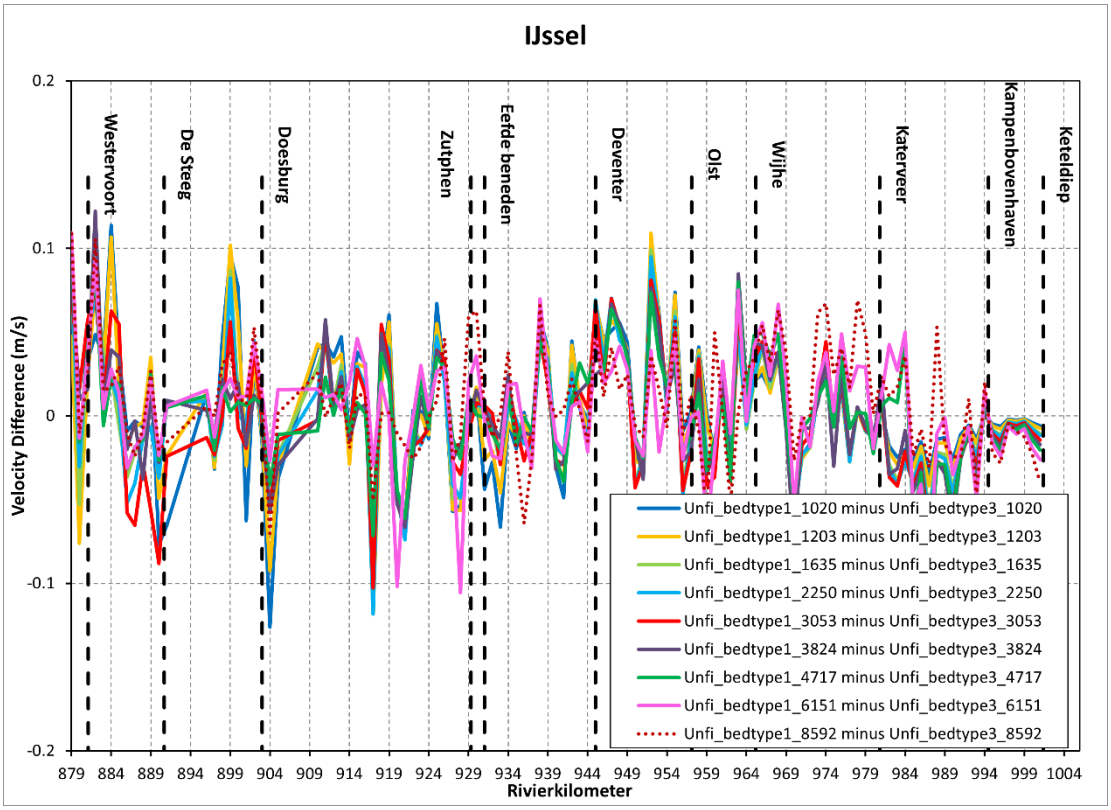

Figure 5.4 Difference in flow velocities (on the river axis) between simulations with bed levels in cell centers from baseline ("Unfilt_bedtype1", morphological model) and bed levels in cell corners ("Unfi_bedtype3", original hydrodynamic model).

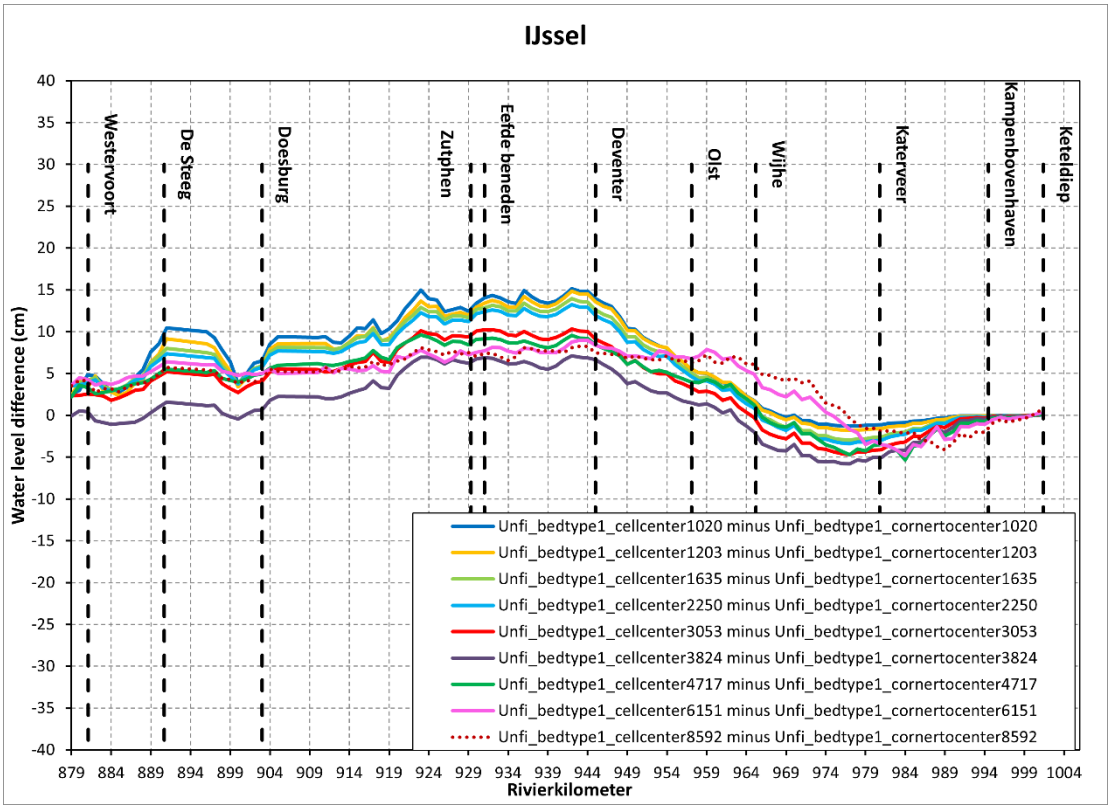

Figure 5.5 Difference in water levels along the river axis between simulations with bed levels in cell centers from baseline ("Unfilt_bedtype1 cellcenter", morphological model) and bed levels in cell centers from corner to center ("Unfi_bedtype1_cornertocenter").

5.2.2 Effect of filtering the bed level

To evaluate the influence of bed level filtering, at first model results of simulations with filtered and unfiltered bed level, both using a bed level definition in cell centers, are compared (Figure 5.6 and Figure 5.7). This shows the influence of purely the filtering. In a next step, Figure 5.8 and Figure 5.9 show the difference with the original hydrodynamic model, i.e. the effect of both filtering and changing the definition of bed levels from cell corners to cell centers.

The filtering of the bed level removes local variations and thus reduces the resistance of the bed level. Therefore, water levels after filtering are lower than before filtering (for the lowest two discharge levels up to 25 cm). This might need to be compensated in the roughness in the following phase. Combined with the effect of defining bed levels in cell centers instead of corners, water level differences are increased significantly (for the low and medium discharge levels up to -50 cm). In both comparisons, velocity differences range between +/- 0.1 m/s, with some local peaks of up to +/- 0.2 m/s. With total flow velocities ranging between 0.8 m/s for the lower discharges and 1.8 m/s for the higher discharges, that results in relative changes of about 1-2%, with peaks of up to 5-25%. Because of the large water level and velocity differences the combination of the different changes (including main channel roughness) in the model are compared with the original model and presented in 5.2.4.

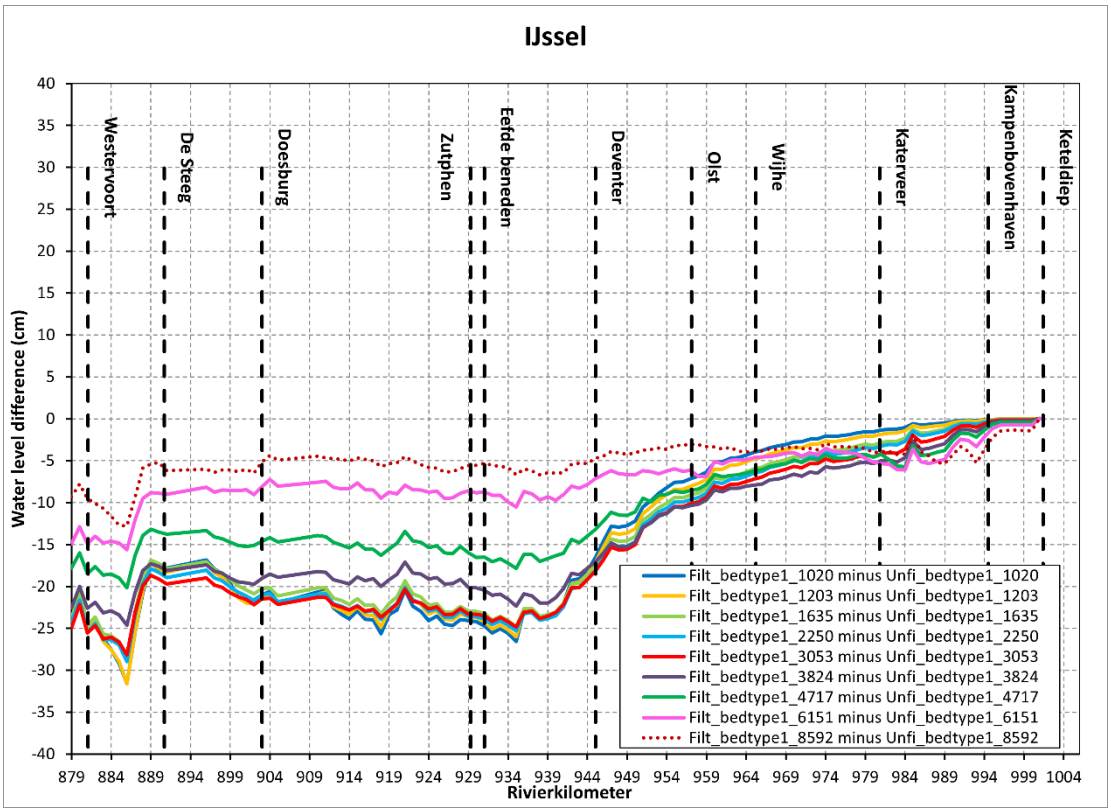

Figure 5.6 Difference in water levels (on the river axis) between simulations with filtered bed levels ("Filt_bedtype1") and unfiltered ("Unfi_bedtype1"). In both cases, bed levels are defined in cell centers.

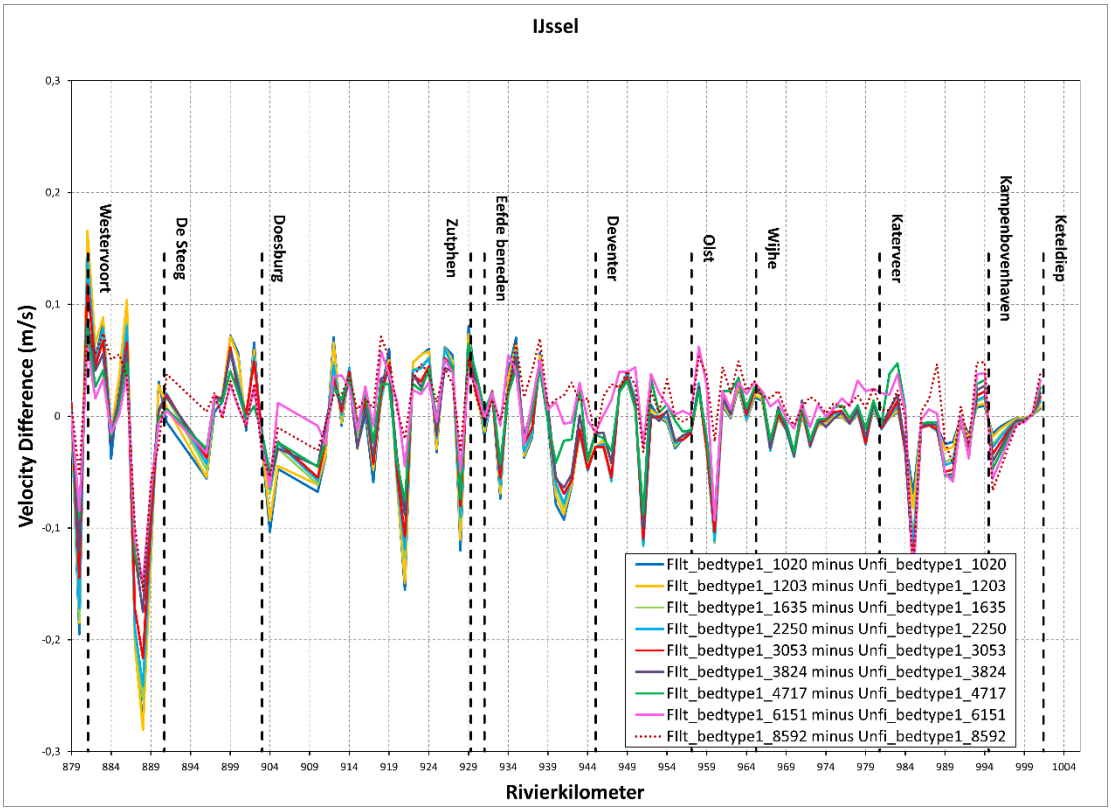

Figure 5.7 Difference in flow velocities (on the river axis) between simulations with filtered bed levels ("Filt_bedtype1") and unfiltered ("Unfi_bedtype1"). In both cases, bed levels are defined in cell centers.

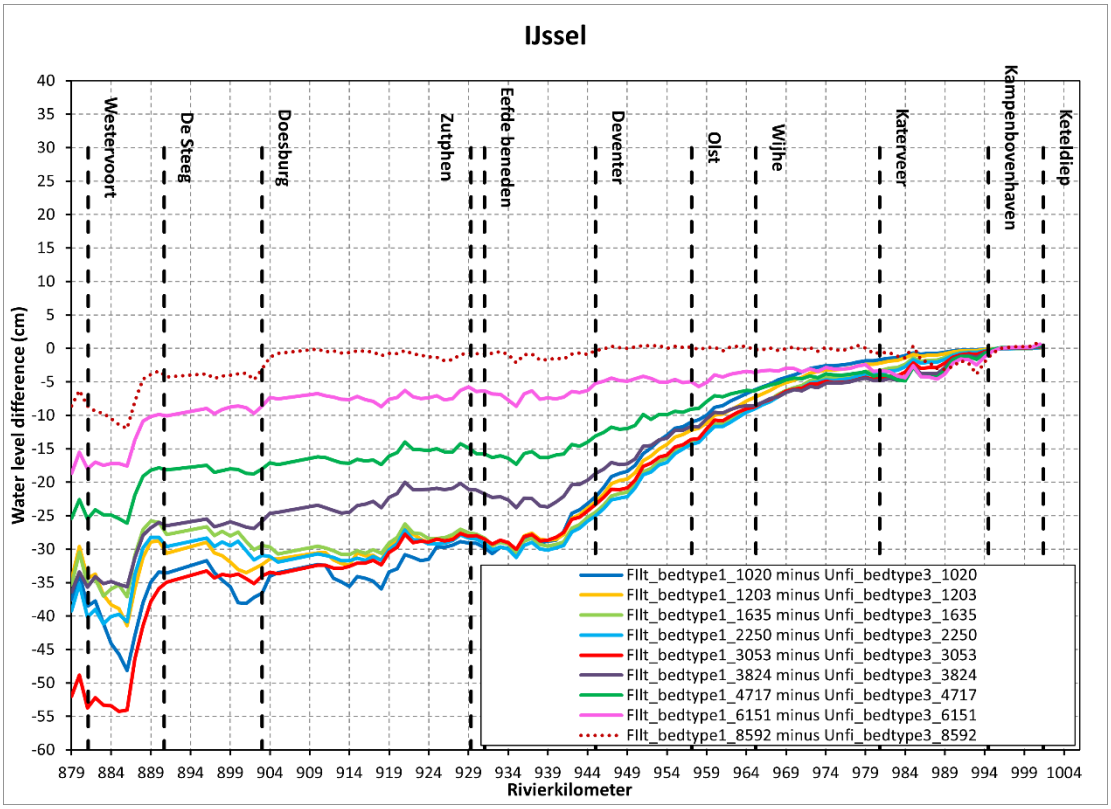

Figure 5.8 Difference in water levels (on the river axis) between simulations with filtered ("Filt_bedtype1", defined in cell centers) and unfiltered bed levels ("Unfi_bedtype3", defined in cell corners).

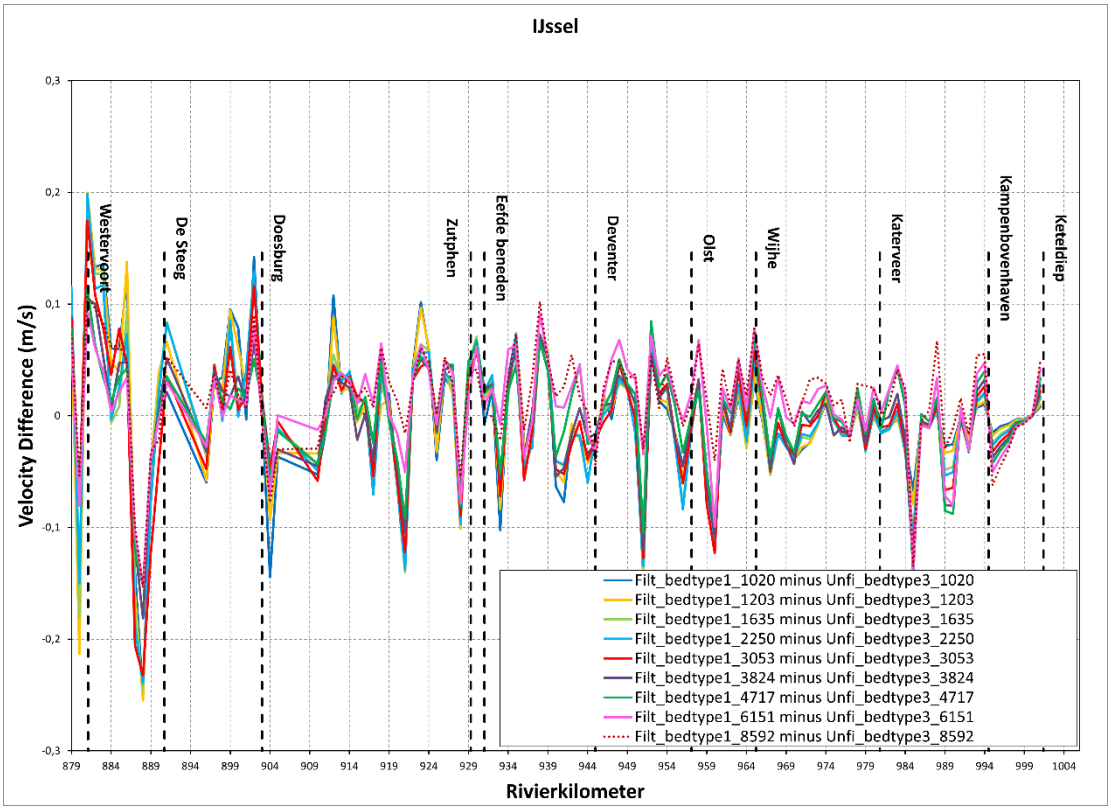

Figure 5.9 Difference in flow velocities (on the river axis) between simulations with filtered ("Filt_bedtype1", defined in cell centers) and unfiltered bed levels ("Unfi_bedtype3", defined in cell corners).

5.2.3 Effect of applying a constant main channel roughness

Another modification in the original settings of the model was to first turn off the use of the calibration factor (i.e. using a constant factor of 1.0 everywhere) and then set a constant main channel roughness. Then, three different constant Chézy values were tested: 41 $m^{1/2}/s$, 45 $m^{1/2}/s$ and 48 $m^{1/2}/s$. In all cases the changes were made, keeping the bed level in cell corners and without filtering.

Figure 5.10 and Figure 5.11 show the effect of not using the calibration factor anymore, keeping the variable base roughness on water levels and flow velocities. For the lower discharges, water levels increase along the entire IJssel. For discharges above average, the water levels decrease for most part of the IJssel. A small increase can be observed only at the upstream part. This is reflected in the flow velocities, which reduce where the water level has increased, and vice versa.

Figure 5.12 compares the water level results between the three fixed roughness and the original model for a discharge of 422 m^3/s (3053 m^3/s at Lobith). Water level differences for Chézy 45 $m^{1/2}/s$ are smaller than for the other two values, ranging from -15 to 15 cm. Therefore, the chosen fixed roughness in the IJssel for the initial tests was 45 $m^{1/2}/s$.

Figure 5.13 and Figure 5.14 compare the results of the model without calibration factor and with the chosen constant main channel roughness to the original hydrodynamic model. Upstream of the IJssel water levels are higher with fixed roughness than with variable roughness, this difference reduces as we move downstream, in the middle IJssel. In general, we observe a slight increase in the water levels downstream in comparison with variable roughness, then the water level differences decrease in the middle part of the analyzed reach.

Figure 5.15 and Figure 5.16 present the absolute water levels for both comparisons.

In a next phase of model development, after a first calibration, we can experiment with more variability in main channel roughness and work towards a compromise between the input of the original hydrodynamic model and the needs of a morphodynamic model. A proposition for how to do that is made in Beker et al. (2023). It is important to keep in mind discharge distribution across the bifurcations in the Rhine branches system when making a choice.

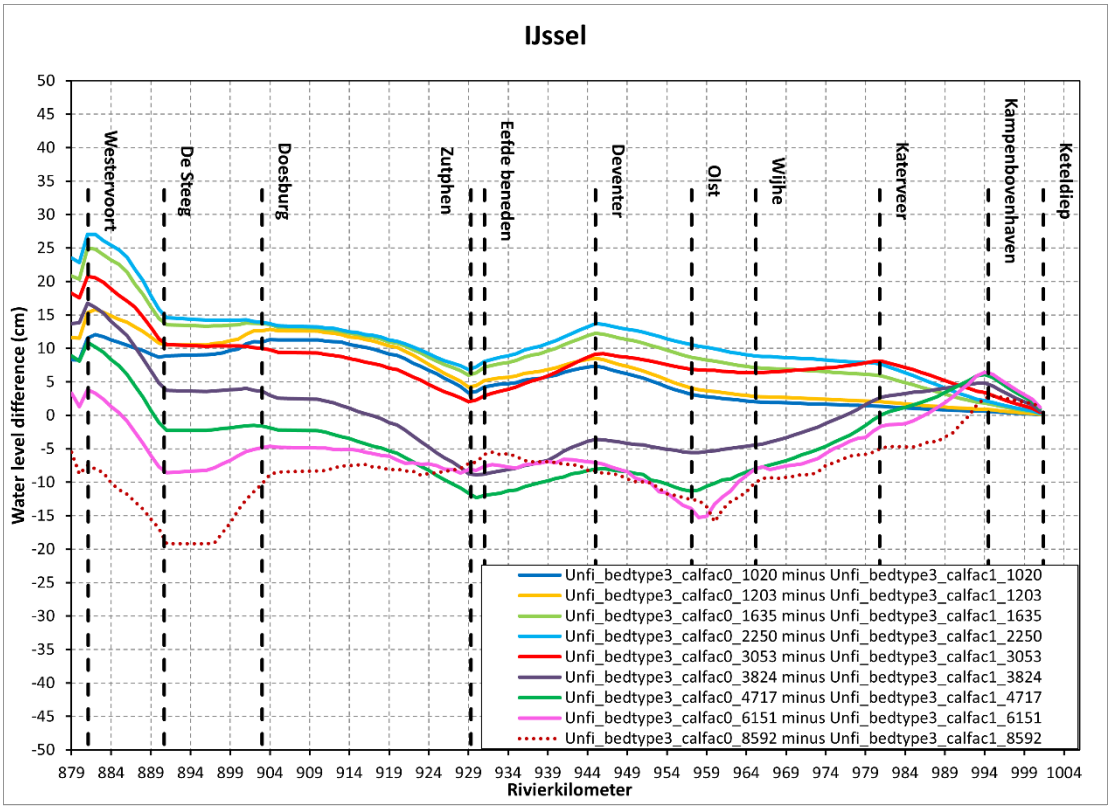

Figure 5.10 Differences in water levels between the simulations without calibration factor ("calfac0") and with calibration factor ("calfac1", original hydrodynamic model).

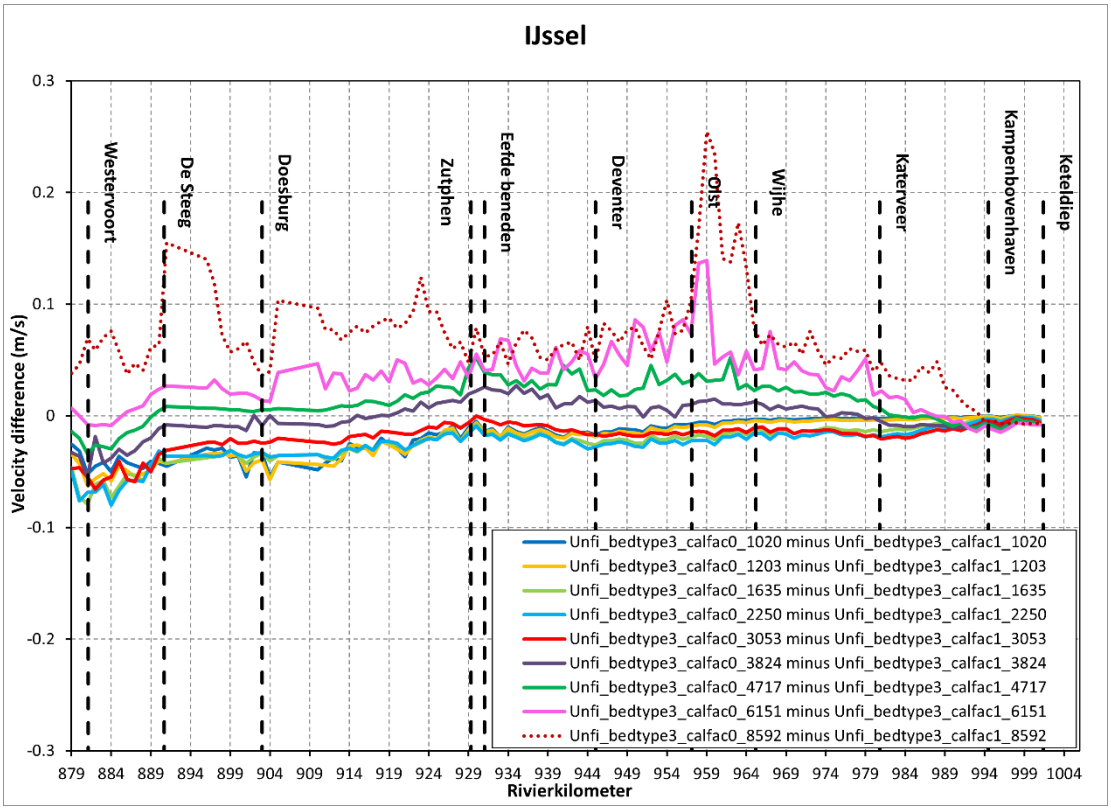

Figure 5.11 Differences in flow velocities between the simulations without calibration factor ("calfac0") and with calibration factor ("calfac 1", original hydrodynamic model).

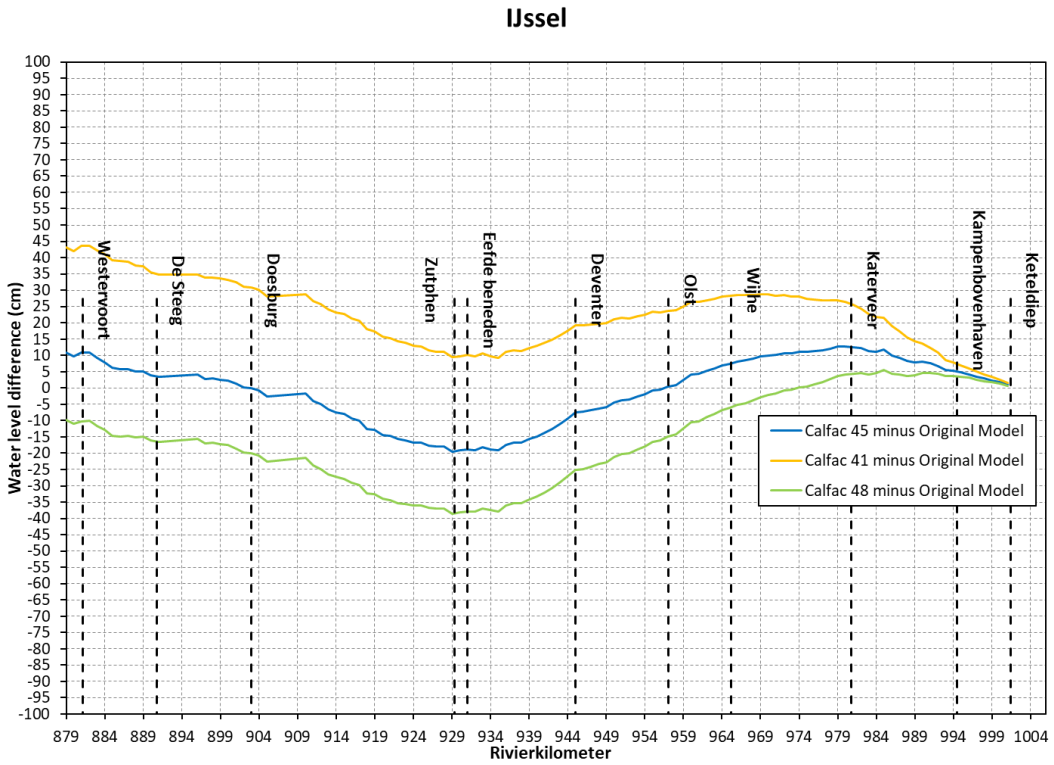

Figure 5.12 Differences in water levels between the different Chézy values (C = 41,45,48 $m^{1/2}/s$ and no calibration factor) and the the original hydrodynamic model ("Original model", varying roughness and calibration factor) for a discharge of 422 m^3/s (3053 m^3/s at Lobith).

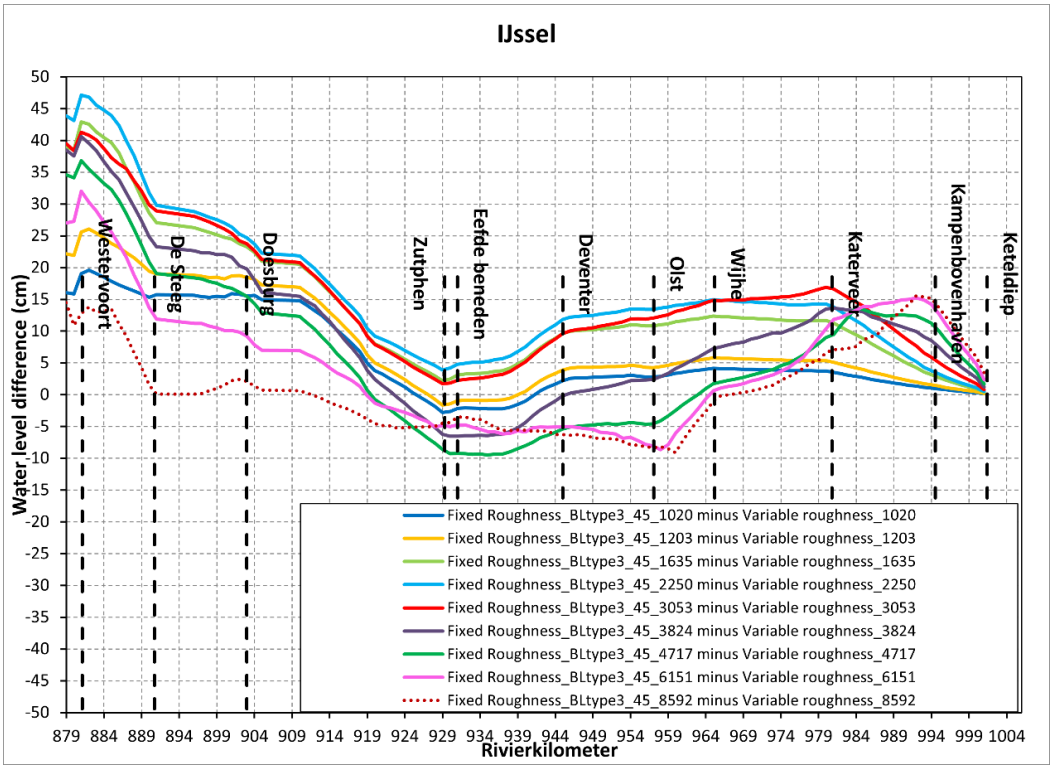

Figure 5.13 Differences in water levels between fixed roughness of 45 $m^{1/2}/s$ and no calibration factor ("Fixed roughness_BLtype3_45") and the original hydrodynamic model ("Variable roughness", varying roughness and calibration factor). All simulations use the bed level defined in corners, as in the original hydrodynamic model.

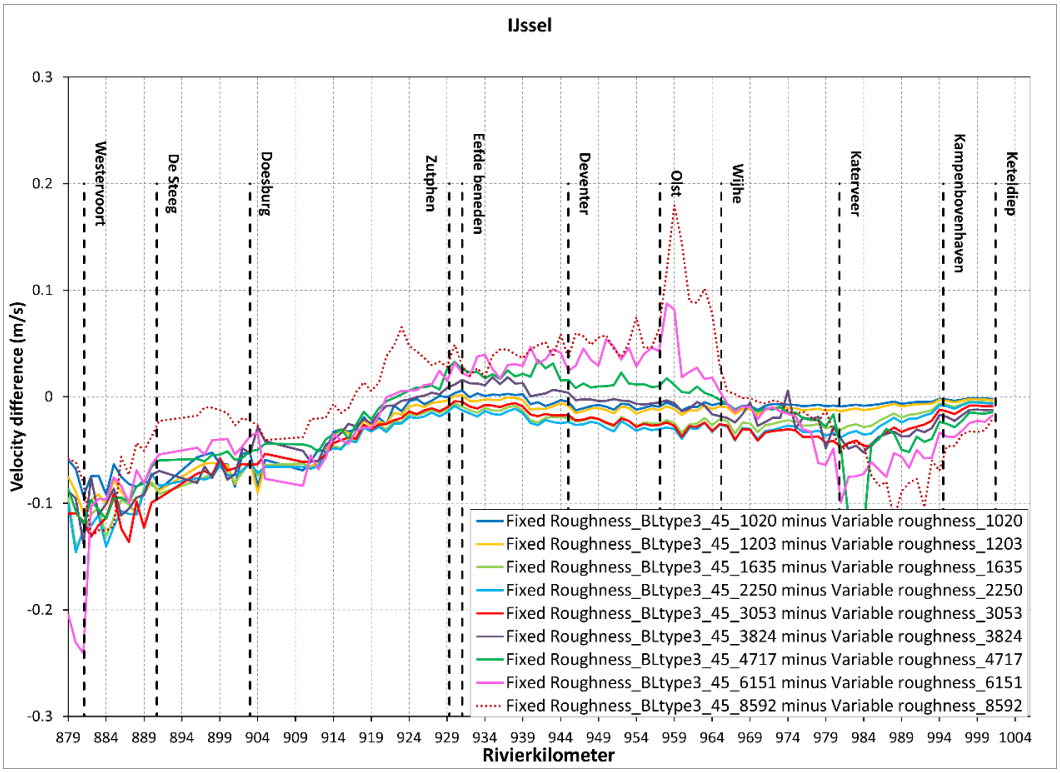

Figure 5.14 Differences in flow velocities between fixed roughness of 45 $m^{1/2}/s$ and no calibration factor ("Fixed roughness_BLtype3_45") and the original hydrodynamic model ("Variable Roughness", varying roughness and calibration factor). All simulations use the bed level defined in corners, as in the original hydrodynamic model.

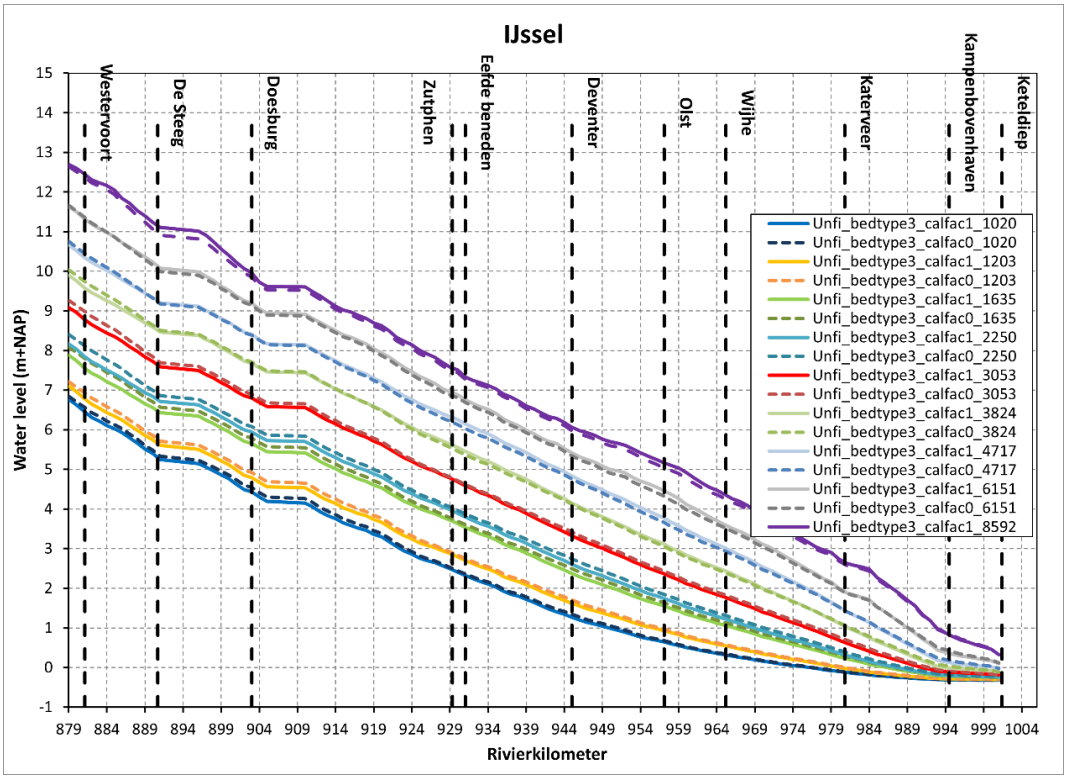

Figure 5.15 Water levels between the simulations without calibration factor ("calfac0") and with calibration factor ("calfac1", original hydrodynamic model). All simulations use the bed level defined in corners, as in the original hydrodynamic model.

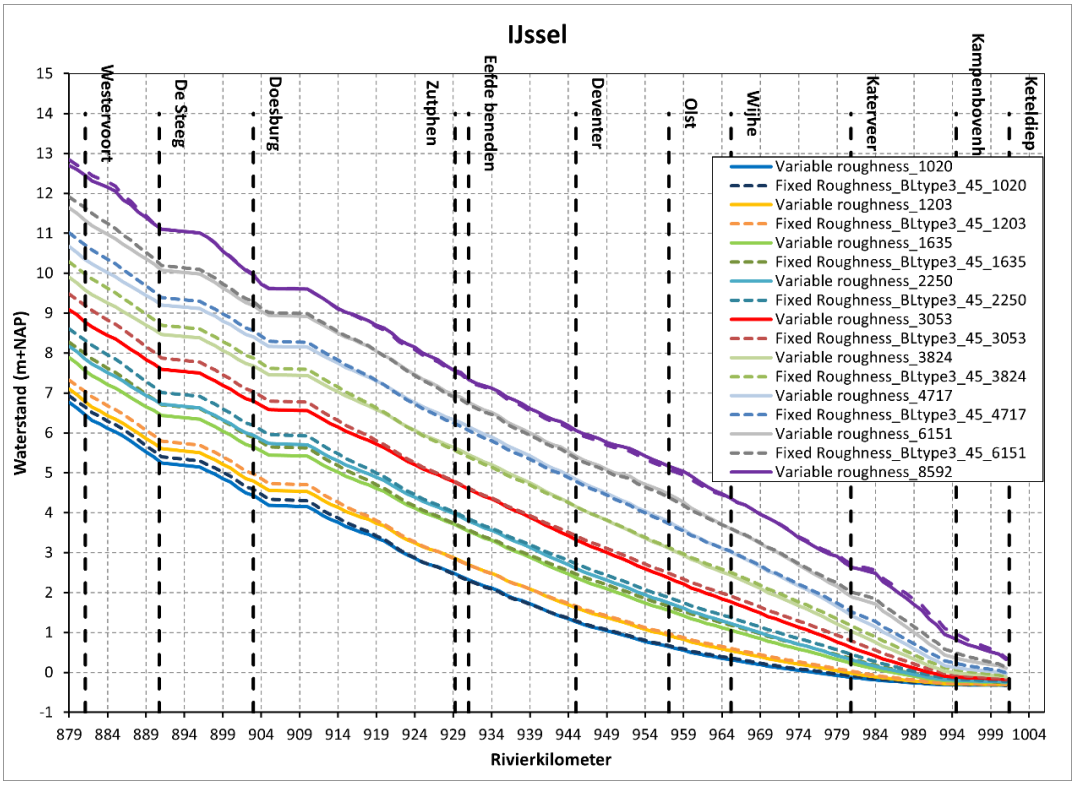

Figure 5.16 Water levels for fixed roughness (C = 45 $m^{1/2}$/s and no calibration factor) and the original hydrodynamic model ("Variable Roughness", varying roughness and calibration factor). All simulations use the bed level defined in corners, as in the original hydrodynamic model.

5.2.4 Effect of combined changes – bedlevel, roughness and filtering

Due to the large differences observed in the IJssel model when changing the bedlevel type or roughness, the combined effect of the two changes in the model was tested in comparison with the original model. This shows that despite the large differences caused by the separate changes, when combined, the differences in water levels and velocities reduce significantly.

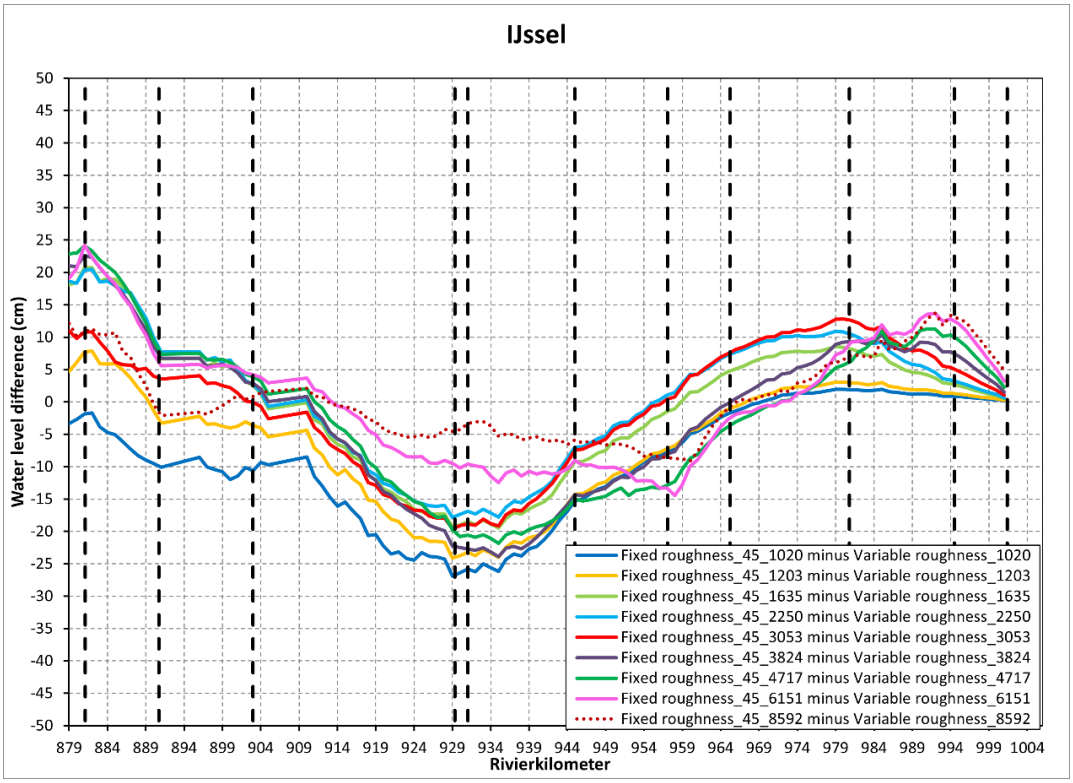

Figure 5.17 Differences in water levels between fixed roughness, no calibration factor, bedlevel type 1, filtered ("Fixed roughness_45") and the original hydrodynamic model ("Variable Roughness", varying roughness and calibration factor with bedlevel type 3).

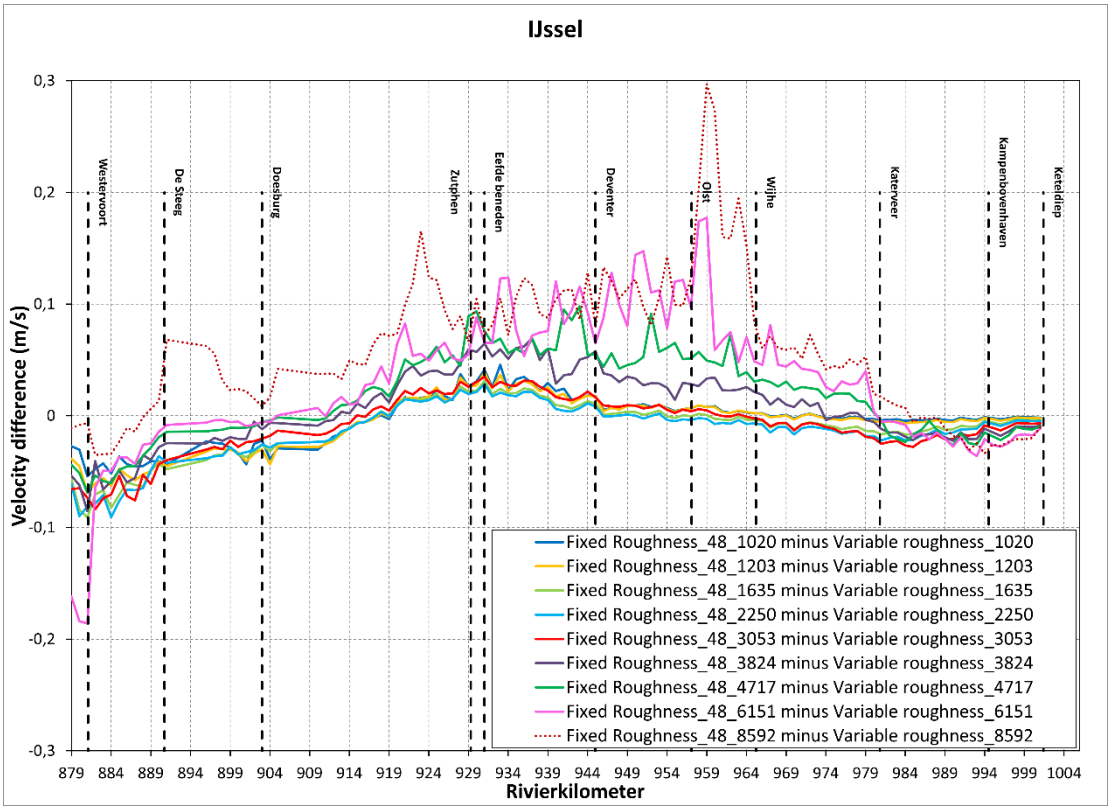

Figure 5.18 Differences in flow velocities between fixed roughness, no calibration factor, bedlevel type 1, filtered ("Fixed roughness_45") and the original hydrodynamic model ("Variable Roughness", varying roughness and calibration factor with bedlevel type 3).

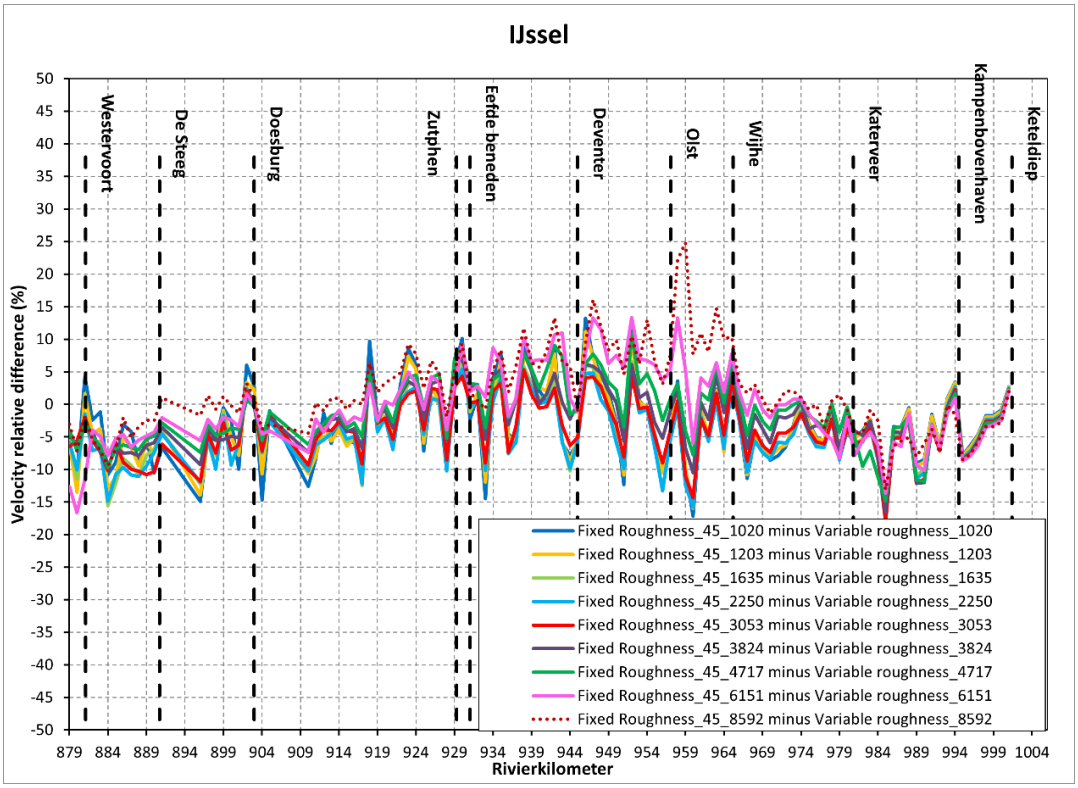

Figure 5.19 Relative differences in flow velocities between fixed roughness, no calibration factor, bedlevel type 1, filtered ("Fixed roughness_45") and the original hydrodynamic model ("Variable Roughness", varying roughness and calibration factor with bedlevel type 3).

5.3 Settings used in morphological simulations

For both the online and offline morphological simulations, it was decided to use the bed levels Baseline picked at cell centers, because using Baseline is easier in the application phase of the model than using a script to average bed levels from corner points, and the results (water levels and flow velocities) are not worse than when using the script. In the main channel (L3R3), filtered bed levels are used. The roughness is set to a constant Chézy-value of 45 $m^{1/2}/s$.

6 Morphological model schematization

6.1 Implementation of graded sediment

6.1.1 Active layer and underlayers

In D-HYDRO, morphodynamic changes for mixed-size sediment (graded sediment) are modelled using the active layer model (Hirano, 1971). In this model, the part of the bed that interacts with the flow is represented by the active layer. Only sediment in the active layer can be set into transport. Sediment in the active layer is perfectly mixed. Computed changes in mean bed elevation per cell result in vertical mixing of sediment between the active layer and the underlayers, and in between underlayers.

D-HYDRO allows to specify spatially and temporally varying active layer thickness, e.g. to model changes in dune height. In the v0 of the IJssel model, however, we will use a constant active layer thickness in order to reduce model complexity and over-parametrization. In the future, we will investigate the impact of the active layer thickness. Based on the results of that analysis, the active layer thickness might be modelled as being dependent on water depth in later model versions. Simulations with the DVR model (predecessor of the new model) have shown that making the active layer thickness directly dependent on the predicted dune heights leads to circular dependencies and therefore unplausible results (Niesten et al., 2017).

As in previous modeling efforts (e.g. Chavarrias et al., 2020), an active layer thickness of 1 m is chosen.

In the DVR model, four layers (1 active + 2 sublayers + 1 thick lowest layer) were used (active layer of 1.0 m thickness, sublayers 0.5 m, and thick underlayer 63 m). That turned out to be rather few: it led to fast mixing of sediment into the lowest thick layer. Therefore, we use a total of 7 layers in the new model: the active layer with an initial thickness of 1 m and 6 layers below with a thickness of 0.5 m for the first 5 and 10 m for the lowest one. So, the thickness of active layer and underlayers stays the same, only the number of underlayers is increased. And the thick lowest layer is reduced in thickness, because it is expected that this will be enough. The initial sediment composition is prescribed for all these layers. The number of underlayers and their maximum thickness is defined accordingly (.mor file) in order to avoid any sediment transfer between layers and immediate mixing during the first time step.

6.1.2 Sediment fractions

The new morphodynamic model does not only need to assess local morphological developments of the navigation channel, but also the large-scale and long-term morphological development of the Rhine river system in the Netherlands. Therefore, it is important to account for the entire variety of processes that play a role in different reaches from upstream till downstream. Most relevant in this respect is the occurrence of grain-size variation and its relevance for sediment-transport processes. Characteristic for the Rhine River is a downstream fining of sediment when looking at it on the length-scale of the German Niederrhein and Dutch Rhine branches, see for example Figure 3.1. The Rhine in Germany (Niederrhein) can be considered as a gravel river, whereas it shows a transition towards a sand-bed river in the Dutch Rhine branches. In the transition zone between the German border and the upper-Waal, Pannerdensch Kanaal and upper-IJssel and Neder-Rijn, both gravel and sand play an important role in sediment transport and morphology.

The river bed of the further downstream-located branches is composed of sand. In the tidal low-land part of Waal and Lek the interaction between sand, silt and mud becomes important. The same applies to the very downstream end of the IJssel.

Therefore, it was decided to apply graded sediment in the entire model. This means that different sediment fractions, from coarse to fine, and their interaction, are modelled separately. This is also important for a proper modeling of sediment management measures affecting sediment composition, such as sediment nourishment.

In order to describe the sieve curves reasonably well, including the bimodal character in Boven-Rijn and Waal, at least approximately 10 fractions are expected to be needed. Since the final goal is to create one model of all upper Rhine branches, including a part of the German Niederrhein, together, all separate branch models should use the same fractions.

The boundaries of the fractions are based on the sieve sizes used in the 2020 measurement campaign (Onjira, 2023). Originally in the data there were 22 fractions available for sieves: 63 µm, 90 µm, 125 µm, 180 µm, 355 µm, 500 µm,710 µm, 1 mm, 1.4 mm, 2 mm, 2.8 mm, 4 mm, 5.6 mm, 8 mm,11.2 mm, 11.6 mm, 16 mm, 22.4 mm, 21.5 mm, 45 mm, 63 mm, 125 mm. For model simplification and computation size reduction, the data was combined into 11 fractions as follows (see also Table 6.1):

- The sediment diameters below 63 µm (clay and silt) are hardly present in the sediment samples of all branches and are not considered in the model. The smallest sediment fraction used in the model is very fine sand.
- The fifth sieve is the smallest that contains significant amounts of sediment on all branches. Therefore, sieves 2 to 5 are summarized in one fraction in the model. The (very small) amount of mud found in the samples is added to this fraction to make all fractions add up to a total of 100%.
- From the following sieves, each two are summarized in one fraction, apart from sieves 12 and 13, which are important for the sand-gravel transition and the bimodal sieve curves on Boven-Rijn and Waal, and sieve 22, which is present in important quantities on the Boven-Rijn.

Figure 6.1 shows that with this distribution, the general characteristics of the sediment mixture, expressed in percentiles D_{10}, D_{50} and D_{90} as well as the geometric mean D_g, are kept approximately the same as when using the information of all sieves, i.e. 22 fractions.

Table 6-1 Sediment fractions included in the first model schematization (v0).

Sieve	Minimum diameter [m]	Maximum diameter [m]	Fraction
Sieve01	0.000008	0.000063	Not considered
Sieve02	0.000063	0.000090	**Fraction01**
Sieve03	0.000090	0.000125	
Sieve04	0.000125	0.000180	
Sieve05	0.000180	0.000250	
Sieve06	0.000250	0.000355	**Fraction02**
Sieve07	0.000355	0.000500	
Sieve08	0.000500	0.000710	**Fraction03**
Sieve09	0.000710	0.001000	
Sieve10	0.001000	0.001400	**Fraction04**
Sieve11	0.001400	0.002000	
Sieve12	0.002000	0.002800	**Fraction05**
Sieve13	0.002800	0.004000	**Fraction06**
Sieve14	0.004000	0.005600	**Fraction07**
Sieve15	0.005600	0.008000	
Sieve16	0.008000	0.011200	**Fraction08**
Sieve17	0.011200	0.016000	
Sieve18	0.016000	0.022400	**Fraction09**
Sieve19	0.022400	0.031500	
Sieve20	0.031500	0.045000	**Fraction10**
Sieve21	0.045000	0.063000	
Sieve22	0.063000	0.125000	**Fraction11**

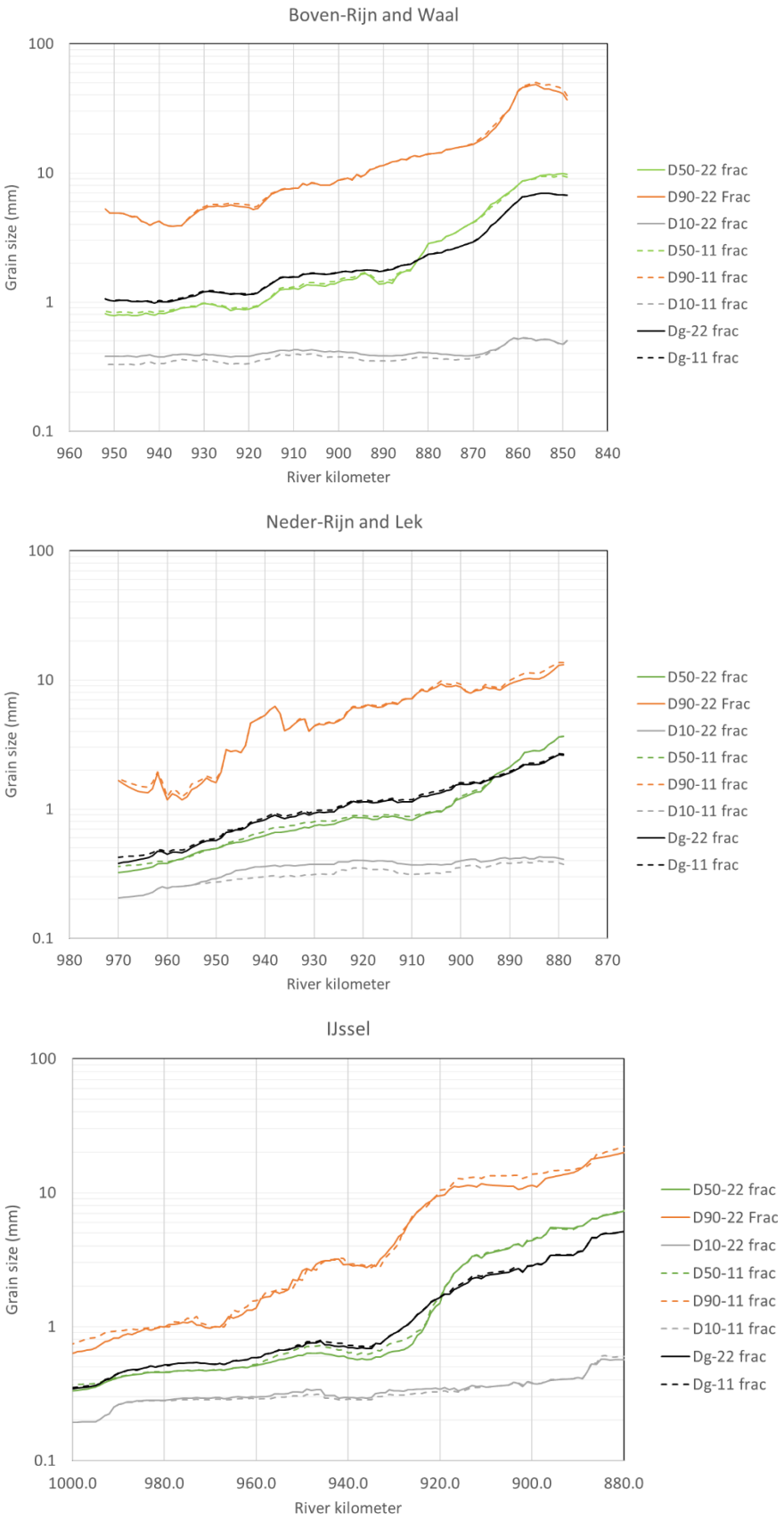

Figure 6.1 Characteristic diameters (10km running average) of the initial sediment composition for all Rhine branches (campaign of 2020) for both the original 22 fractions (solid lines) as well as the combined 11 fractions (dashed lines).

6.1.3 Initial sediment composition in top layer

The initial sediment composition in the model largely determines the large-scale gradient in sediment transport and hence morphological trends. It has long-lasting effects on morphology, even after a long period of model spin-up. Sediment composition data come from sampling the top layer of the riverbed and show large variation in space and time. For the model, it is important to derive an average composition that adequately characterizes the bed material.

Data from the most recent measurement campaign in 2020 (section 3.3) were chosen for the initial bed composition of the model.

Sloff (2022) describes a number of possible causes for the large spatial variability both in longitudinal as in transverse direction. Many of these processes, such as sorting due to bed forms, take place on a too small scale to be represented on the computational grid of the new model. They therefore need to be filtered out. Processes on the scale of river bends or several times the width of the main channel (several hundreds of meters to a few kilometers) can be calculated by the model. They are, however, small-scale enough to be introduced into the model by means of a spin-up simulation of one to a few years length. Research into a statistical method for spatially averaging the data is not yet complete (Becker et al., 2023), and therefore it was decided to use a 'running average' of 10 km in longitudinal direction to filter out small-scale variability.

On several sections of the Waal and other branches, there is a difference between the left (finer) and right side (coarser) of the riverbed. These differences are – for lack of other reasons – for now attributed to the influence of return flow and propeller radius of shipping. During the set-up of a first model (v0.8) for the Waal, it was found that Coriolis force might play a role as well. This still needs to be analyzed further before we can draw any conclusions. Since the model only calculates the natural sediment transport and sorting processes by river flow, it is not able to simulate the differences in transverse sorting due to shipping. Therefore it was decided to average (i.e. blend) the sieve curves of samples in the transverse direction for all rays where three samples (left, axis, right) are available. The samples lying in between, on the river axis, are therefore not used.

Note that the 10 km running average was continued across Pannerdensche Kop bifurcation, because there are no indications for a sudden “jump” in sediment composition. On the IJsselkop bifurcation, however, there is a sudden jump in composition towards the Upper IJssel and the averaging was not continued across the bifurcation. Instead, the data on the first 5 km of the IJssel is a linear extrapolation of the gradient in fraction sizes between km 884 and km 885.

Furthermore, it should be noted that in the Upper Waal some samples are very different from surrounding values due to possible armour layers (Sloff, 2022). Applying running averages of 10 km spreads the effect of these isolated anomalous samples over large distances, leading to a false increase in sediment size. These anomalous samples were therefore not included in the averaging.

Figure 6.2 shows the resulting geometric mean for the IJssel branch. Appendix C shows the resulting median (black lines) and geometric mean (dashed red lines) sediment diameters in comparison to the measurement data of 2020 and other years for all branches, distinguishing between left and right side of the river as well as the river axis. Figures were made with logarithmic and linear scaling on the y-axis. Since the model initially uses a constant sediment composition across the width, the lines for median and geometric mean sediment diameter are the same on all three figures (left, axis and right). Along the IJssel, grain size strongly decreases up to approximately km 935.

Downstream of that, grain size still decreases but with a smaller gradient. In general, the averaged initial composition falls within the bandwidth of the measurements. The variation in the measurements is larger on the left and right bank than on the river axis, which makes sense, because the influence of bends is larger along the edges of the main channel. Up to approximately km 935-950, the variation in grain size is larger than further downstream because of the presence of gravel and sand. In such a non-uniform mix of sediment, the sieve curve found for a sample depends strongly on the location on which the sample was taken. Large variation between locations close to each other is introduced by, amongst others, sorting due to dunes or general patchiness of the river bed (see Sloff, 2022, for more details).

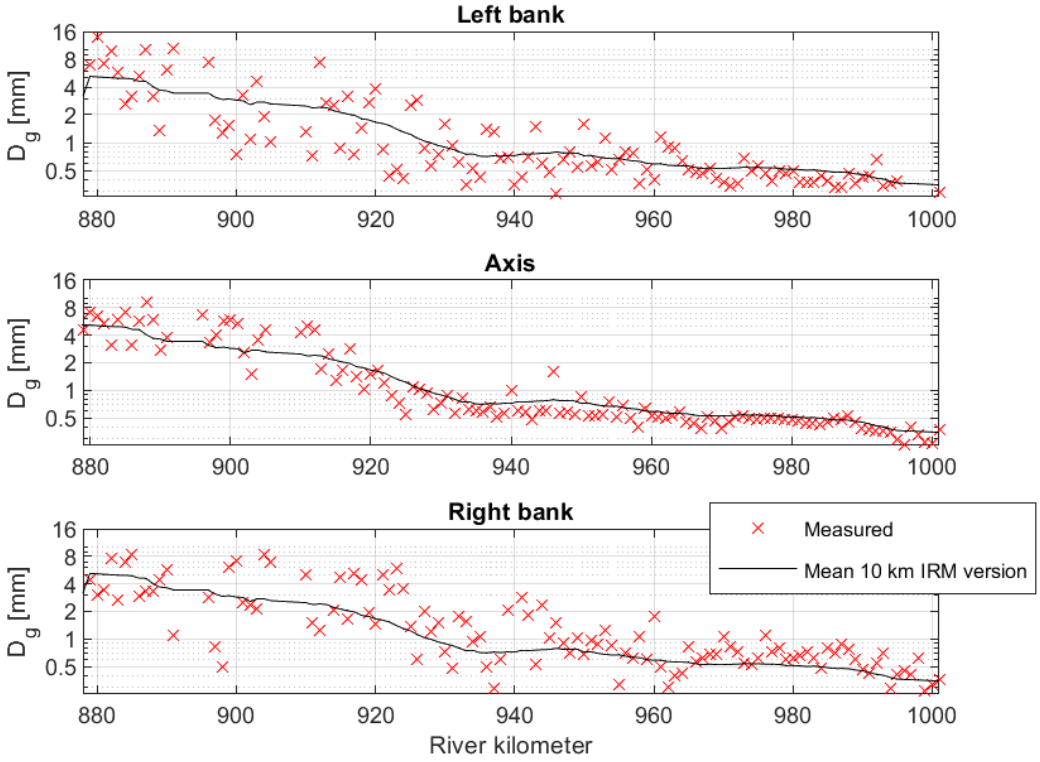

Figure 6.2 Geometric mean of the sieve curves on the IJssel derived from the 2020 measurements (red crosses) and derived using the rolling mean (solid black line).

6.1.4 Initial sediment composition in underlayer

There is not enough data available to define the composition of underlayers in the IJssel. Therefore, we will use the same (initial) composition for the underlayers as for the top layer.

6.1.5 Hiding and exposure

Hiding and exposure is a relevant process in transport and sorting processes in poorly sorted sediments. Due to hiding processes fine sediments are hidden behind coarse grains and have a lower mobility, whereas the coarse particles are more exposed and get a higher mobility. This effect is accounted for by a modification factor on critical shear stress in the transport formula. For hiding and exposure, the ration between grain-size of a fraction D_i and the median grain-size D_m of the sediment mixture is used to increase (for coarse fractions) or reduce (for fine fractions) the critical shear stress.

The hiding exposure options are listed in Table 6-2. The DVR model used the Ashida & Michiue formulation (see e.g. Becker, 2021). For the new model in D-HYDRO, a sensitivity test of the possible hiding and exposure factors was tested and is presented in chapter 7.

Since the hiding and exposure factor works on the critical shear stress, it is only used in sediment transport formulations that contain a critical shear stress (e.g. Meyer-Peter-Müller, see section 6.2).

Table 6-2 Hiding and Exposure formulation options (Deltares, 2022)

Hiding and Exposure	
0 = No hiding and exposure	$\xi = 1$
1 = Egiazaroff (1965)	$\xi = \left(\frac{\log_{10} 19}{\log_{10} 19 + \log_{10} {}^{D_i}/_{D_m}} \right)^2$
2 = Power law (Parker, Klingeman & McLean or Soehngen, Kellerman & Loy)	$\xi = \left(\frac{D_i}{D_m}\right)^{\alpha}$, with alpha as calibration factor, e.g. -0.8
3 = Ashida-Michiue (1972)	$\xi = 0.8429 \frac{D_i}{D_m}$ if $\frac{D_i}{D_m} < 0.38889$ $\xi =$ as Egiazaroff otherwise

with D_i the characteristic grain size of the sediment fraction considered [m] and D_m the mean grain size of the total sediment mixture [m].

6.2 Sediment transport formula

In principle, the choice of a suitable sediment transport formula is part of the calibration of a model. For the first version (v0) of the IJssel model, experiments were run with the settings used in previous calibration efforts for the DVR model (Sloff et al., 2009). These settings are presented in Table 6-3. The use of Meyer-Peter and Müller was decided based on the Integral River Management (IRM) morphological 2D model (Sloff, Becker, Paarlberg, & van Denderen, 2024).

Sloff et al. (2009) found that the formula of Meyer-Peter and Müller (1948, MPM) was well suited for the upstream part of the DVR model (Boven-Rijn, Pannerdensch Kanaal, Boven-Waal). The model domains further downstream were never modelled using graded sediment. When developing the fully graded sediment 1D model for IRM, Chavarrías et al. (2020) found that it was impossible to correctly predict both the sand and gravel load for all Rhine branches with only one load relation. They decided to use the formula of Engelund and Hansen (1967, EH) for the sand fractions and the one of Meyer-Peter and Müller for the gravel fractions, as these were most accurate for the independent fractions. (Sloff, Becker, Paarlberg, & van Denderen, 2024) tested both sediment transport options and concluded that it would be better to use the same transport relation (MPM) for the following reasons:

- Using EH+MPM, an explicit choice is made for the ratio between sand and gravel transport in the model, while in reality we have very little information on this ratio.
- Using EH+MPM might lead to unrealistic sorting effects if the transport relations are not tuned carefully, or if the model is changed in the future e.g. by a model update or a set of measures.
- There is little scientific basis for using EH+MPM combined in one model.

Based on the aforementioned background, in this version of the model an offline sensitivity test was made to identify an initial combination of parameters suitable for the IJssel and the Waal branches using only the Meyer-Peter and Müller (MPM) sediment transport formula.

Offline model calibration results were used to test these parameters and define an initial parameter setting. Tests were also made for hiding and exposure and ripple factor. Table 6-2 and Table 6-4 indicate the available hiding and exposure options that can be used in the model. MPM default parameters are also indicated in Table 6-3. Recent analysis by (Wong & Parker, 2006) proposed a correction on these parameters. The definition of the parameter settings to be used in this version of the model also took this correction into account.

The final goal is to set-up morphological models for all Rhine branches separately and one model of all branches together. It still needs to be decided if we allow the use of separate settings per branch or not. Depending on this decision, we might need to change the transport formula settings for the IJssel at a later stage.

Table 6-3 Sediment transport formulations tested in the first model version (v0).

Abbreviation	Sediment transport formula	Parameters	Source
IRM00	Fractions 1 – 4 Engelund-Hansen (EH) Fractions 5 – 11: Meyer-Peter-Müller general formula (MPM)	a = 0.18, n = 5 a = 2.56, b = 1.5, θ_c = 0.025, μ = 1	Chavarrías et al. (2020)
DVR00	Meyer-Peter-Müller general formula (all fractions) (MPM)	a = 5, b = 1.5, θ_c = 0.025, μ = 0.7	Sloff et al. (2009)
Original MPM	Meyer-Peter-Müller general formula (all fractions) (MPM)	a =8, b = 1.5, θ_c = 0.047, μ = 1.0[5]	(Meyer-Peter & Müller, 1948)
Corrected MPM	Meyer-Peter-Müller general formula (all fractions) (MPM)	a = 4.93, b = 1.6, θ_c = 0.047, μ = 1.0	(Wong & Parker, 2006)

with:

$$S_{EH,i} = \frac{a \cdot 0.05 u^n}{\sqrt{g} C^3 \Delta_{\square}{}^2 D_i}$$

$$S_{MPM,i} = a D_i \sqrt{\Delta g D_i} (\mu \theta_i - \xi_i \theta_c)^b$$

$$\theta_i = \left(\frac{q}{C}\right)^2 \frac{1}{\Delta D_i}$$

with u the flow velocity magnitude [m/s], C the Chézy friction coefficient [$m^{1/2}/s$], Δ_i the relative density of the sediment fraction i [-], D_i the characteristic grain size of the sediment fraction considered [m], μ the ripple factor, θ_i the actual Shields parameter for the sediment fraction considered, θ_c the critical Shields parameter, ξ_i the hiding and exposure factor for the sediment fraction considered, q the flow velocity, and n, a and b calibration parameters.

Table 6-4 Ripple factor model options (Deltares, 2022)

Ripple factor	
1	μ = constant (user input)
2	$\mu = \min\left(\left(\frac{C}{C_{g,90}}\right), 1.0\right)$

[5] In the original formulation of Meyer-Peter & Müller, the ripple factor did not yet exist. For better comparability between the different settings used, we put its value to 1.0 in this overview.

Where C is the Chézy friction coefficient [m$^{1/2}$/s], and $C_{g,90}$ is the Chézy coefficient related to grains, given by:

$$C_{g,90} = 18 \log\left(\frac{12(d+\zeta)}{D_{90}}\right)$$

With D_{90}specified in [m].

6.3 Constructions and morphologically active area

In general, in the v0- and v1-version of the new model we follow the approach used in the DVR model, i.e. only the main channel of the river is morphologically active, because morphological processes in the flood plains and e.g. of side channels in the flood plains are more complex due to vegetation, summer dikes etc. More research is needed to model these processes sufficiently well (see Spruyt, 2023).

In the flood plain, sedimentation can take place, and sediment that has been deposited there during the simulation can be moved away again, but at the start of the simulation no sediment is present in the flood plain and thus no erosion can take place.

The main channel is defined as the grid cells that fall in between the normal lines. All grid cells neighboring the tips of groynes or fixed banks are also made inactive, because the bed level of these cells contains parts of the groynes. If these cells were kept active, the groynes would erode at the beginning of the simulations. For the same reason, cells with a steep slope were excluded from the active part. Figure 6.3 shows the resulting active part for a river stretch around km 898. Since the computational grid on the IJssel is rather coarse in transverse direction, the fixed weirs of steep banks are often projected further towards the land side than the groyne tips, which often leaves 2 non-active cells between the projected fixed weirs and the start of the active area, see left bank on the right of Figure 6.3.

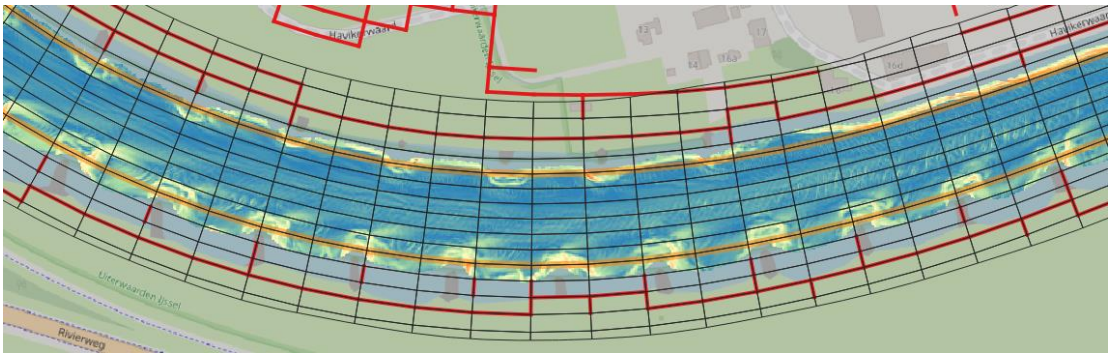

Figure 6.3 Morphologically active area (orange polygon), fixed weirs for e.g. groynes (red lines) presented on top of the computational grid (black) and the slope of the multibeam measurements (autumn 2020) around IJssel km 898.

6.4 Secondary flow

In the simulations including sediment transport and morphology, secondary flow is switched on, without coupling it back to hydrodynamics. The calibration parameter for bend effects is initially given the same value as was used in the DVR model (e.g. the model used in Becker, 2021):

- Espir = 1.0

This value will be changed during 2D calibration.

6.5 Bed slope effects

The parameters for taking into account bed slope effects are initially given the same values as were used in the DVR model (e.g. the model used in Becker, 2021):

- AShld = 1.1
- BShld = 0.5

In a next phase of the model development, the values will be used as calibration parameters for calibrating 2D bank patterns.

6.6 Upstream boundary conditions (morphology)

In a river model, with flow in only one direction, a morphological boundary condition has to be prescribed at the upstream model boundary. In the IJssel model, that is the boundary at IJsselkop (section 4.3.1). D-HYDRO offers different possibilities for prescribing these.

For the IJssel model the rate of bed level change was prescribed. A constant rate was derived from the bed level measurements processed by De Joode (2023). The trend was derived for the most upstream 100 m sections of the IJssel as shown in Figure 6.2 from which the trend for the entire period of analysis was chosen to be the average of the 5 sections (-1.86 cm/y). In combination with a bed level trend one also has to impose information on upstream sediment composition. It was assumed that composition stays constant.

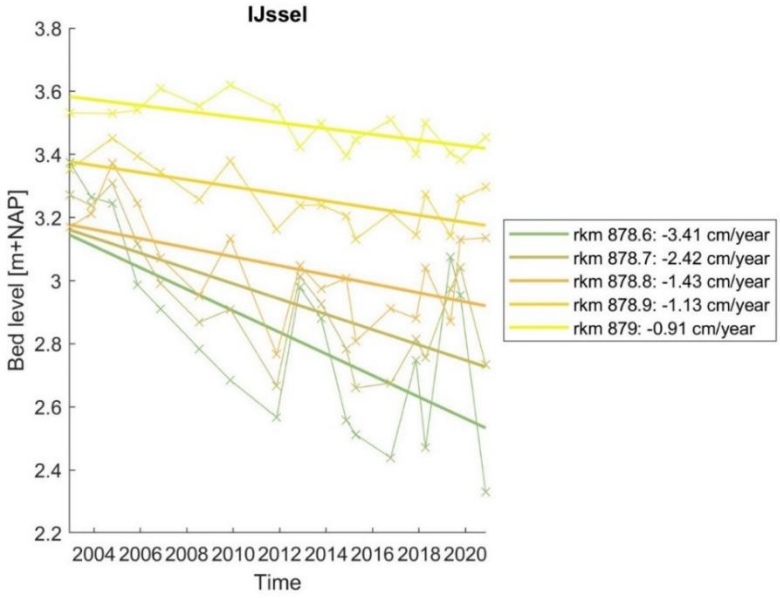

Figure 6.4 Bed level trend for the full period of analysis (2004-2020) in the most upstream 100 m sections of the IJssel.

7 Offline calibration

7.1 Methodology

Within the offline calibration, sediment transport is calculated based on hydrodynamic model simulations. This means that the computed sediment transports are not translated into bed level changes in the model, which in turn would influence hydrodynamics. Because this feedback mechanism is not included, we call this an offline calibration. The objective is to compute the expected sediment transport of an average year for varying sediment transport relations and parameters in order to be able to select suitable values for the start of the 1D calibration. To do so, the calculated sediment transport is compared to the estimates by Frings et al. (2019) and Sloff (2019) that are described in section 3.4.2 (“trend Pmap 20 yr”).

For the offline calibration, use was made of the bed level schematization from Baseline without further modification, so bed level specified in corners and no averaging procedure. Given the uncertainty in sediment transport, the limited differences in water depth and velocity due to these adjustments are not expected to have any significant impact on the conclusions regarding yearly sediment transport rates.

The basis of the offline calibration is formed by the steady-state hydrodynamic results for nine different discharge levels as described in section 4.4. The final state of each hydrodynamic simulation (i.e., the steady-state for each discharge) is used to construct a schematized hydrograph. This step was carried out before the discharge hydrographs for calibration and validation were constructed (see section 4.4.1) and thus still used the hydrograph of the old DVR model.

As in the offline calibration there is no coupling between hydrodynamics and bed level changes, the order in which discharge levels occur does not influence the results. We can therefore simply take the total duration of each discharge level within the standard hydrograph, without dividing this duration over different periods through the year.

The hydrodynamic output is combined with morphodynamic input regarding the characteristic sediment sizes and the bed composition, defined as the available sediment volume per fraction in each grid cell. For the offline calibration, the rolling mean interpolation of the data from the 2020 measurement campaign was used (see Section 3.3 and 6.1.3) in combination with 11 sediment fractions (Section 6.1.2).

For each flow field (i.e., for each discharge level), the sediment transport rate is computed given the morphodynamic input. The yearly sediment transport is obtained by multiplying each sediment transport rate by the duration of each discharge level.

The offline calibration of the IJssel consisted of comparing the sediment transport results for variations of the parameters a, θ_c and b of the Meyer-Peter & Müller formula presented in section 6.2, to the sediment transport values from section 3.4.2. Table 7-1 shows the parameters tested in the offline calibration.

Table 7-1 Parameter list used in the offline calibration tests

Abbreviation	Sediment transport formula	Parameters	Source
Sensitivity test	Meyer-Peter-Müller (all fractions)	• a = [2,4,6]; b = [1.1,1.3,1.7]; θ_c =[0.015,0.035,0.055] • a = 4.93, b = 1.6, θ_c = 0.047 • a = 8 b =1.5 θ_c =0.047	• Sensitivity test • (Wong & Parker, 2006) • Default
Final test	Meyer-Peter-Müller (all fractions)	• a = 2, b = 1.6, θ_c = 0.047	• Defined

7.2 Results

7.2.1 Offline sediment transport

Figure 7.1 to Figure 7.3 shows the total (so including both sand and gravel) yearly sediment transport for all parameter variations. Comparing the parameter variations to the default MPM case the following conclusions can be drawn:

- Looking at the case in which all parameters are fixed except for the calibration parameter (a) (green solid lines), we see that sediment transport increases significantly by varying the parameter from 2 to 6. The order of magnitude using a calibration parameter of 2 is the closest to the sediment transport estimates by Frings et al.(2019) and Sloff (2019) ("*trend PMAP 20yr*"). Note that the estimate of Frings (2019) is one value per river section, that is why it appears as a constant value in the figures. Also note that the estimate of Sloff (2019) is based on an analysis of bed level changes for a period (2000-2018) that is different from our calibration period (2002-2012). So both should be regarded as estimate.
- Sediment transport is sensitive to small variations in parameter b, the exponent (dashed blue lines). The higher the parameter value, the smaller the sediment transport. This is because the difference between actual and critical shear stress on average is smaller than 1.0 on the IJssel.
- Downstream of rkm 930, sediment transport is less sensitive to variations of the critical shields (c) (orange dotted-dashed lines). Increasing c by 0.02 decreases sediment transport by less than 20.000 m³/year. On the upper part of the IJssel, the critical shear stress significantly influences the yearly sediment transport. This is because the sediment here is more graded, and the critical shear stress determines which fractions are mobile. For the same reason, the critical shear stress also influences the transport gradient on the upstream part of the IJssel.
- Default parameters for MPM (grey solid line) strongly overestimate the yearly sediment transport.
- Adopting the parameters suggested by Wong and Parker (2006) provides a better estimate of the sediment transport than the default parameters for MPM, because the calibration parameter is lower (4.93 instead of 8) and the exponent is higher (1.6 instead of 1.5).
- Changes in the calibration parameter (a) and the exponent (b) also affect the gradients upstream and downstream. The smaller (a)/higher (b) the parameter, the smaller the gradients.
- With all parameter sets, gradients in transport are overestimated compared to the Pmap analysis (except for the most downstream section where Pmap gives a high gradient). That gradient probably results from the strong bed level change caused by the implementation of the summer bed lowering within the Room for the River bed project.

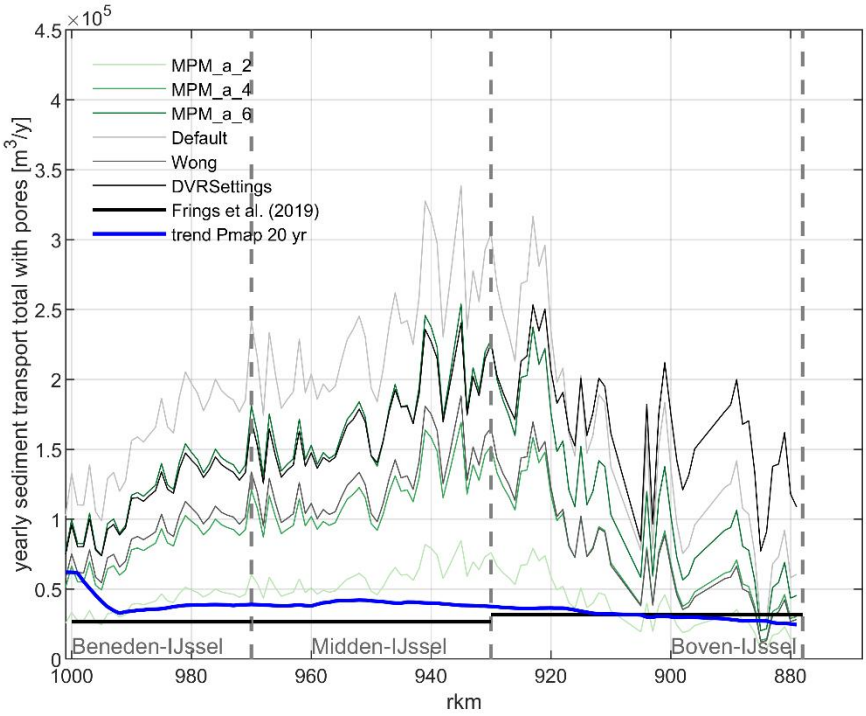

Figure 7.1 Yearly total sediment transport with pores, changing parameters a (green solid lines) compared to MPM default setting (light grey), Wong et al. (2009) (grey), DVR settings (black), and sediment transport estimates from Frings et al. (2019) and Pmap (20 years).

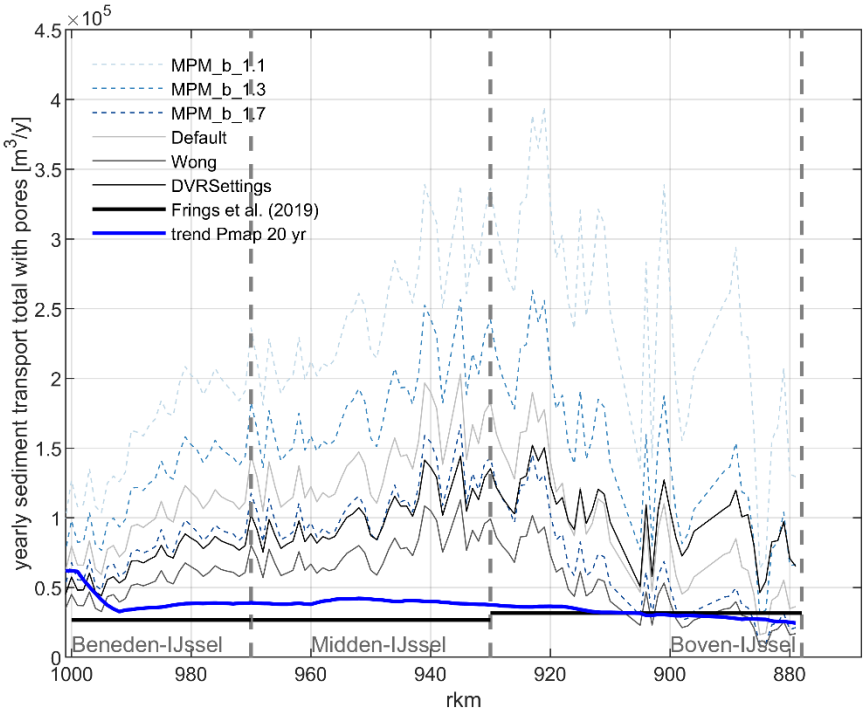

Figure 7.2 Yearly total sediment transport with pores changing parameter b (blue dashed lines) compared to MPM default setting (light grey), Wong et al. (2009) (grey), DVR settings (black), and sediment transport estimates from Frings et al. (2019) and Pmap (20 years).

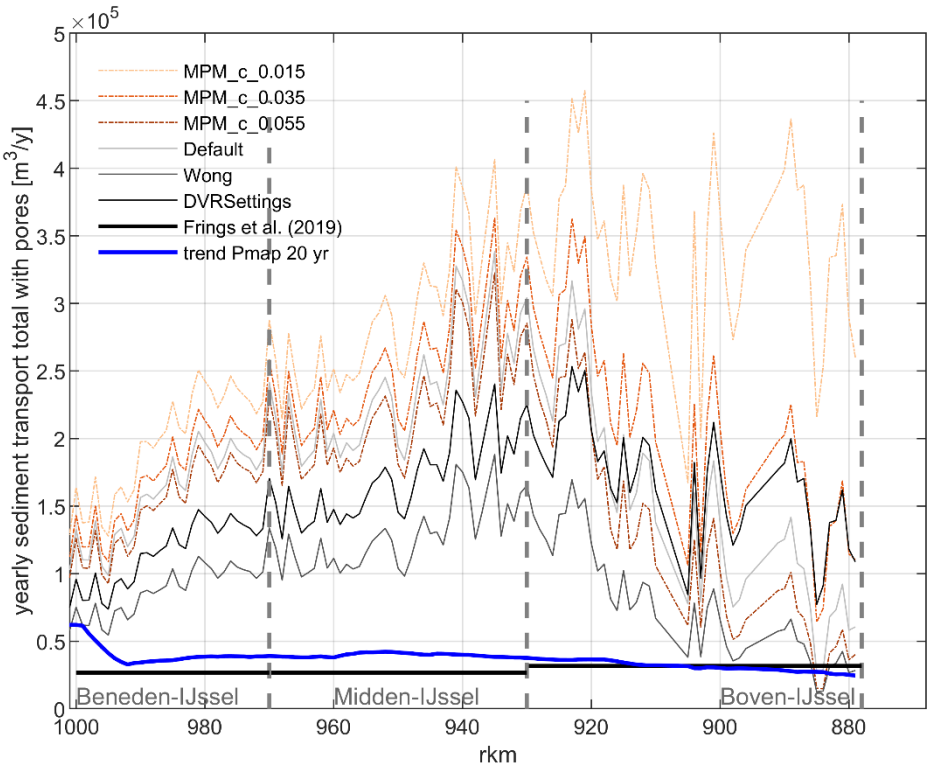

Figure 7.3 Yearly total sediment transport with pores changing parameter c (orange dashed-dotted lines) compared to MPM default setting (light grey), Wong et al. (2009) (grey), DVR settings (black), and sediment transport estimates from Frings et al. (2019) and Pmap (20 years).

Similar conclusions are drawn when analyzing the offline sediment transport results for gravel and sand separately (Figure 7.4 to Figure 7.9). Plotting gravel and sand separately shows that the fractions respond differently to the change in parameters. Gravel transport is more sensitive to changes in c than sand. On the other hand, the sediment transport in sand is more sensitive to changes in the calibration parameter a.

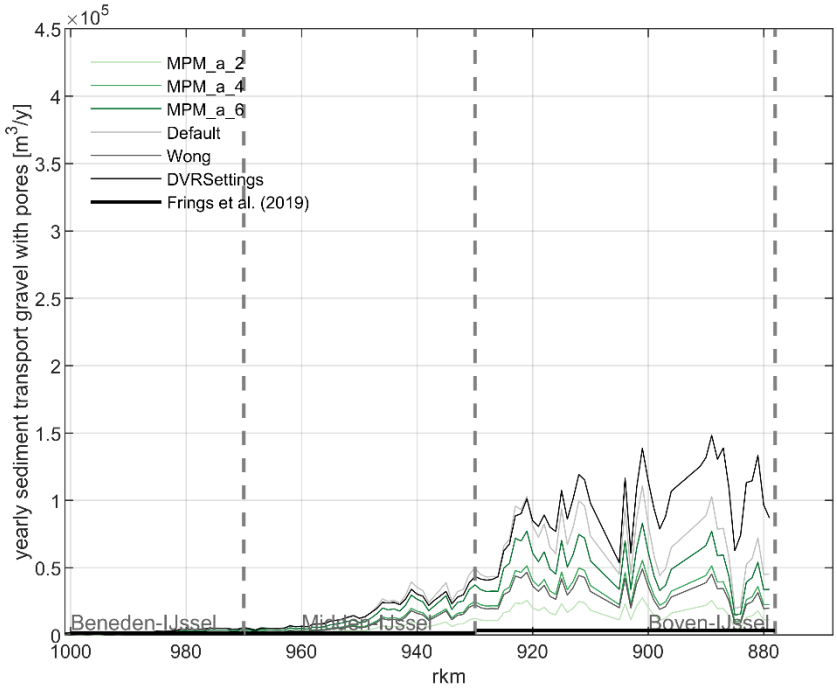

Figure 7.4 Yearly sediment transport for gravel with pores changing parameter a (green solid lines) compared to MPM default setting (light grey), Wong et al. (2009) (grey), DVR settings (black), and sediment transport estimates from Frings et al. (2019).

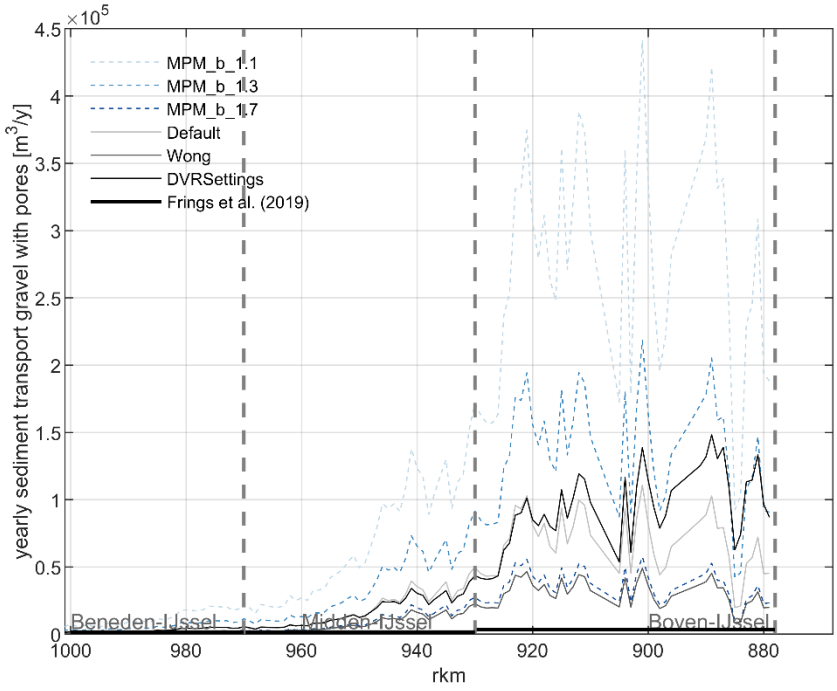

Figure 7.5 Yearly sediment transport for gravel with pores changing parameters b (blue dashed lines) compared to MPM default setting (light grey), Wong et al. (2009) (grey), DVR settings (black), and sediment transport estimates from Frings et al. (2019).

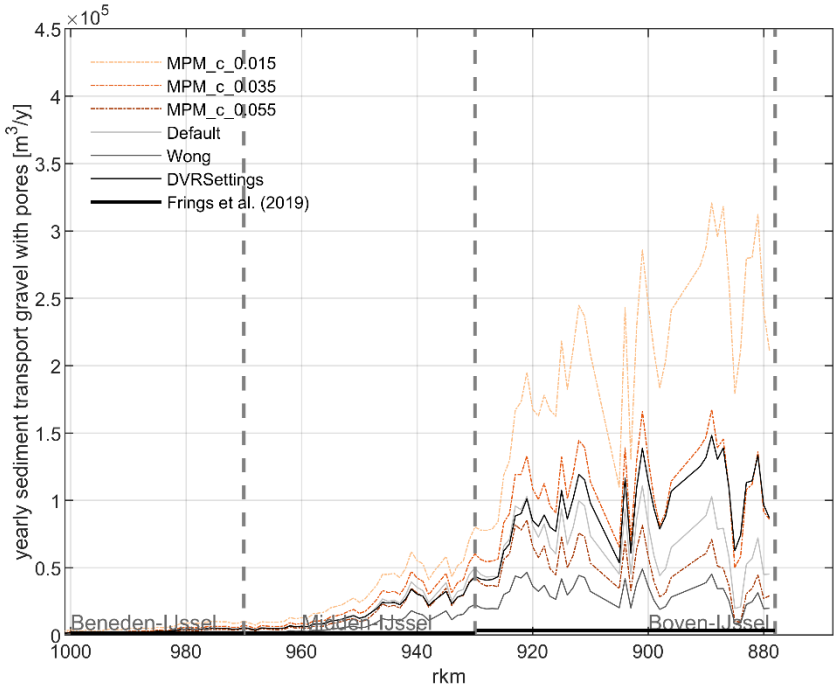

Figure 7.6 Yearly sediment transport for gravel with pores changing parameters c (orange dashed-dotted lines) compared to MPM default setting (light grey), Wong et al. (2009) (grey), DVR settings (black), and sediment transport estimates from Frings et al. (2019).

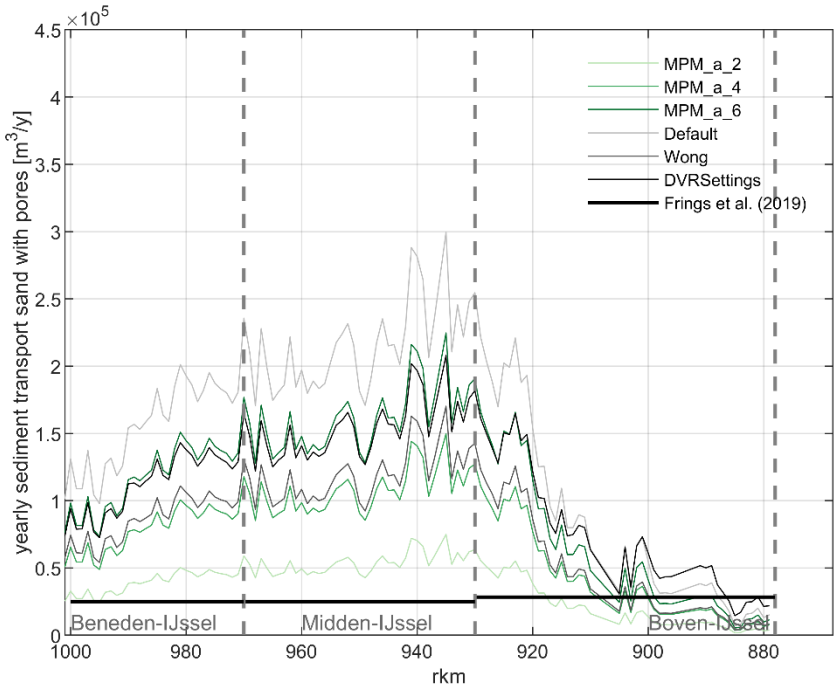

Figure 7.7 Yearly sediment transport for sand with pores changing parameter a (green solid lines) compared to MPM default setting (light grey), Wong et al. (2009) (grey), DVR settings (black), and sediment transport estimates from Frings et al. (2019).

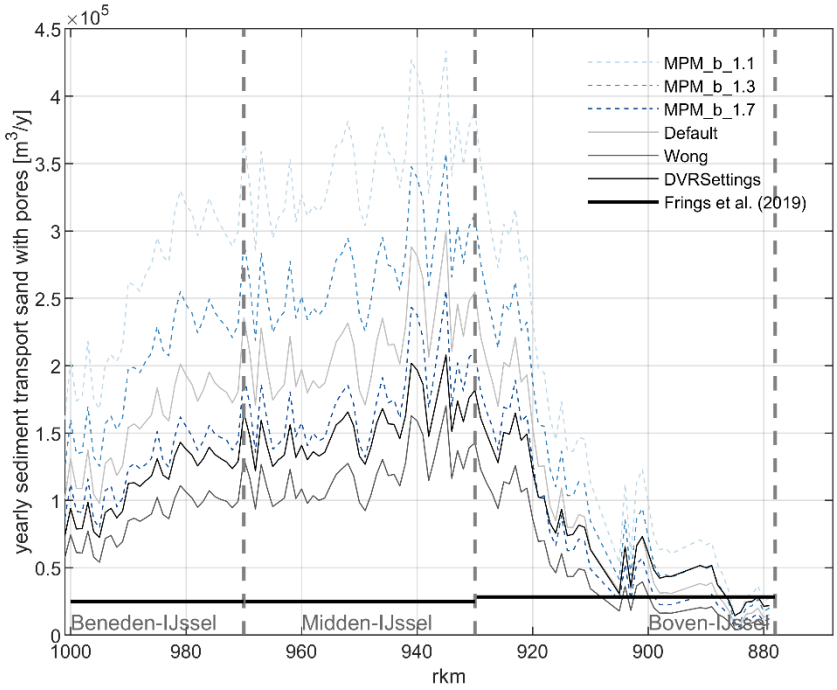

Figure 7.8 Yearly sediment transport for sand with pores changing parameters b (blue dashed lines) compared to MPM default setting (light grey), Wong et al. (2009) (grey), DVR settings (black), and sediment transport estimates from Frings et al. (2019).

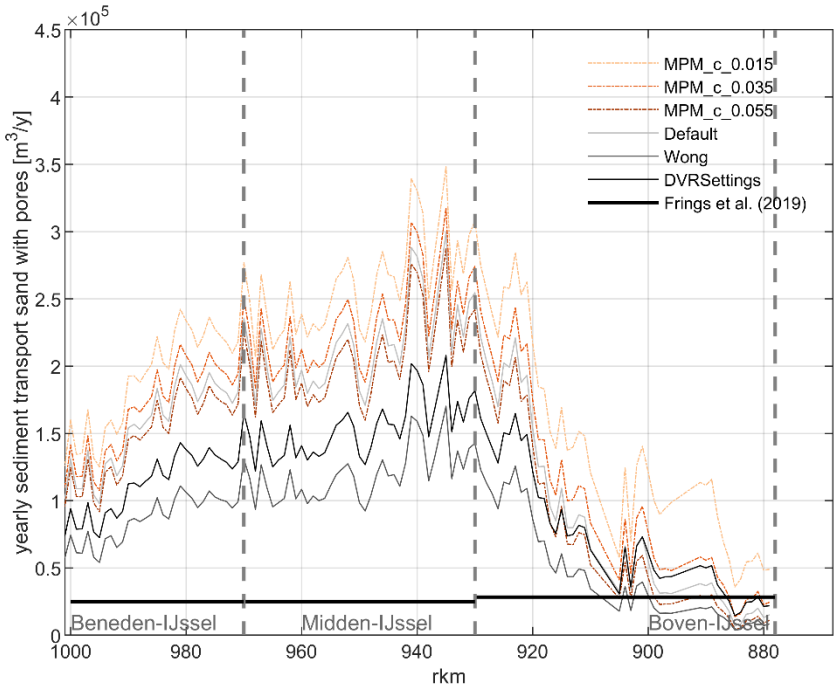

Figure 7.9 Yearly sediment transport for sand with pores changing parameters c (orange dashed-dotted lines) compared to MPM default setting (light grey), Wong et al. (2009) (grey), DVR settings (black), and sediment transport estimates from Frings et al. (2019).

Hiding and exposure and the ripple factor were also tested. Hiding and exposure formulas 0,1,2 and 3 (see Table 6-2) were tested. In 2 (Hiding and exposure formula 2 = Power law (Parker, Klingeman & McLean or Soehngen, Kellerman & Loy), the hiding coefficient was fixed to -0.8, no variations were tested.

Sediment transport was not very sensitive to changes in the hiding and exposure settings (Figure 7.10), also not upstream in the section with clearly graded sediment in the bed. The ripple factor, on the other hand, has a larger effect on the sediment transport. Decreasing the ripple factor from 1 to 0.4 (using method 1 – constant μ, see Table 6-4) leads to a decrease of approximately 200.000 m³/year in the Waal (Becker et al., 2023). This test was not conducted for the IJssel, since similar results were expected.

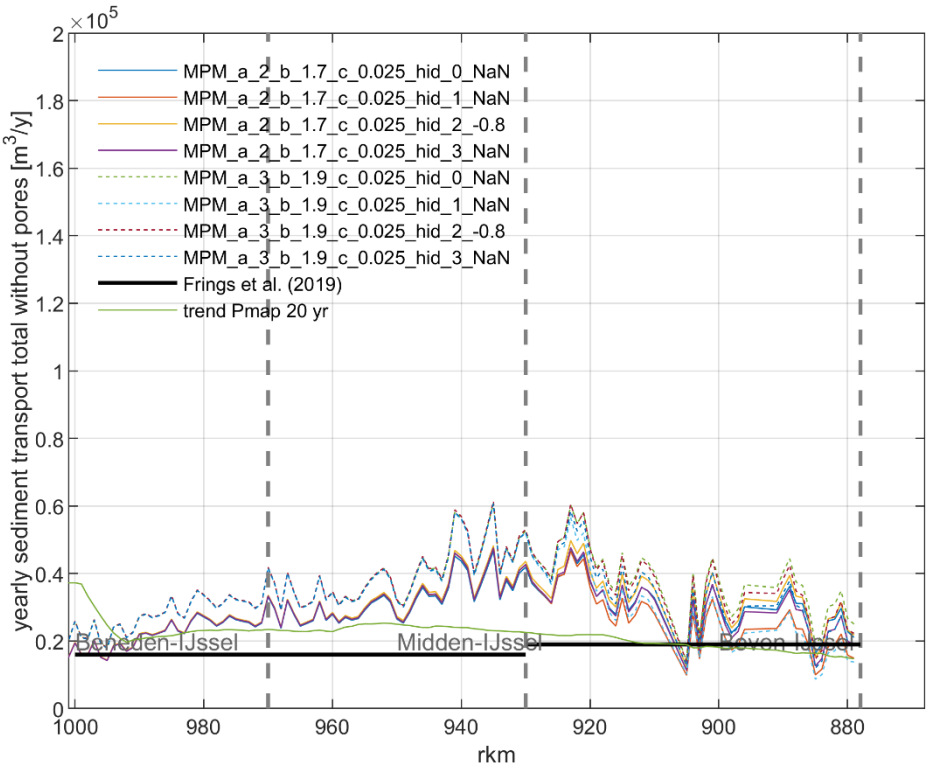

Figure 7.10 Sensitivity test of sediment transport for different hiding and exposure settings.

Based on the results and discussions with Rijkswaterstaat, the decision was made to use parameters based on the recent literature of (Wong & Parker, 2006). The main reason was that we did not want to deviate from a formulation that was published in scientific literature, because that would change the character of the transport formula into something that has not been tested scientifically. The only parameter that got a different value is the calibration factor (a), which is meant to be varied for calibration to better fit the measured data. It still needs to be decided whether the same set of parameters should be used for all branches, or if we want to build separate branch models with each using the ideal settings per branch. This will be done once the models of Boven-Rijn, Pannerdensch Kanaal and Neder-Rijn/Lek have been set up as well.

For the Waal and IJssel, the set of parameters presented in Table 7-2 was used for initial calibration runs.

Table 7-2 – Final parameters settings used in the model

Settings	Sediment transport formula	Parameters
Final parameter set	Meyer-Peter-Müller (all fractions)	a = 2; b = 1.6; θ_c = 0.047
	Hiding and Exposure	Power Law with α = -0.8
	Ripple factor	Constant user input = 1.0

Final results of the offline run with these parameters can be seen in Figure 7.11.

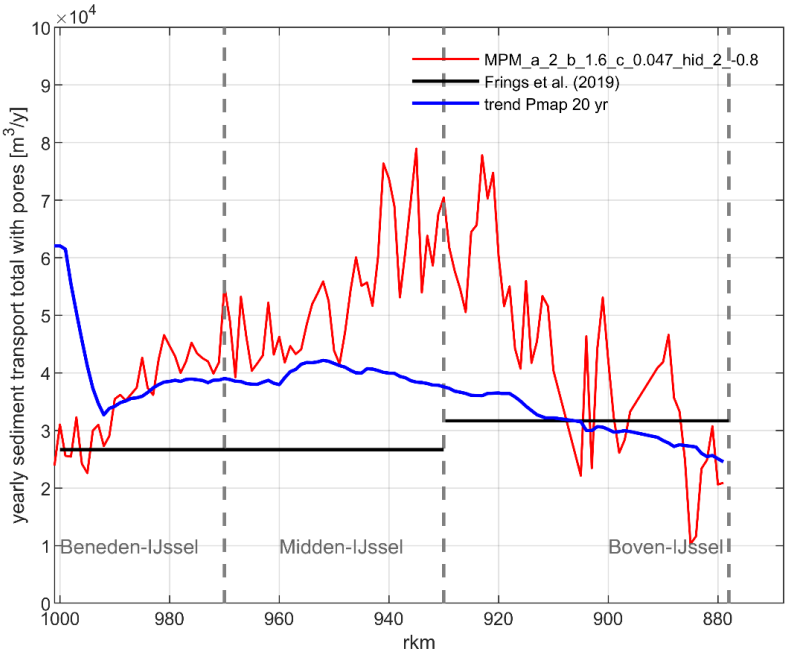

Figure 7.11 Offline yearly total sediment transport with MPM sediment transport formula with a =2, b=1.6 , c =0.047.

7.2.2 Gradient analysis

As part of the offline calibration, the sediment transport results were compared to velocity and grain size (Figure 6.2) gradients. As the sediment transports, velocities were averaged within the main channel and per river kilometer. Figure 7.12 shows the results of the sediment transport per fraction (1-11) and the velocities for three flow conditions. Based on these outputs the following conclusions can be drawn:

- For low flows moving in the downstream direction up to km 930, we see that although velocity decreases, there is a positive gradient in sediment transport. This is due to the reduction of the mean particle size in this transition between gravel and sand. After km 930 there is an inflection point in the grainsize fining, and the downstream fining is less strong. Then the negative gradient in velocity plays a bigger role, leading to a reduction in the sediment transport.
- Similar results are observed for medium flows. In medium flows, also larger particles are entrained (5-11).
- For high flows, the influence of grain size on sediment transport is still visible in the upstream part, especially for the finer fractions. From approximately km 930, the velocity gradient takes over.

Especially upstream, between km 880 and 930, the transport gradient is too high. This can be explained by

1. a slightly too strong fining in the grain sizes (see Figure 6.2), and
2. an underestimation of flow velocities upstream and overestimation around Zutphen (km 930), resulting in a too strong decrease in velocity.

The best way to improve model results in terms of transport would be to improve the flow velocities, because initial grain sizes are more difficult to modify in a graded sediment model and will change again during morphological spin-up of the model.

Flow	Sediment transport / fraction	Velocity
Low flow (1020 m³/s at Lobith)	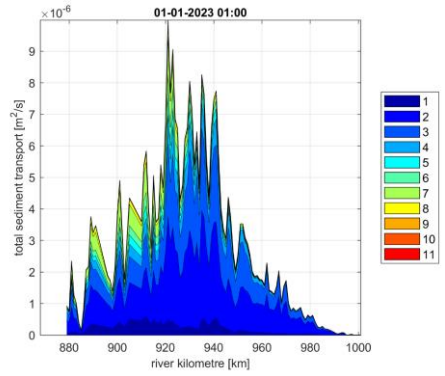	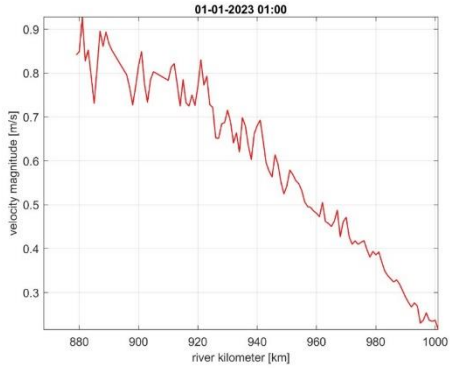
Medium flow (3053 m³/s at Lobith)	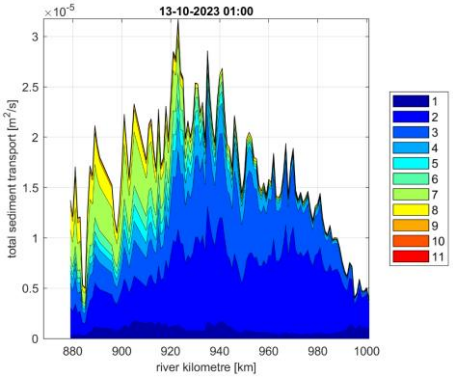	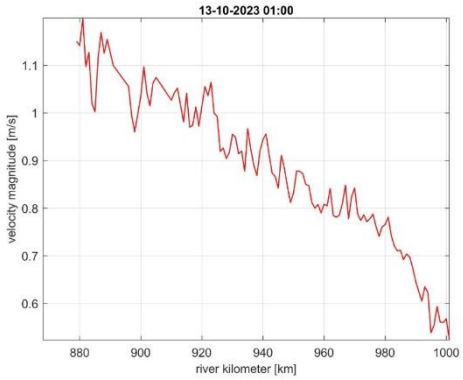
High flow (8592 m³/s at Lobith)	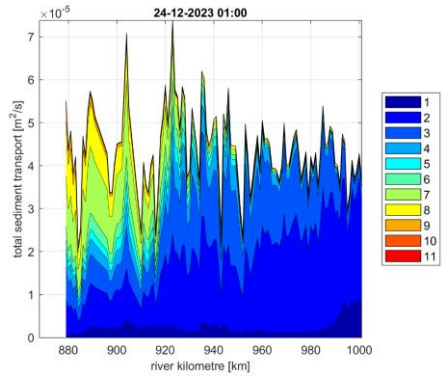	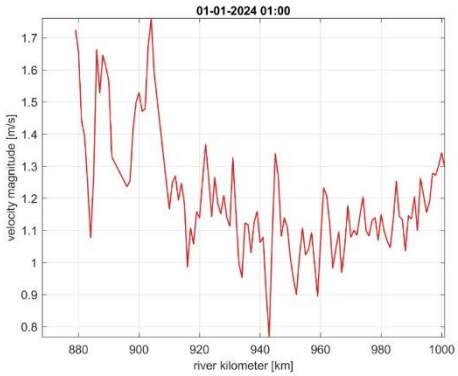

Figure 7.12 – Total sediment transport per fraction and velocity gradient for low, medium and high flows in the IJssel for Meyer-Peter and Müller transport formula (a = 2, b = 1.6, c=0.047).

8 First steps in 1D calibration

8.1 Calibration procedure

Calibration will be carried out in 2 steps, a 1D and a 2D calibration, as described in the “plan van aanpak” (Spruyt, 2022). The 1D calibration focusses on the following parameters:

1 Yearly sediment transport rates and transport gradients (longitudinal profiles of sediment transport) as described in paragraph 3.4.2
2 width averaged bed levels and bed level trends (longitudinal profiles L3R3 per km, as described in paragraph 3.4.1)
3 Celerities (propagation speeds) of local disturbances in the bed level. This step has not yet been carried out. Indicative values for the celerities have been derived by Sieben (2020), see paragraph 3.4.3, these will have to be verified with the data by De Joode (2023) (see paragraph 3.4.1).

The 2D calibration is meant to adjust

4 2D patterns, e.g. transverse slope in bends (longitudinal profiles along the river axis and lines to the left (L3) and right (R3) of the river axis)

For the 1D calibration, first a test simulation was run with a parameter set that seemed promising according to first results of the offline calibration. Then, a new simulation was tested, which uses the settings reported in literature (Wong & Parker, 2006) for the critical Shields parameter and for the exponent b, in order to keep the character of the transport formula (its non-linearity) based on literature. Table 8-1 indicates the parameters used for each simulation.

Table 8-1 Calibration parameters tested

Settings	Sediment transport formula	Parameters
Test simulation	Meyer-Peter-Müller (all fractions)	a = 2; b = 1.7; θ_c = 0.025
Offline Calibration		a = 2; b = 1.6; θ_c = 0.047

In the following sections, the first morphological simulations for the calibration period are analyzed. Note that these results are coming from simulations that start from initial bed levels and composition without prior spin-up. These results thus have to be regarded as preliminary, which is why the resulting model version is called v0.5. In 2025, we intend to finish 1D calibration to reach model version v0.8 and then continue with 2D calibration leading to model version v1.0.

8.2 Calibration and validation periods

For the IJssel branch, an analysis of bed developments and dredging activities by Sieben (2023) has shown that the following periods can be regarded as approximately homogeneous:

- 2002 - 2010 (Boven-IJssel up to km 901, Doesburg) and 2013 (rest of the IJssel)
- 2016 - 2020

We suggest to use the first (and longer) period for calibration and the latter and shorter period for validation. The following paragraph presents first results for the period 2002-2012.

8.3 1D calibration – first results

8.3.1 Yearly sediment transport rates and transport gradients

Sediment transport of sand and gravel on the upstream part of the IJssel should be around 32.000 m³/y including pores and decrease towards approximately 26.000 m³/y as it moves downstream (Frings, 2019, and section 3.4.2). Note that the gradients estimated based on bed level changes (Sloff, 2019) do not take into account the influence of sedimentation and erosion waves.

Results for yearly sediment transport (with pores) along the IJssel for the 10 years simulation from both calibration simulations presented in Table 8-1 can be seen in Figure 8.1 and Figure 8.2.

Figure 8.1, which was the test simulation, shows a clear sedimentation wave upstream, that cannot be physically explained by any of the initial conditions and boundaries of the model. Conclusion is that the model is ill-posed, leading to numerical instability. This was further analyzed and explained by Chavarrías (2024), see Appendix D.

As detailed in the memo, for the new parameter set from the offline calibration the model is on the edge of stability. So Figure 8.2 does not show such a sedimentation wave, and the sediment transport seems reasonable when comparing to the data (Pmap and Frings). However, this does not mean that the ill-posedness issue is solved. Small changes in the model, such as an update of the geometry to a more recent state or the implementation of an intervention, can still lead to instability.

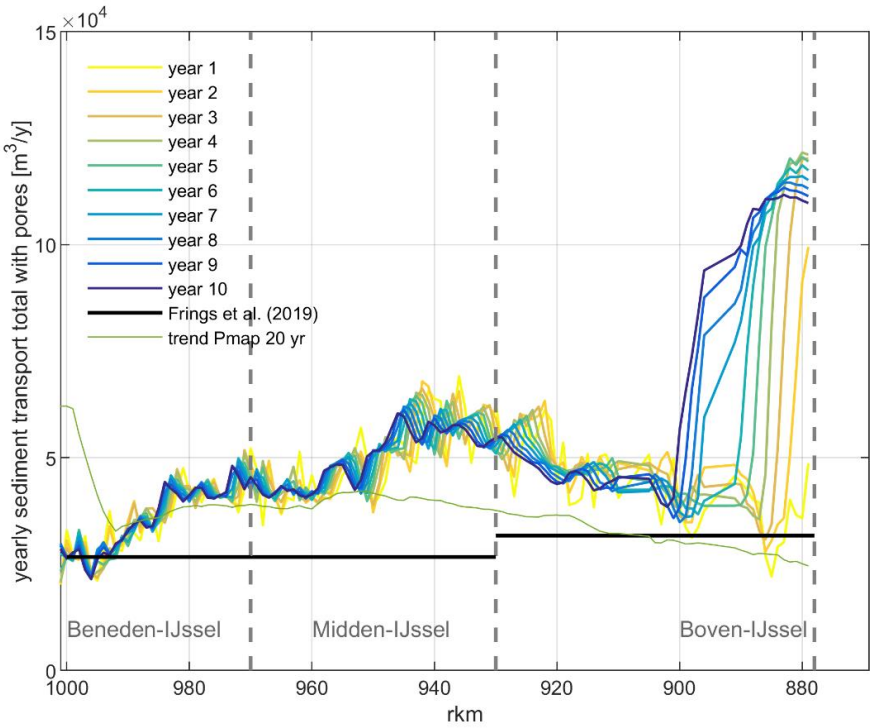

Figure 8.1 Yearly sediment transport rates (total with pores for all fractions) using the test parameter settings online (10 years) and sediment transport estimates by Frings et al.(2019) and Sloff (20219) ("trend PMAP 20yr").

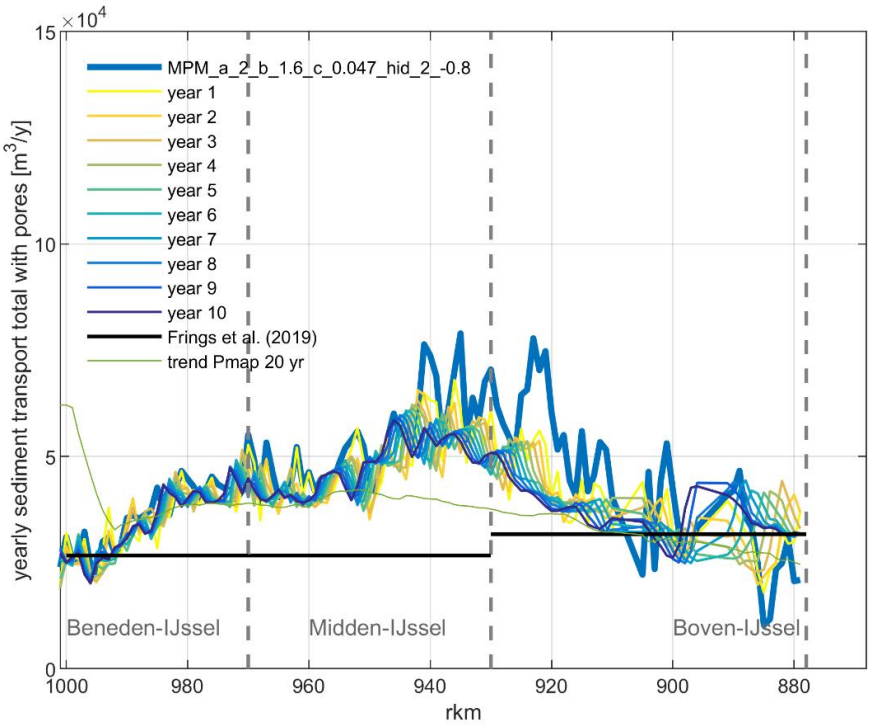

Figure 8.2 Yearly sediment transport rates (total with pores for all fractions) using the final parameter settings online and offline(10 years) and sediment transport estimates by Frings et al.(2019) and Sloff (20219) ("trend PMAP 20yr").

For this "stable" scenario we can see that the simulated transport up to km 990 is similar to the sediment transport estimates. There is an increase in sediment transport upstream up to an inflection point in the Midden-Ijssel, similar to what is estimated by Sloff (2019). This reflects the gradient analysis in section 7.2.2. In the downstream part, we see a decrease of sediment transport in the model, whereas in the estimate of Sloff (2019) there is a steep increase. Probably the estimate of Sloff (2019) was based on bed level changes that included the summer bed lowering that was realized in 2015/2016 between km 992.9 and km 1000.6, which is not present in the model, since the model represents the state of approximately 2002.

In terms of order of magnitude, we see that the model overestimates the sediment transport in the Midden and Beneden-IJssel in comparison to Frings et al. (2019) estimates, while it remains close to the estimate of Sloff (2019). Only between km 920 and km 950 the modelled sediment transport is somewhat higher than estimated by Sloff (2019).

8.3.2 Bed level development

Figure 8.3 compares the width-averaged (L3R3) and km-averaged bed level development in the model to measurements. The increase in sediment transport between km 878 and km 945 is reflected in the erosion trend in the Boven-IJssel. This trend can be seen both in the measurements and in the model results. Moving downstream, a sedimentation trend is present with some differences between the model and the measurement. At km 960, for example, we see sedimentation in the measurements, whereas in the model there is erosion. This differences between model and measurements will be further analyzed in the next phases of the project.

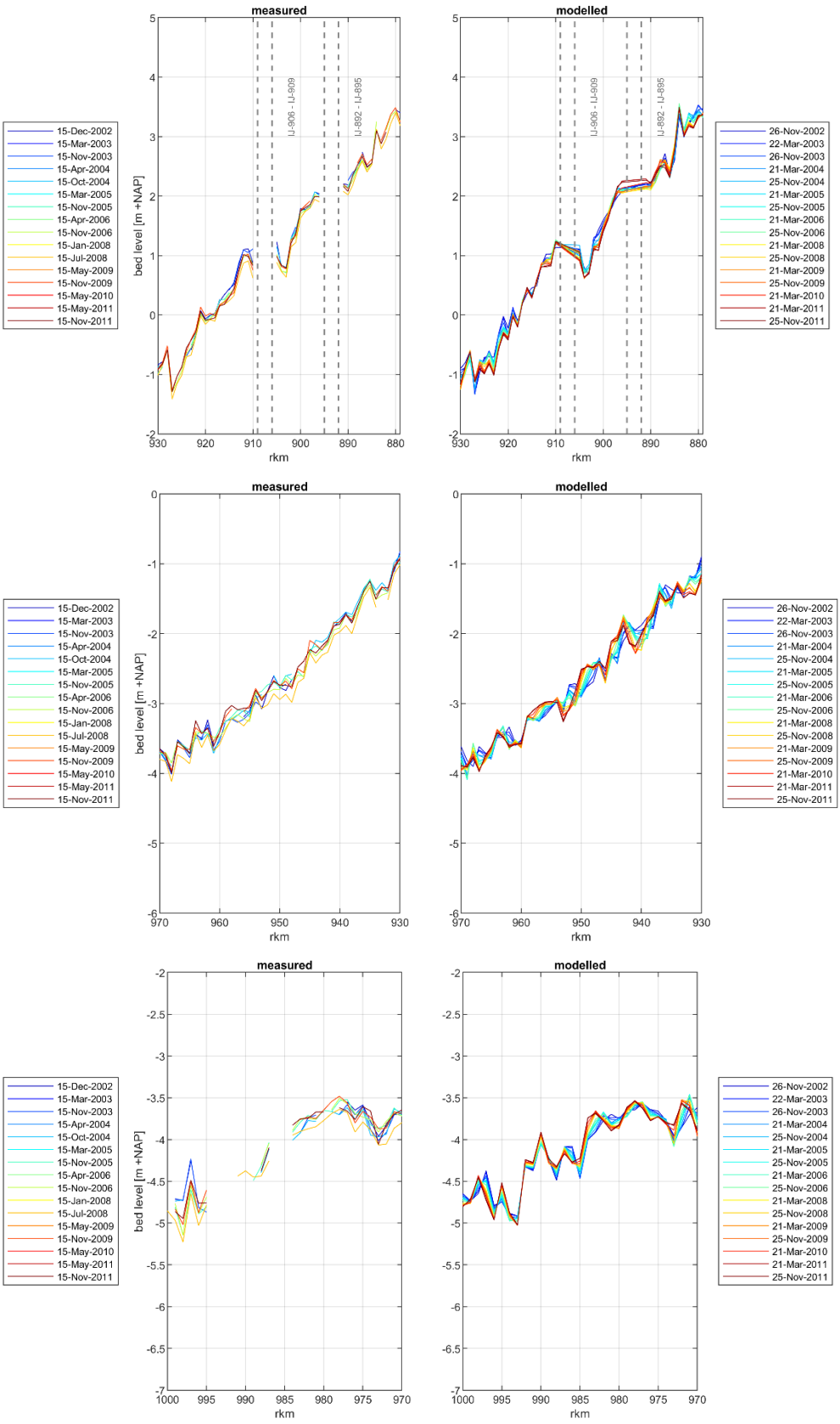

Figure 8.3 Km-averaged bed levels along the Boven IJssel. Left: observed (2002-2012); right: modelled using the final sediment transport formula settings (10 years-with initial bed level from 2002).

8.4 Recommendations for following calibrations steps

Based on these first calibration results, the following steps are recommended for the next phase of this project:

- Create the possibility to add extra diffusion to the model in case of an ill-posed situation.
- Analyze whether the results of the model can still be improved by adding lateral inflows.
- Repeat the simulations after proper spin-up of the model to see which part of the bed level and composition development is due to spin-up.
- Analyze the result and differences between model and measurements in more detail than was done so far, e.g.:
  - How to improve the gradients in yearly sediment transport?
  - At which locations do we see large deviations between modelled and observed bed level trends, and why?
  - Check propagation speed (celerity) of bed disturbances in the model and compare to the estimates of Sieben (2020) and the data of De Joode (2022)
- Run simulations for the validation period using the j16 model, and do the same analyses.
- Add dredging and dumping to the model and compare volumes to available data.
- Once the model is sufficiently calibrated for the long-term and on the larger scale, proceed to a detailed 2D calibration.

9 Conclusions and recommendations

A first version of the morphological model of the IJssel (v0.5: including offline calibration but not yet a full 1D calibration) was set-up based on existing 6th generation hydrodynamic models. Schematizations for two moments have been made: j02 (start of calibration period), and j16 (start of validation period). An offline calibration and first 1D calibration runs have been carried out with j02. The results for width averaged bed level changes and sediment transport are promising. Local deviations between model behavior and reality need to be removed in the next phase during more detailed (2D) calibration.

A serious issue was discovered in the model stability (ill-posedness) close to the upstream model boundary. Possibilities on how to solve this issue were discussed, and implementation of the most promising solution (introduction of additional diffusion where needed) will be taken up in 2025.

The 6th generation hydrodynamic model was changed in several points to make it usable for morphological simulations. The most important ones were the definition of main channel roughness and the schematization of bed levels. In the hydrodynamic model there are sharp transitions between different roughness values, which result in strong morphological reactions that do not occur in reality, where bed resistance usually has smooth gradients. In order to remove sharp transitions, and to decrease model complexity, the model is currently run using constant main channel roughness. In Becker et al. (2023), a proposition was made on how to improve the approach to implement main channel roughness in future hydrodynamic models, so that they can be used for morphological simulations as well. These can be tested in the following phase, once the model is better calibrated. The influence of the change of bed level schematization from “cell corners” to “cell centers” is significantly larger in the IJssel model than in the Waal model. This is because the grid resolution on the IJssel is much lower than on the Waal (only 6 cells across the width on the IJssel, while there are about 12 cells across the width on the Waal). The influence of the change in bed level schematization could partly be removed by an appropriate choice of summer bed roughness.

All steps in model development and the main steps in analysis of model results have been defined in Matlab scripts to make them reproducible and re-usable for model development for other branches or future scenarios. To make these accessible to future users, who will have to derive new model schematizations, it is recommended to group them in a clear workflow using software like Snakemake. In such a way, the order of the steps and input and output for/of each step are clearly defined. Snakemake also visualizes which steps have already been carried out, and which ones still need to be taken. Care should be taken to define which of the steps can be incorporated in future versions of Baseline, and how. These can then be kept outside the Snakemake workflow.

Table 9-1 recommends which steps to take next year. For the IJssel, the 1D calibration should be finished (leading to model version v0.8) and the 2D calibration carried out (leading to model version v1). For 1D validation, a dredging and dumping module should be added, following the set-up that was prepared for the Waal in 2024. For 2D calibration, attention should be paid to possible locations of non-erodible or partially erodible layers. Olink & Sieben (2024) prepared a method for this, and maps that visualize the bed characteristics of both Waal and IJssel branches are available now. Furthermore, the possibility to add extra diffusion to the model in case of ill-posedness should be added in the software and then used in the model.

Next to the work on the IJssel, the calibration of the Waal model will be refined further (leading to model version v1), and first models (v0) for Boven-Rijn, Pannerdensch Kanaal, Neder-Rijn and Lek will be set up.

Table 9-1 Recommended steps to continue model development in 2025.

activity areas	associated activities	model version	steps for 2025
data collection	• Collection of all data needed to set-up a model, e.g. boundary conditions, calibration data hydrodynamics and sediment transport and morphology, bed composition, etc.	v0 v1	non- or less erodible layers IJssel v1 (data analysis has been prepared by RWS in 2024)
morphodynamic model schematization: towards a well-working basic model (v0)	• set-up of a first running model including: a. dynamic river bed b. representative initial bed elevation (e.g. smoothing of bed forms) c. suitable roughness formulation for morphology d. sediment (grain sizes and sediment layers, with focus on active/upper layer) e. secondary flow f. first choice of transport formula and parameters (uncalibrated) g. non-erodible and less erodible layers h. suitable grid resolution • testing phase v0 model, identification of problems and modification of the schematization accordingly	v0	improving stability around upstream boundary (ill-posedness)
extending the basic model to a v1 model	• more sophisticated description of a. main channel roughness b. composition and thickness of underlayers, including non-erodible layers • set-up of a dredging and dumping module • testing phase v1 model, and iterative modification of model schematization if necessary	v1	IJssel v1: Non-erodible layers; Testing phase; dredging and dumping module
development of methodologies and tools for running the model	• approach and tools for model simulation (i.e. Simulation Management Tool) • strategy for model spin-up • strategy and tools for model evaluation and presentation of results • strategy and tools for simplification of model set-up and improving reproducibility	v0 v1	IJssel v1: Snakemake workflows, analysis time dependent morfac
model calibration and validation	• calibration and validation strategy • adapting the hydrodynamic model to make it suitable for morphodynamic simulations • hydrodynamic validation • “offline” calibration giving a first estimate of morphological response based on the flow field in the hydrodynamic simulations • 1D morphodynamic calibration and validation (focusing on width-averaged, large-scale and long-term trends) • 2D morphodynamic calibration and validation (focusing on 2D patterns in the river bed, such as bank patterns and bend profiles) • validation of dredging and dumping module	v1	IJssel v1: finish 1D calibration and carry out 2D calibration

activity areas	associated activities	model version	steps for 2025
exploring model uncertainties	• influence of unknown physical variables (e.g. roughness in transport, bed composition, active layer thickness) • influence of model settings (e.g. initial geometry/composition and boundary conditions) or modelling concepts (e.g. Hirano model) • influence of simulation strategy and approaches (e.g. methods for optimizing simulation time, schematization of the hydrograph, choice of simulation period)	v1-v3	-
development of modeling strategies and development for future use of the model	• identifying types of application and requirements • development of strategies for application of the model (e.g. choice of scenarios, choices for model settings and geometry, type of interventions) • identifying needs for further development of the model schematization (including needs for knowledge development and data requirements) • implementation and testing	v1-v3	-
verification of model application	testing the model application in test cases of a. effect of interventions b. planning study (“planstudie”) c. (long-term) forecast of system behaviour improvement of the model schematization, modeling strategies, methodologies and tools based on the outcomes of the test cases	v1-v3	-
Implementation of new functionality in D-HYDRO	• Identifying requirements of new functionality • functional design of needs • design of implementation • implementation and testing • updating user manuals	v2-v3	extra diffusion to in case of ill-posedness

10 Literature

Baseline. (2024, March). User Manual Baseline 6.3.

Becker, A. (2021), Slim suppleren Boven-Waal, rapport Deltares 11206792-014-ZWS-0001, Deltares, Delft, 156 pp.

Becker, A., A. Kosters, A.L. Nunes de Alencar Osario, V. Chavarrías, W. Ottevanger (2023): Morphological model for the river Rhine. First model (v0) of the Waal branch. Deltares report 11209261-003-ZWS-0002. Dec. 2023.

Brinke, W. ten (2019): Effecten morfologische ontwikkelingen op functies Rijn en Maas. Blueland Consultancy BV. Rapport B19.01, Oct. 2019.

Chavarrías, V., Busnelli, M. and Sloff, K. (2020). Morphological models for IRM. Rhine branches 1D. Deltares report 11206792-014-ZWS-0001.

De Jong, J., and W. Ottevanger (2020): Analyse van de bodemhoogte Rijntakken van 1999 tot 2018. Deltares-memo 11202744-003-ZWS-0001, 2 april 2020.

Deltares. (2022). User Manual Delft 3D FM Suite.

Engelund, F., and E. Hansen (1967): Monograph on sediment transport in alluvial streams. Tech. Rep., Hydraulics Laboratory, Technical University of Denmark, Copenhagen, Denmark.

Frings, R.M., G. Hillebrand, N. Gehres, K. Banhold, S. Schriever and T. Hoffmann (2019): From source to mouth: Basin-scale morphodynamics of the Rhine River. Earth-Science Reviews, Volume 196, ISSN 0012-8252, https://doi.org/10.1016/j.earscirev.2019.04.002.

Hirano, M. (1971): River bed degradation with armouring. Proc. Jpn. Soc. Civ. Eng. 195: 55-65. DOI: 10.2208/jscej1969.1971.195_55.

Joode, A. de (2022): Bodemparameters voorbereiding 2D model Rijntakken. 20 december 2022.

Kosters, A., Spruyt, A.S. and Niesten, I. (2022). Ontwikkeling zesde-generatie Rijntakken model: Modelbouw, kalibratie en validatie. Deltares report 11206813-003-ZWS-0012.

Kosters, A., A. Becker, W. Ottevanger, V. Chavarrías, A. Nunes de Alencar Osario (2024): Morphological model of the river Rhine. Partially calibrated (v0.8) model of the Waal branch.

Meyer-Peter, E., and R. Müller (1948): Formulas for bed-load transport. In: Proc. 2nd IAHR World Congress, 6-9 June, Stockholm, Sweden, pages 39-64.

Minns, T., A. Spruyt, D. Kerkhoven (2022): Specificaties zesde-generatie modellen met D-HYDRO. Generieke technische en functionele specificaties (v1-2023). Preliminary version, 22 december 2022.

Niesten, I., W. Ottevanger, A. Becker (2017): Riviersuppleties in de Rijntakken Conclusies 1e suppletie Boven-Rijn en advies voortzetting monitoring. Deltares report 11200877-000-ZWS-0005.

Olink, E., and J. Sieben, J. (2024): Korte verkenning scan rivierbodem met hardere ondergrond. Memo RWS-WVL of 11-06-2024.

Onjira, P. (2023), Living lab Rhine (LiLaR): Comparison of sediment measurement methods between the Netherlands and Germany, Tech. Rep., BfG.

Sieben, J., R. van der Veen, D.F. Kroekenstoel and M. Schropp (2005): Morfologsiche effecten Ruimte voor de Rivier in het Bovenrivierengebied. Tech. Rep. 20005.044X, RIZA, Directoraat-Generaal Rijkswaterstaat, Arnhem, The Netherlands.

Sieben, J. (2020): Notitie update kentallen lokale 1D bodemdynamiek Rijntakken. Memo 1-9-2020.

Sieben, J., D. Beyer, M. Reneerkens (2023): Definitie calibratie perioden, RWS concept-memo 11-5-2023.

Sloff, K., A. Paarlberg, A. Spruyt, M. Yossef (2009): Voorspelinstrument Duurzame Vaardiepte Rijndelta. Continued development and application of morphological model DVR Part 2: model adjustment. Deltares report 1002069-002-ZWS-0005, June 2009.

Sloff, K. (2019): Prognose bodemligging Rijntakken 2020-2050. Trends voor scheepvaart en waterbeschikbaarheid. Deltares-rapport 1203738-005-BGS-0008, 20 december 2019.

Sloff, K. (2022): Ruimtelijke en temporele interpretatie van bemonstering bodemsamenstelling Rijntakken. Deltares report 11208033-012-ZWS-0001, 22 December 2022.

Sloff, K., Becker, A., Paarlberg, A., & van Denderen, P. (2024). Integraal Rivier Management, morfologisch model, 2D morfologie, DVR, Delft3D.

Spruyt, A. (2023): Plan voor ontwikkeling 2D morfologisch modelinstrumentarium van de Rijntakken in D-HYDRO. Functioneel en technisch ontwerp. Deltares report 11208033-014-ZWS-0001, 23 february 2023.

Spruyt, A., T. Minns, M. Yossef, D. Kerkhoven, F. Zijl, M. Genseberger (2016): Advies voor algemeen functioneel ontwerp voor de 6e-generatie modellen van RWS. Deltares rapport 1230071-011-ZWS-0009, December 2016.

Van Putten, D. (2023): Methodiek vereffenen afvoerverdeling. Versie 1, 15 februari 2023.

Ylla Arbós, C., A. Blom, S. van Vuren, R.M.J. Schielen (2019): Bed level change in the upper Rhine Delta since 1926 and rough extrapolation to 2050. Delft University, Nov 2019.nWong, M., & Parker, G. (2006). Re-analysis and correction bedload relation of Meyer-Peter and Muller using their own database. Journal of Hydarulic Engineering, Volume 132, Issue 11.n

Yossef, M. F. M., H. R. A. Jagers, S. van Vuren and A. Sieben (2008): Innovative techniques in modelling large-scale river morphology.” In M. Altinakar, M. A. Kokpinar, ˙Ismail Aydin, S¸ evket Cokgor and S. Kirgoz, eds., Procedings of the 4th International Conference on Fluvial Hydraulics (River Flow), 3-5 September, Cesme, Izmir, Turkey. Kubaba Congress Department and Travel Services, Ankara, Turkey.

A Baseline measure lists

A.1 Measure list baselijne-rijn-j95_6-j02_6-v1

```
*******************************************************************************
#
#  De naam voor deze variant is  : baseline-rijn-j02_6-v1
#  De basis voor deze variant is : baseline-rijn-j95_6-v1
#
# *******************************************************************************
#
#  RWS Oost-Nederland
#  25 april 2024
#
#  Met deze maatregel_lijst kan een selectie van de beschikbare wijzigingen
#  tussen 1995 en 2002 ingemixt worden. De volgorde van de maatregelen is
#  oplopend in de tijd en er is rekening gehouden met de inmixvolgorde. Het
#  resultaat van deze variant geeft de actuele situatie weer van de Rijntakken
#  voor het jaar 2002, ten behoeve van de ontwikkeling van D-MOR.
#
# Padnaam aangepast door Deltares: 26-4-2024
#
# *******************************************************************************
#
#  Actualisatiemaatregelen
#
# *******************************************************************************
#
../../rijn-maatr_6/act/ij_havikrw_a1
../../rijn-maatr_6/act/ij_tichel_a1
../../rijn-maatr_6/act/ij_dvldeve_a2
../../rijn-maatr_6/act/ij_engelse_a1
../../rijn-maatr_6/act/ij_rheder_a2
../../rijn-maatr_6/act/rt_zbhgt02_a1
#
# *******************************************************************************
#
#  Einde lijst
#
# *******************************************************************************
```

B Modified calibration factor file

```
#-------------------------------------------------------------------------------
#2014 DISCHARGE PK_872.5_QR_Pannkop_IJsselkpop #Pannkop-Pannerden - removed the discharge dependency because we don't have PK in our model
2014 1.0
#-------------------------------------------------------------------------------
#2015 DISCHARGE PK_872.5_QR_Pannkop_IJsselkpop #Pannkop-Pannerden - removed the discharge dependency because we don't have PK in our model
2015 1.0
#-------------------------------------------------------------------------------
2024 DISCHARGE IJ_880.4_QR_IJsselkop-Westervoort # IJsselkop-Hpleij
2024 0175 0.852
2024 0320 0.708
2024 0380 0.708
2024 0520 0.87
2024 1100 0.586
2024 1725 0.506
#-------------------------------------------------------------------------------
2025 DISCHARGE IJ_880.4_QR_IJsselkop-Westervoort # Hpleij_ijssel-Westervoort
2025 0175 1.082
2025 0320 1.106
2025 0520 1.088
2025 1100 1.163
2025 1725 1.33
#-------------------------------------------------------------------------------
2026 DISCHARGE IJ_884.8_QR_Westervoort-Doesburg # Westervoort-Desteeg
2026 0175 0.901
2026 0320 0.857
2026 0520 0.883
2026 1100 0.98
2026 1725 1.121
#-------------------------------------------------------------------------------
2027 DISCHARGE IJ_884.8_QR_Westervoort-Doesburg # Desteeg-Doesburg
2027 0187 0.95
2027 0345 0.941
2027 0520 0.987
2027 1100 1.127
2027 1725 1.289
#-------------------------------------------------------------------------------
2028 DISCHARGE IJ_915.4_QR_Doesburg-Zutphen # Doesburg-Zutphen
2028 0187 0.913
2028 0345 0.938
2028 0550 0.971
2028 1150 1.091
2028 1775 1.033
#-------------------------------------------------------------------------------
2029 DISCHARGE IJ_928.4_QR_Zutphen-Eefdebeneden # Zutphen-Eefdebeneden
2029 0195 1.032
2029 0363 1.031
2029 0550 1.055
```

2029 1175 1.133
2029 1775 0.955
#----------
2030 DISCHARGE IJ_945.0_QR_Eefdebeneden-Deventer # Eefdebeneden-Deventer
2030 0195 0.982
2030 0363 0.989
2030 0560 1.065
2030 1220 1.053
2030 1825 0.887
#----------
2031 DISCHARGE IJ_956.3_QR_Deventer-Olst # Deventer-Olst
2031 0195 0.93
2031 0363 0.93
2031 0560 1.015
2031 1220 1.065
2031 1825 0.897
#----------
2032 DISCHARGE IJ_957.4_QR_Olst-Wijhe # Olst-Veessen
2032 0195 0.969
2032 0363 0.938
2032 0560 1.048
2032 1220 1.219
2032 1825 1.054
#----------
2033 DISCHARGE IJ_957.4_QR_Olst-Wijhe # Veessen-Wijhe
2033 0195 0.969
2033 0363 0.938
2033 0560 1.048
2033 1220 1.219
2033 1825 1.054
#----------
2034 DISCHARGE IJ_980.1_QR_Wijhe-Katerveer # Wijhe-Wapenveld
2034 0195 0.983
2034 0363 0.953
2034 0560 1.051
2034 1240 1.077
2034 1825 0.931
#----------
2035 DISCHARGE IJ_980.1_QR_Wijhe-Katerveer # Wapenveld-Katerveer
2035 0195 0.983
2035 0363 0.953
2035 0560 1.051
2035 1240 1.077
2035 1825 0.931
#----------
2036 DISCHARGE IJ_987.2_QR_Katerveer-Keteldiep # Katerveer-Reevediep
2036 0195 0.975
2036 0363 0.913
2036 0560 1.013
2036 1240 1.05
2036 1825 0.977
#----------
2037 DISCHARGE IJ_987.2_QR_Katerveer-Keteldiep # Reevediep-Kampen
2037 0195 0.975

```
2037 0363 0.913
2037 0560 1.013
2037 1240 1.05
2037 1825 0.977
#-------------------------------------------------------------------------------------
2038 DISCHARGE IJ_997.1_QR_Kampen-Keteldiep-2 # Kampen-Keteldiep
2038 0195 0.804
2038 0363 0.804
2038 0560 0.804
2038 1240 0.991
2038 1825 0.887
#-------------------------------------------------------------------------------------
2039 DISCHARGE IJ_997.1_QR_Kampen-Keteldiep-2 # Keteldiep-eindeketdiepkatdiep
2039 0195 0.917
2039 0363 0.917
2039 0560 0.917
2039 1240 0.887
2039 1825 0.887
#-------------------------------------------------------------------------------------
2040 DISCHARGE IJ_880.1_QO_IJssel # Ketelmeer-Ketelbrug
2040 0195 1.0
2040 0363 1.0
2040 0572 1.0
2040 1135 1.0
2040 1825 1.0
#-------------------------------------------------------------------------------------
2041 DISCHARGE IJ_880.1_QO_IJssel # Vossemeer
2041 0195 1.0
2041 0363 1.0
2041 0572 1.0
2041 1135 1.0
2041 1825 1.0
```

C Figures of sediment composition

C.1 Boven-Rijn and Waal, width- and 10 km-averaged, log scale

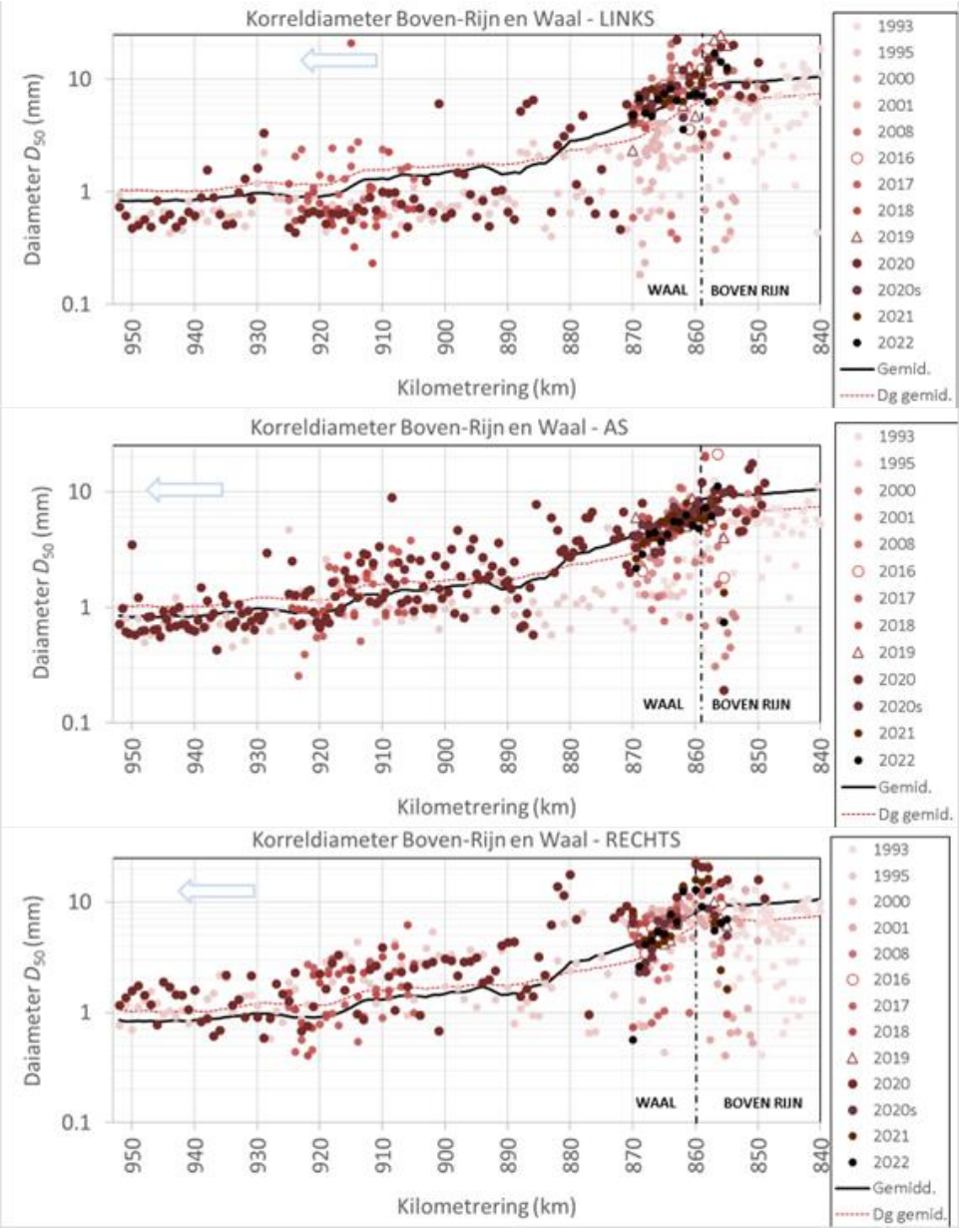

C.2 Boven-Rijn and Waal, width- and 10 km-averaged, linear scale

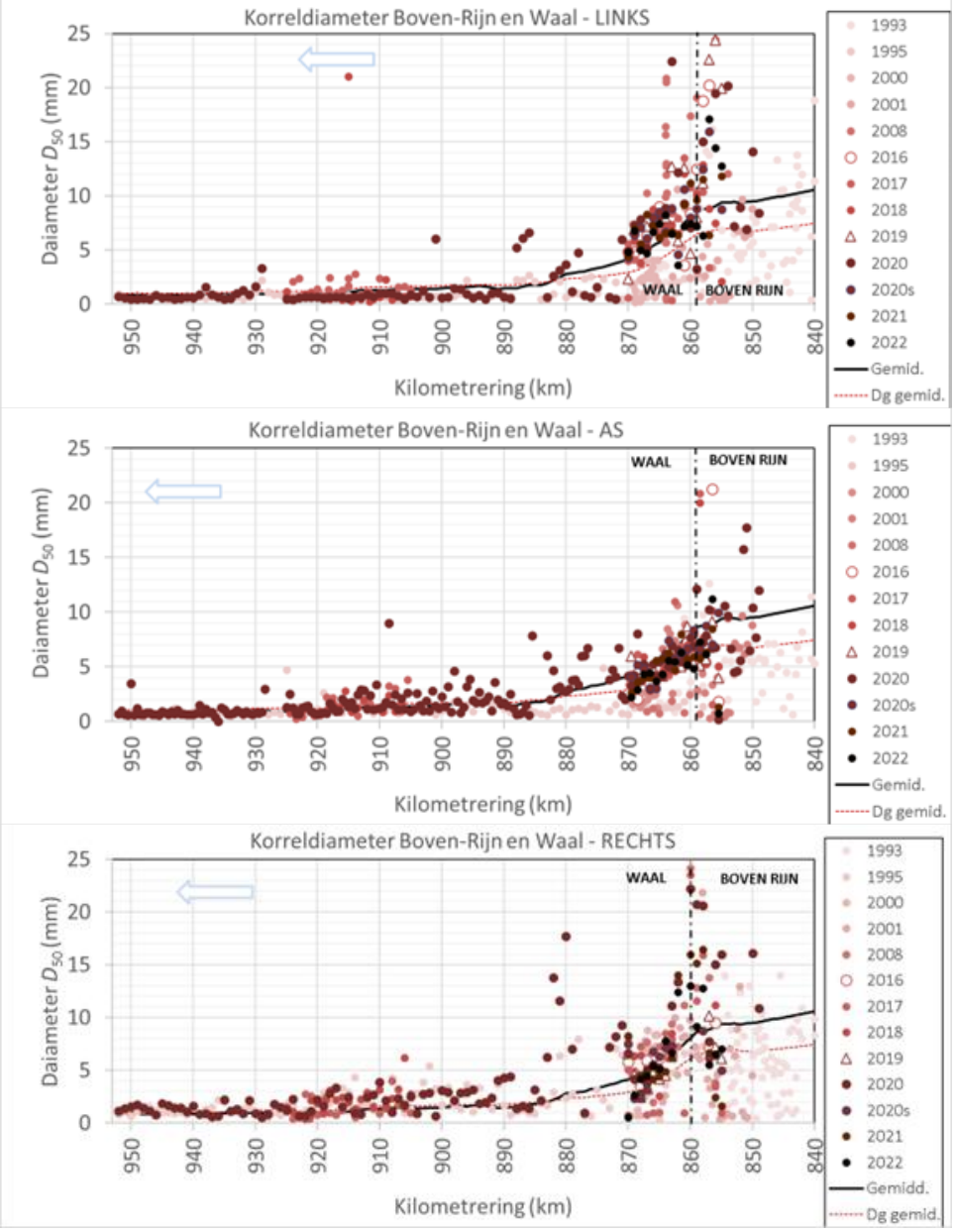

C.3 IJssel, width- and 10 km-averaged, log scale

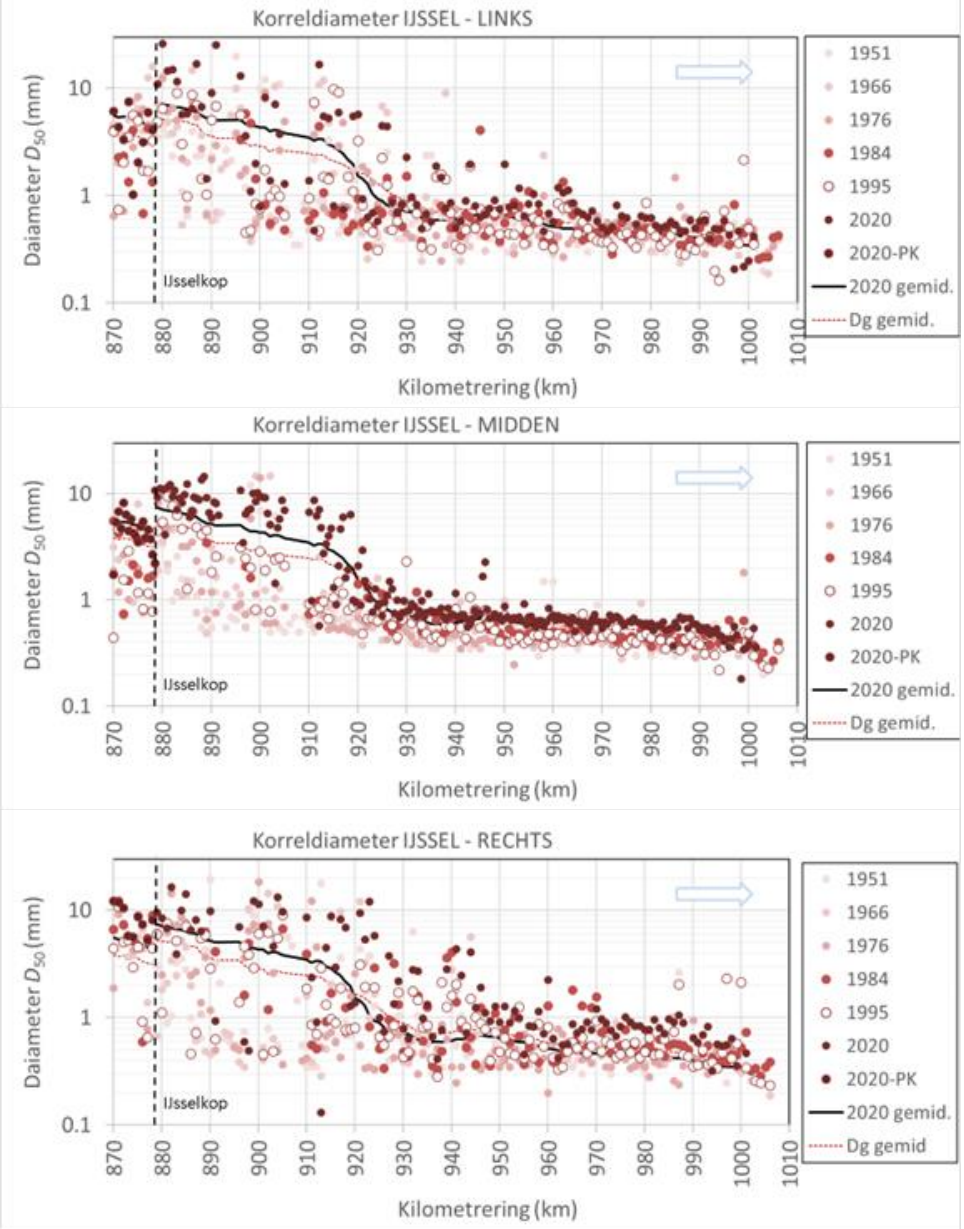

C.4 IJssel, width- and 10 km-averaged, linear scale

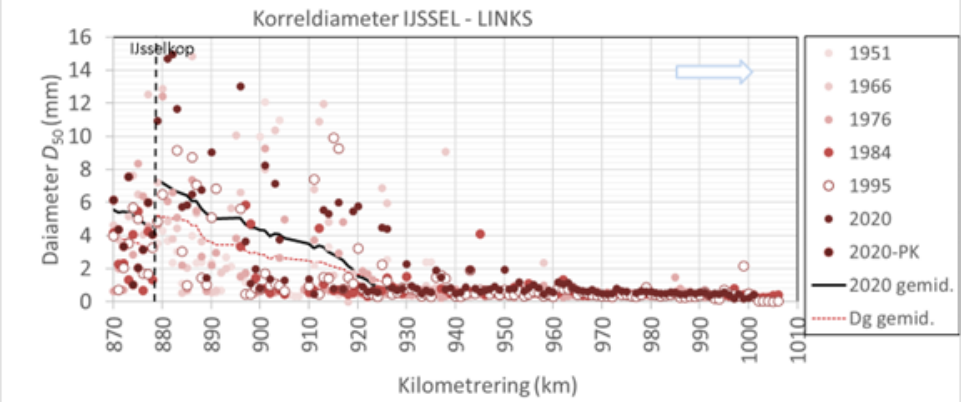

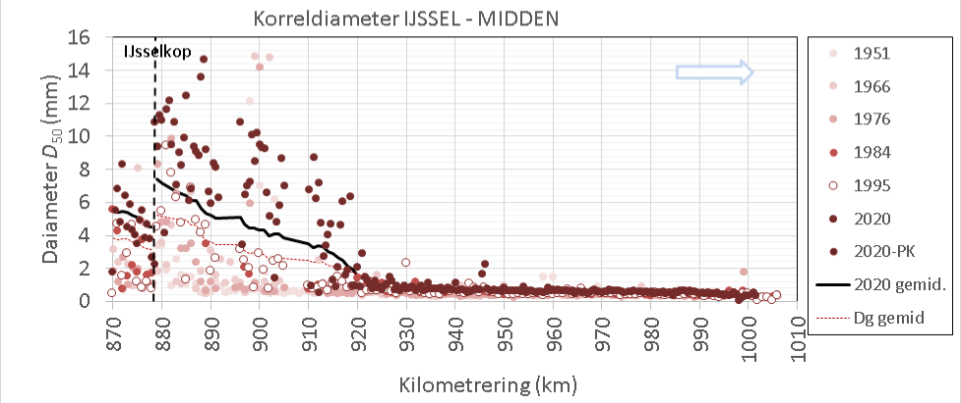

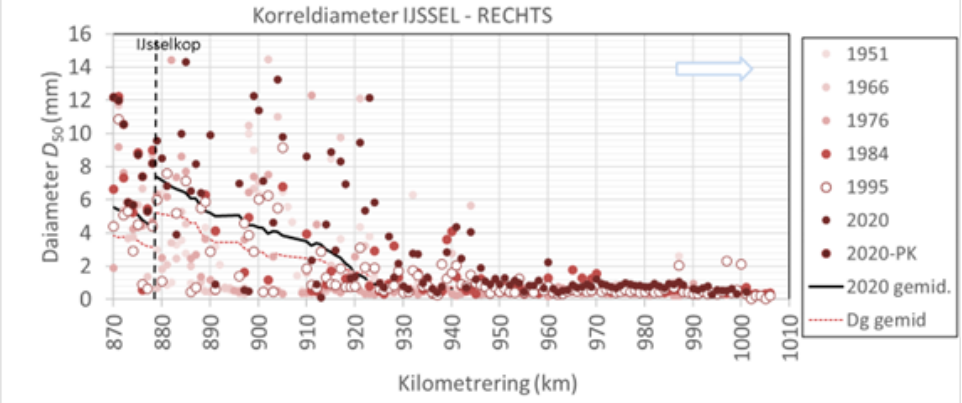

C.5 Pannerdensch Kanaal, Neder-Rijn and Lek, width- and 10 km-averaged, log scale

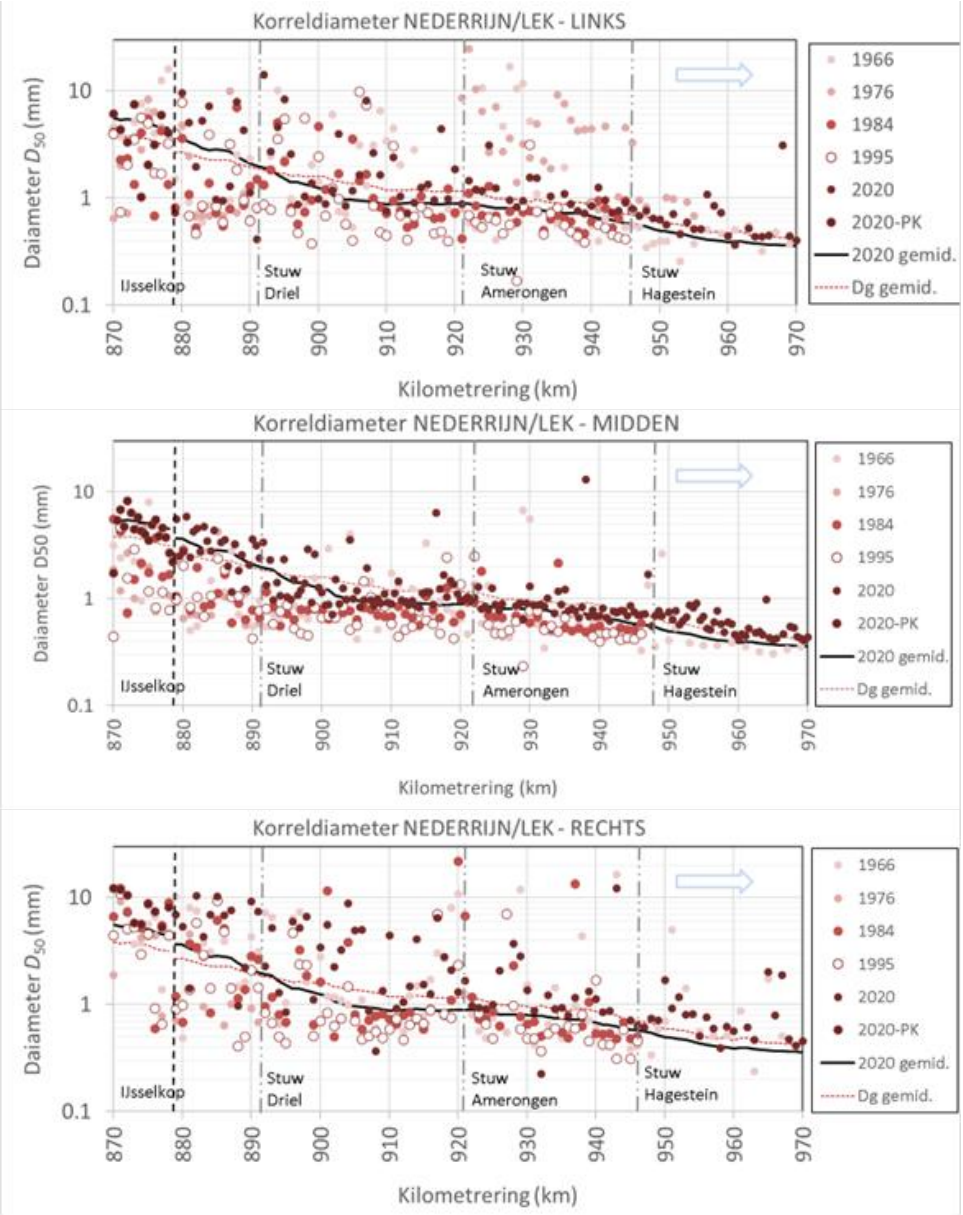

C.6 Pannerdensch Kanaal, Neder-Rijn and Lek, width- and 10 km-averaged, linear scale

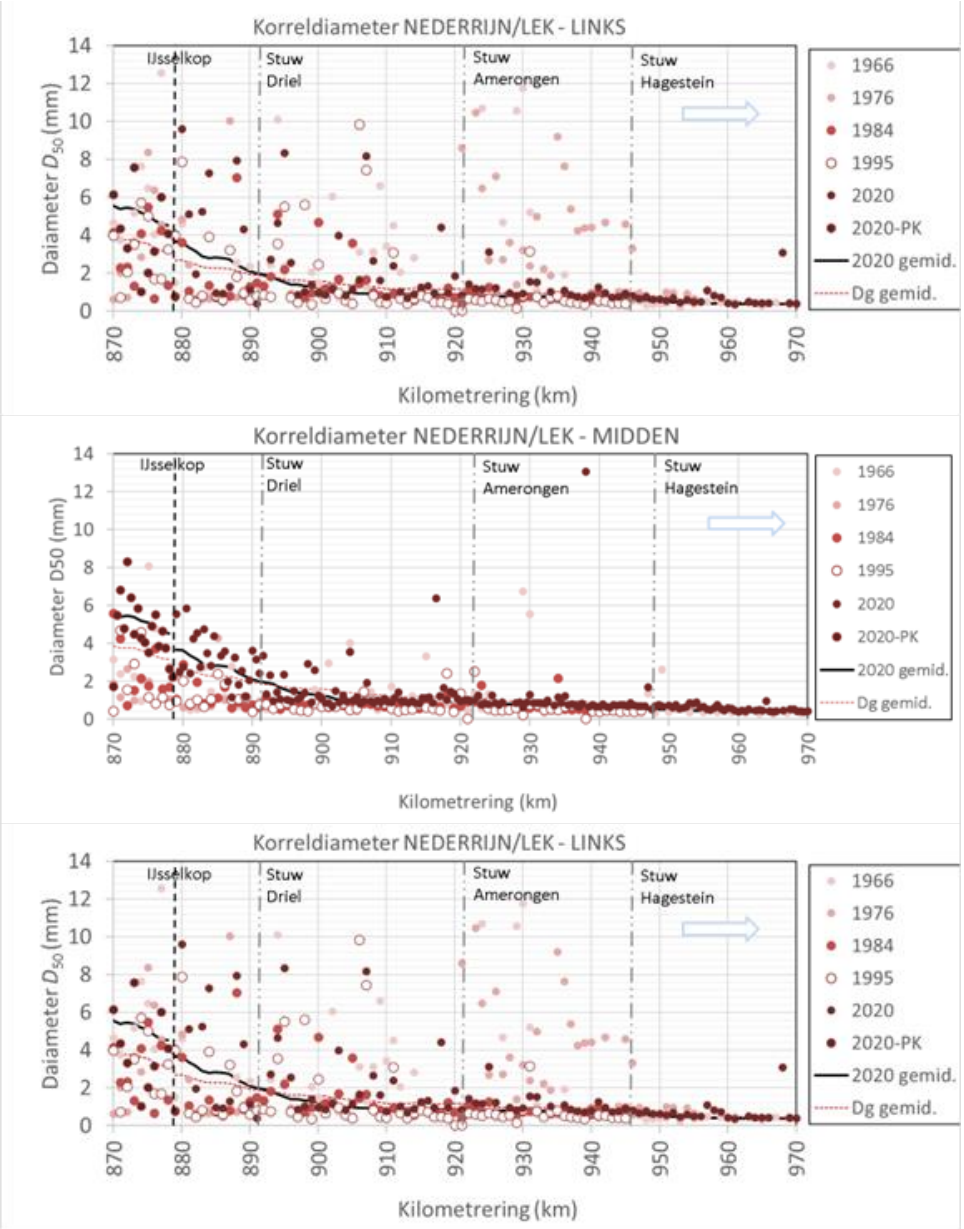

D Ill-posedness problem at the upstream end of the IJssel model

Deltares is een onafhankelijk kennisinstituut voor toegepast onderzoek op het gebied van water en ondergrond. Wereldwijd werken we aan slimme oplossingen voor mens, milieu en maatschappij.

Deltares

www.deltares.nl